

Geotechnical Extreme Events Reconnaissance

Geotechnical Reconnaissance:
The 28 September 2018 M7.5 Palu-Donggala, Indonesia Earthquake

(Version 1.0; 3 April 2019)



GEER Members: H. Benjamin Mason (United States team leader), Aaron P. Gallant, Daniel Hutabarat, Jack Montgomery, A. Nicole Reed, Joseph Wartman

HATTI Members: Masyhur Irsyam (Indonesian team leader), Widjojo Prakoso, Didiek Djarwadi, Dandung Harnanto, Idrus Alatas, Paulus Rahardjo, Pintor Simatupang, Aksan Kawanda

PusGen Members: Rahma Hanifa

ACKNOWLEDGEMENTS

The GEER reconnaissance was led by H. Benjamin Mason (Oregon State University) and included team members Aaron Gallant (University of Maine), Daniel Hutabarat (University of California, Berkeley), Jack Montgomery (Auburn University), and Joseph Wartman (University of Washington). A. Nicole Reed (Auburn University) provided support to the field team through pre-reconnaissance damage mapping and was responsible for mapping displacements of buildings using satellite images. We had incredible in country partners, which helped open many doors for us during the reconnaissance efforts. In particular, we thank the HATTI and PusGen organizations for all of their support and in particular, the in country collaborators: Masyhur Irsyam (Indonesian team leader), Widjojo Prakoso, Didiek Djarwadi, Dandung Harnanto, Idrus Alatas, Paulus Rahardjo, Pintor Simatupang, Aksan Kawanda, and Rahma Hanifa, who are co-authors of the report. The government of Indonesia was very supportive of our travel and issuing our research permits. We would like to particularly thank Ardito Kodijat, of the UNESCO Office in Jakarta, and Laura Kong, of the International Tsunami Information Center, for helping us quickly process the research permits and establish ourselves in Indonesia. We are sure that many more hands went into the process of helping, opening doors, and making us feel welcome in Indonesia. We would like to thank everyone who had a hand in our collective success.

The GEER team would like to thank Yuamar Imarrazan Basarah and Youssef Hashash (University of Illinois, Urbana-Champaign) for helping with the logistics of getting research permits and traveling to Indonesia, as well as Jake Dafni (University of Washington) for helping with the NSF-funded RAPID center's gear logistics. We would also like to thank the GEER Steering Committee and in particular David Frost and Fangzhou Albert Liu (Georgia Tech) for providing us with abundant support, guidance, and contacts during the reconnaissance effort. Before traveling to Indonesia, Hermann Fritz (Georgia Tech) and Ian Robertson (University of Hawaii) also provided us with abundant advice regarding traveling and performing reconnaissance in Palu.

The work of the GEER Association is based upon work supported in part by the National Foundation through the Geotechnical Engineering Program under Grant No. CMMI-1266418. The GEER Association is made possible by the vision and support of the NSF Geotechnical Engineering Program Directors: Dr. Richard Fragaszy and the late Dr. Cliff Astill. Reconnaissance mission field support was provided by the Natural Hazards Reconnaissance Facility (known as the "RAPID") under NSF grant 1611820. GEER members also donate their time, talent, and resources to collect time-sensitive field observations of the effects of extreme events. Any opinions, findings, and conclusions or recommendations expressed in this material are those of the authors and do not necessarily reflect the views of the NSF.

TABLE OF CONTENTS

ACKNOWLEDGEMENTS	ii
TABLE OF CONTENTS	iii
LIST OF FIGURES	iv
1 INTRODUCTION	1
2 GEOLOGIC BACKGROUND	5
2.1 Bedrock Geology and Tectonic Features	5
2.2 Surficial Geology: Palu Basin	8
2.3 Seismicity	9
3 LANDSLIDES IN THE PALU BASIN	11
3.1 Petobo Landslide	16
3.1.1 <i>Field observations and landslide morphology</i>	18
3.1.2 <i>Interpreted slide progression</i>	25
3.1.3 <i>Factors contributing to and hypothesized mechanisms of the Petobo flowslide</i>	28
3.2 Jono Oge Flowslide	31
3.2.1 <i>Field Observations and Morphology</i>	33
3.2.2 <i>Eyewitness accounts</i>	42
3.2.3 <i>Interpreted slide progression and hypothesized mechanisms</i>	43
3.3 Lolu Village Landslide	45
3.3.1 <i>Field Observations and Morphology</i>	46
3.3.1 <i>Interpreted Slide Progression and Hypothesized Mechanisms</i>	54
3.4 Sibalaya Landslide	57
3.4.1 <i>Field Observations and Morphology</i>	58
3.4.2 <i>Interpreted Slide Progression and Hypothesized Mechanisms</i>	65
3.5 Balaroa Landslide	68
4 SUMMARY AND CONCLUSIONS	72
5 REFERENCES	74

LIST OF FIGURES

Figure 1.1: Location of main earthquake, foreshocks, and aftershocks (from JRC, 2018).	3
Figure 1.2. Areas surveyed by the GEER Team.	4
Figure 2.1. North-south displacements mapped along the Palu-Koro Fault from optical satellite data after earthquake (Valkaniotis et al. 2018).	6
Figure 2.2. Geology of Sulawesi showing principal structures and geographical features (from Maulana et al. 2016).	7
Figure 2.3. Geologic map of the Palu area (from Watkinson 2011).	8
Figure 2.4. Surficial geology and sediment thickness in the Palu Valley (adapted from Hanifa 2018 and Thein et al. 2014).	9
Figure 2.5. Contours of peak ground acceleration (PGA) given by the United States Geologic Survey (USGS). The star is the earthquake’s epicenter and the red dot is a location of a “Did You Feel It?” respondent, which is near Palu City (after USGS; https://earthquake.usgs.gov/earthquakes/eventpage/us1000h3p4/shakemap/pga ; accessed 1 April 2019).	10
Figure 3.1. Locations of landslides in the Palu Basin surveyed by the GEER Team.	12
Figure 3.2. East-west ground deformations in Palu Basin interpreted from optical satellite data (adapted from Valkaniotis et al., 2018).	13
Figure 3.3. East-west ground deformations on western edge of Palu Basin interpreted from optical satellite data.	14
Figure 3.4. Elevation contours interpreted from optical satellite data on the western edge of the Palu Basin in the vicinity of the Peotobo, Lolu Village, and Jono Oge flowslides.	16
Figure 3.5. Orthomosaic map indicating limits of Petobo landslide, location of sand boils, vector displacements, and zones delineated by morphological features and key observations.	17
Figure 3.6. Digital elevation model illustrating 3D morphological features in the northeast section of the slide.	18
Figure 3.7. Observations in Zone A: a.) cracking in the irrigation canal (-0.93791, 119.92157); b.) collapse of canal walls near head scarp (-0.93832, 119.92154); c.) damage and vertical displacement of gates in northeast corner of slide where the canal turns and runs east to west (-0.936019, 119.920635); d.) back-rotated blocks near head scarp at the center of the slide (-0.938349, 119.921008); e.) back-rotated blocks and head scarp in northeast corner of the slide (-0.93623, 119.92018); f.) overlooking back-rotated block field in the southeast corner of the slide (0.94071, 119.92258).	20

Figure 3.8. Sand boils: a.) typical sand boil ejecta (-0.93850, 119.92092); b-c.) representative height and width of typical sand boils found preserved between blocks (-0.938503, 119.920425).
..... 21

Figure 3.9. Zone B: a.) relatively large block/mound in this zone with limited vegetation and a shape that is not as well-defined as blocks in Zone A (-0.939489, 119.917507); b.) debris flow deposits and mounds in the foreground of picture near the margin of Zone C, which forms an elevated plain at the boundary of these two zones (-0.939664, 119.918263)..... 21

Figure 3.10. Zone C: a.) view facing south-southeast at the margin of Zones B and C, with a clear difference in elevation and visible water in Zone C (-0.93971, 119.91859); b-c.) observed rill network and drainage channels carrying water through the zone (-0.939725, 119.918577 and 0.93974, 119.91859); d.) an erratic, relatively intact, block in the zone (-0.940918, 119.917806)
..... 23

Figure 3.11. Zone D: a.) compressed and uplifted blocks, ridges, and mounds along the western margin of the zone (-0.941527, 119.917471); b.) evidence of debris flow through a home in Zone D1 (-0.940627, 119.912096)..... 24

Figure 3.12. Zone E: a.) reworked areas in the center of the zone where earthwork has made morphological features unrecognizable (-0.93952, 119.90387); b.) flooded areas on the northern margins of Zone E (-0.94672, 119.90939); c.) flooded are on the southern margin of Zone E (-0.94090, 119.91040); d-f.) area along the southern margins of Zone E4 where debris flows infiltrated adjacent neighborhoods (-0.94072, 119.90413; -0.94141, 119.90977; -0.94150, 119.9068). 25

Figure 3.13. Perspective of eyewitness account (facing west-southwest) from northeast corner of slide (-0.93622, 119.920207). 27

Figure 3.14. Pre-slide cross-sections and topography and post-earthquake satellite imagery of slide at Petobo..... 28

Figure 3.15. Aerial view of destroyed water gate and breach point captured by drone. 31

Figure 3.16. Orthomosaic map indicating limits of Jono Oge landslide, location of sand boils, vector displacements, and zones delimited by morphological features and key observations. 32

Figure 3.17. Digital elevation model and drone-derived shaded relief image illustrating 3D morphological features in the eastern region of the slide. 33

Figure 3.18. (a) Final location of the Patra Poultry Market (-0.98786, 119.90844), which displaced approximately 1,230 m ; (b) final location of the Pusdiklat GPIID Patmos Jono Oge (-0.98942, 119.91007), which displaced approximately 1,080 m (image from Antara Foto 2018)..... 33

Figure 3.19. Zone A: (a) View of an intact rice paddy and the head scarp of the flowslide at Jono Oge (-0.98540, 119.92580); (b) intersection of the head scarp with the canal (-0.98423, 119.92607); (c) formation of rotated blocks and extensional cracks in the area of the canal breach

(note the sand deposited by the subsequent flooding; -0.98478, 119.92423); (d) damage to a road along the southern edge of the flowslide (0.98623, 119.92383)..... 34

Figure 3.20. Zone B: Zone B consists of rafted blocks that moved into the main failure area after the soil in this area was displaced (-0.98211, 119.91760). 35

Figure 3.21. Zone C: (a) Much of Zone C was low-lying and areas between blocks were often saturated (-0.98539, 119.91938); (b) collapsed structure located in Zone C (-0.98364, 119.92071). The metal roofing was removed after the earthquake; (c) collapsed structure and tree, which had moved approximately 470 meters on a relatively intact block of crust (-0.98436, 119.91995); (d) cluster of sand boils between two blocks of crust (-0.98410, 119.92163). Note the pen on one of the sand boils in the foreground is approximately 15 cm long. 37

Figure 3.22. Drone imagery of the secondary failure zone along the southern edge of the flowslide at Jono Oge. 38

Figure 3.23. Screenshot of a video recorded during the initial failure. The person recording the video is standing on the roof of a building, which is moving. The red roofed house in the video is not moving and is located at -0.98579, 119.91965. The buildings behind the red roofed house have not moved at the time the video was recorded, but were displaced by a secondary failure. 38

Figure 3.24. Zone D: (a) Tree in between two intact blocks of rice paddies (-0.98554, 119.22403); (b) small sand boils in a low-lying area between blocks of crust (-0.98483, 119.92223); (c) view of the red roofed house looking northeast (-0.98595, 119.91951); (d) damage to the side of the red roofed house looking southwest (-0.98566, 119.91973). The person in the photo is approximately 1.87 meters tall..... 39

Figure 3.25. Zone E: (a) Structure damaged by the flowslide deposits (-0.98898, 119.90891); (b) Existing structure surround by debris and soil deposited by the flowslide at Jono Oge (-0.98985, 119.90922); (c) A vehicle damaged by the flowslide (-0.98838, 119.90895); (d) debris, blocks of crust and trees within the deposition area of the flowslide (-0.98893, 119.90881)..... 40

Figure 3.26. Approximate extent of the mudflow caused by the canal breach at Jono Oge..... 41

Figure 3.27. (a) Mudflow deposits filled the streets, but left structures undamaged near the margins of the slide (-0.99025, 119.90926); (b) mudflow deposits within the river channel (-0.98440, 119.90143); (c) mudflow deposits left the river channel and flooded the surrounding community after reaching a bridge (-0.98279, 119.89848); (d) height of the mudflow on one of the homes near the bridge (-0.98253, 119.89817). The person in the photo is approximately 1.75 meters tall.... 42

Figure 3.28. Interpreted progression of the flowslide at Jono Oge. The large red arrows indicate initial movements, while the yellow arrows indicate secondary movements. 44

Figure 3.29. Pre-earthquake profile of the Jono Oge flowslide. 44

Figure 3.30. Orthomosaic map with sand boil locations and vector displacements at Lolu Village. 46

Figure 3.31. Orthomosaic map in area of the lower slide area indicating vector displacements. Also shown are the deformation patterns of ground masses near the center of the slide area (dashed green lines) and previous location of roads (brown dashed lines). 47

Figure 3.32. Drone-derived digital elevation model illustrating 3D morphological features at Lolu Village..... 47

Figure 3.33. a.) Aerial view of cracking in irrigation canal; b.) crack in canal (-0.96974, 119.92249); c.) sluice gate that remained largely intact (-0.970496, 119.922598). 48

Figure 3.34. a.) Lateral extension of ground in fields above (east) of the main road (-0.970407, 119.918776); b.) damage to residential structure and laterally extended ground near main road (-0.970327, 119.916775); c.) damage to residential structure and partial scarp development near main road (-0.971073, 119.919248). 49

Figure 3.35. Sand boils between laterally extended ground above (east of) the main road (-0.970349, 119.916787). 49

Figure 3.36. Damaged gas station on western side of main road: a.) view of facility (-0.970627, 119.916465); b.) splitting and cracking of concrete pavement (-0.970753, 119.916406). 50

Figure 3.37. Damaged structures in Zone B: a.) laterally extended ground and collapsed home (0.97051, 119.91515); b.) partially collapsed mosque and repaired access road left (-0.97050, 119.91492); c.) collapsed structures and rafted blocks in the foreground (-0.97037, 119.91531). 50

Figure 3.38. Area uphill and adjacent to sheared housing complex: a.) laterally extended and partially disintegrated blocks and mounds in field above housing complex (-0.97000, 119.91361); b.) extent of heavily reworked and disintegrated debris flow and rafted trees near margin of Zones B and C (-0.97034, 119.91374); c.) partially eroded sand boils near margin of debris flow deposits in Zone B (-0.97030, 119.91360). 51

Figure 3.39. Housing complex in Zone C: a.) view of split housing complex that slid around papaya tree field (-0.97025, 119.91304); b.) east-facing view showing rotated and uplifted street with papaya tree field still visible to the left (-0.97039, 119.91268); c.) view of destruction and evidence of compression and uplift in street in lower portion of apartment complex (-0.97069, 119.91304); d.) western view behind separated portion of housing complex showing sand boils and margin of debris flow and disintegrated blocks to the right (-0.97034, 119.91380); e.) west-northwest view of upper portion of housing complex with margin of debris flow and disintegrated blocks (-0.97036, 119.91375); f.) height of mudflow through lower portion of housing complex (-0.97040, 119.91292). 52

Figure 3.40. Zone D: a.) sand boil field and heavily reworked and disintegrated debris (-0.97100, 119.91171); b.) compression ridge near margin of Zones C and D (-0.97048, 119.91188); c.) forward-rotated trees near toe of slide (-0.97091, 119.91104). 53

Figure 3.41. Sand boil field near the eastern margin of Zone D..... 53

Figure 3.42. Pre-slide topography and interpreted slide progression indicating initial (red arrows) and secondary (yellow arrows) movements.....	56
Figure 3.43. Orthomosaic map indicating limits of Sibalaya landslide location of sand boils, and zones delimited by morphological features and key observations.....	57
Figure 3.44. Orthomosaic map indicating locations of sand boils, vector displacements, and zones delimited by morphological features and key observations.....	58
Figure 3.45. Zone A: a.) scour channel and damaged box culvert (-1,14844, 119.92477); b.) east-southeast facing perspective of southern scour channel where scour channels converge (-1.14788, 119.92281); c.) damaged gate and cracking in the canal on southeastern margin of slide (-1.149652, 119.924991); d.) damaged liner between box culvert and gate and sloughing of canal walls in the background (-1.14915, 119.92493).	59
Figure 3.46. Zone B1: a.) head scarp (-1.149536, 119.924125); b.) back-rotated blocks (-1.149580, 119.924053); c.) sand boils (-1.49620, 119.923225).....	60
Figure 3.47. Zone C: a.) view facing southeast of back-rotated blocks (-1.146946, 119.919843); b.) view facing south of back rotated blocks (-1.146946, 119.919843); c.) view facing southeast of back-rotated blocks and sand boils (-1.146575, 119.919432); d.) sand boils (-1.146419, 119.920662); e.) sand boils near margins of Zone C and D (-1.146422, 119.919374); f.) large sand boil (-1.147622, 119.921125).	61
Figure 3.48. Zone D: a.) block compression and uplift near northern margin of zone C (-1.145940, 119.919559); b.) relatively intact portion of road and apparent closure of crack on left side (-1.146440, 119.919162); c.) notable difference in elevation immediately adjacent to depression in zone C (-1.146422, 119.919289); d.) relatively intact residential homes near the center of the zone D (-1.146385, 119.919055); e.-f.) greater distress and collapse of structures near the northwestern margins of zone D (-1.145904, 119.919079 and -1.145963, 119.918827).....	63
Figure 3.49. Zone E: a.) runout block field and seam of previously liquefied sediment in seam between blocks (-1.144891, 119.917555); b.) sediment in depressed seam between blocks (-1.14496, 119.91769); c.) forward-rotated and uplifted collision blocks near the terminus of the slide (-1.144893, 119.917708); d.) thickness of debris at the terminus of the slide (-1.144651, 119.915743).	64
Figure 3.50. Pre-slide topography and interpreted slide progression indicating initial (red arrows) and secondary (yellow arrows) movements as well as runout displacements (blue arrows).....	67
Figure 3.51. Landside in the Balaroa neighborhood.....	68
Figure 3.52. Photos of the scarp of the Balaroa landslide (left -0.906689°, 119.839557°) and of the slide area (right, -0.906687°, 119.839372°) after clean-up had occurred.....	69
Figure 3.53. Displacement mapping of the Balaroa landslide.	69
Figure 3.54. Toe of the Balaroa landslide, showing multiple structures stacked on top of each other (-0.904367, 119.846528).....	70

Figure 3.55. Pre-slide topography of the Balaroa landslide..... 71

1 INTRODUCTION

The M_w 7.5 Palu-Donggala earthquake occurred on 28 September 2018 at 6:02 PM local time, and was caused by strike-slip faulting along the north-south trending Palu-Koro fault that extends through Palu City and the Central Sulawesi region of Indonesia. The United States Geological Survey (USGS) reports the epicenter was approximately 72 km north of Palu City at a depth of 10 km, and geodetic evidence indicates rupture of the fault over a length of 150 km Figure 1.1 shows the prescient earthquake ruptures as well as intensities caused by the mainshock (JRC, 2018). The earthquake triggered a series of massive landslides, resulted in the collapse of both unreinforced and reinforced structures, and generated tsunami waves that impacted coastal areas in Palu Bay, devastating Central Sulawesi.

The National Disaster Mitigation Agency in Indonesia (BNPB) estimates \$911 Million in economic losses in Central Sulawesi (Tehusijarana, 2018). Areas of Central Sulawesi most affected include Palu, Donggala, Sigi, and Parigi Moutong. According to the governor of Central Sulawesi, there were 4,340 fatalities as a result of the earthquake and tsunami (Jakarta Post, 2019). This count includes 667 people who had been declared missing. Search and rescue operations were halted on October 12 and the landslide areas were considered to be mass graves for those buried by the slides. The earthquake has also resulted in 4,438 major injuries, damage to 68,451 homes, and displacement of 206,494 people (AHA, 2018). The provincial capital of Palu City, which has a relatively large population of approximately 350,000 inhabitants, suffered the most significant human and economic losses. The large loss of life makes the Palu-Donggala earthquake the deadliest natural disaster worldwide in 2018, and the deadliest earthquake to affect Indonesia since the 2006 Yogyakarta earthquake. A substantial majority of the fatalities were directly related to landslides, making this one of the most significant landslide disasters of the past several decades.

The U.S. National Science Foundation (NSF)-funded Geotechnical Extreme Events Reconnaissance (GEER) team arrived in Palu City on 11 November 2018, and conducted six days of extensive fieldwork. The GEER team, which included U.S.-based five members, was hosted and accompanied by a team of geologists, geotechnical engineers, and researchers from Indonesia's Center for Earthquake Studies (PusGen) and the Indonesian Society of Geotechnical Engineers (HATTI). **Given our close-knit field operations, we collectively refer to the U.S.-Indonesian field reconnaissance team as the GEER team herein.**

Upon arrival, the GEER team surveyed coastal areas affected by the tsunamis. However, based on other reconnaissance teams' extensive tsunami-based surveys, the GEER team decided to focus

more efforts on the five large landslides within and just outside Palu City (see Figure 1.2 for GPS tracks), which were judged to be more geotechnically interesting. The GEER team's primary objectives were to collect and document perishable data that may be used to understand the sequence of events and general mechanisms resulting in these large landslides. Aside from the catastrophic loss of life and ongoing physical and emotional toll still burdening survivors in this region, several aspects of the events that unfolded after the Palu-Donggala earthquake make this one of the most significant geologic disasters in recent history.

A noteworthy issue is the paucity of strong motion data around the greater Palu area. In total, there were three seismic stations: one in Palu, one in Sabang, and one in Poso. At the time of this writing, the digitized seismic records were not publicly available.

Some aspects of the landslides studied by the GEER team that are significant to the engineering and science communities include:

1. Landslides occurred along ground with relatively low relief (i.e., average grades of approximately 2 to 4 percent). Portions of these landslides transitioned to flowslides (using the landslide classification of Hungr et al. 2014) after initiation that traveled approximately 1 km in several instances. In at least one location, a breached canal triggered a mudflow that over-rode the initial landslide mass. The enormous size of these slides is largely responsible for the significant loss-of-life during the Palu-Donggala earthquake.
2. The presence of sand boils at or near the landslides indicates that seismically-induced liquefaction occurred at each site. Soil liquefaction is believed to be the mechanism responsible for initiating the landslides. Important landslide morphological features including ground cracking (both tension and shear cracking), extension, back-rotated soil blocks, compression and uplift of soil blocks, sand boil "volcanoes", and erosional features, were well preserved and documented during the field reconnaissance.
3. An unlined irrigation canal forms the upper boundary or crest of slides that occurred on the eastern side of the Palu basin. The canal contributed to saturation of the ground (typically used as agricultural fields and rice paddies) at these locations, where the groundwater table would otherwise be at greater depths. The canal was breached by the landslides at several locations and contributed water to later stage mudflows at some locations. Thus, the canal is believed to have played a critical role in the initiation and progression of the landslides on the east side of Palu basin.

4. Geomatic and photogrammetric information collected via drone and satellite images assisted in understanding the evolution and progression of the landslides. These images captured the three-dimensional geomorphological features produced during these slides, and assisted in evaluating the displacement of structures and runout distances that manifested during these events.
5. Eyewitness accounts of the landslides were obtained from multiple survivors, many of whom witnessed the initiation and subsequent progression of the debris and mudflow that followed. Access to smartphones and cameras allowed local residents to capture video footage as some of the landslides occurred, which is one of the first instances where large scale landslides have been documented by multiple individuals on video. Links to these recordings on social media sites are provided in Chapter 3 and the videos have been archived along with this report on DesignSafe (designsafe-ci.org) to ensure they remain available to other researchers.

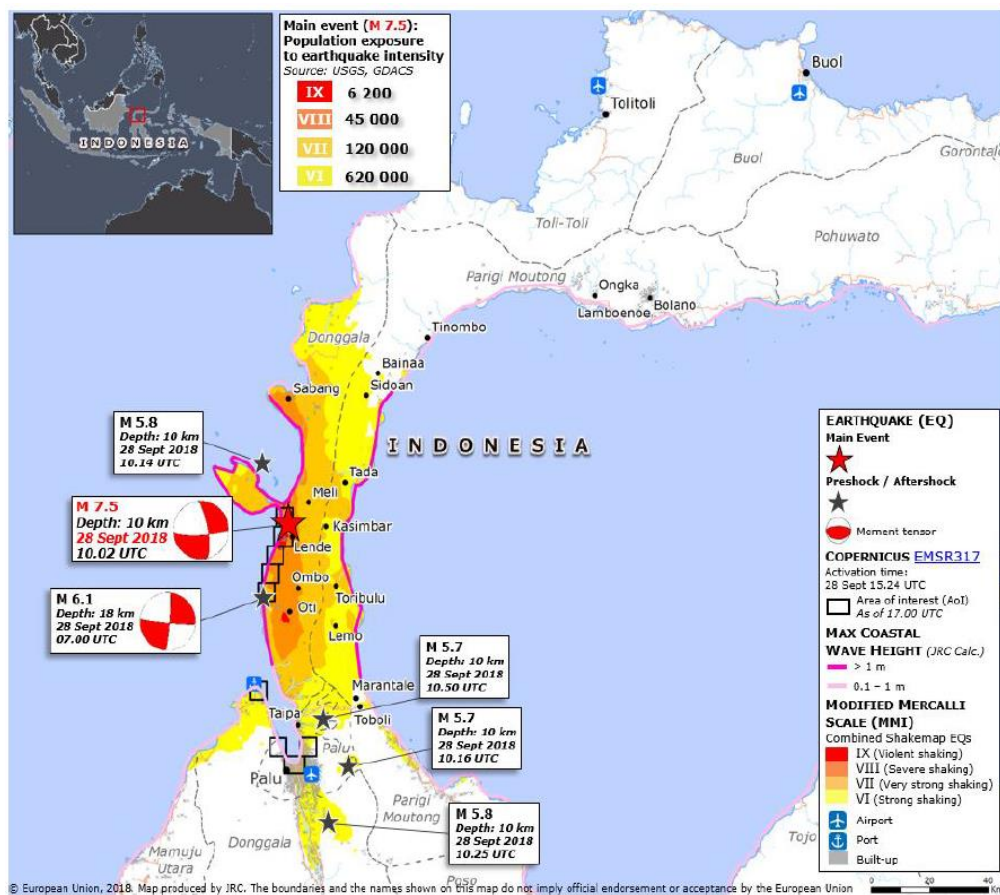


Figure 1.1: Location of main earthquake, foreshocks, and aftershocks (from JRC, 2018).

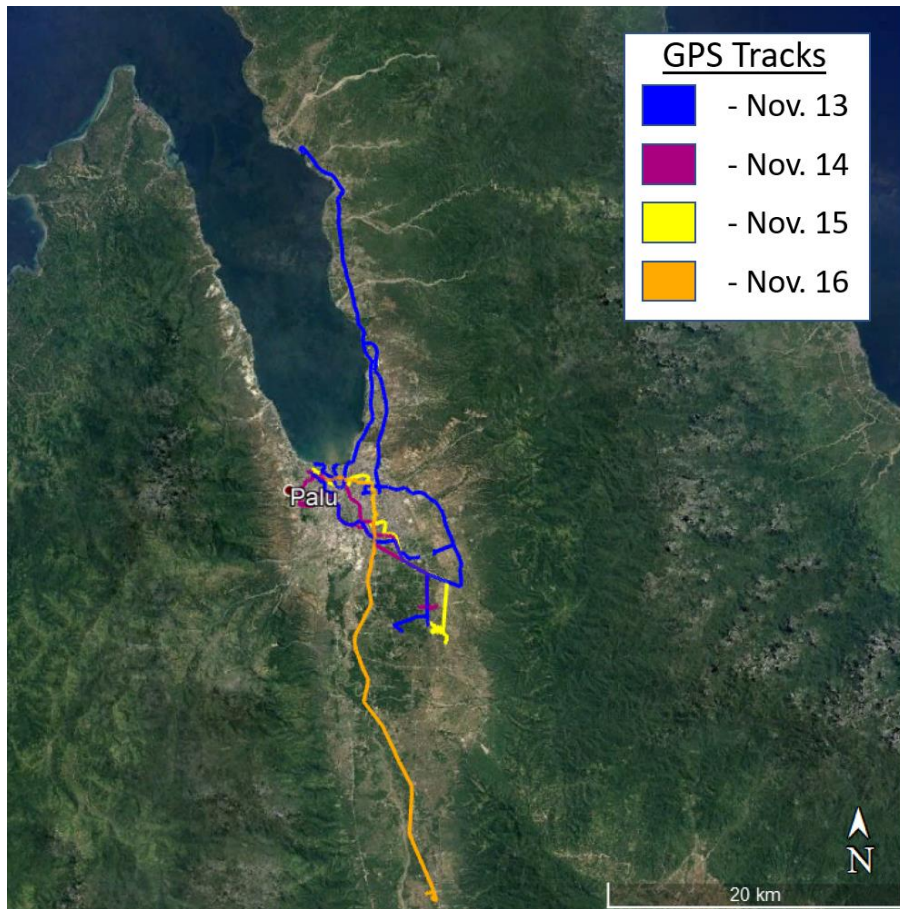


Figure 1.2. Areas surveyed by the GEER Team.

2 GEOLOGIC BACKGROUND

2.1 Bedrock Geology and Tectonic Features

The Sulawesi Island in Eastern Indonesia is located at the convergence of the Eurasian, Indo-Australian and Philippine tectonic plates, which have been interacting from the Mesozoic to the present day (Figure 2.1). The island's unique K-shape and four characteristic arms have been formed by a complex geologic history of subduction, accretion, ophiolite obduction, and collision (Hamilton 1979). The island is subdivided into four main geologic provinces that are distinguished by large-scale tectonic dislocations and thrust faults: i.) West Sulawesi, where Tertiary sediments and magmatic rocks are prominent, ii.) Central and South-East Sulawesi, comprised mainly of early Cretaceous metamorphic rocks, iii.) East Sulawesi, where Mesozoic and Paleozoic sedimentary rocks underlie ophiolitic nappe, and iv.) the Banggai-Sula Microcontinent comprised of continental basement rock (van Leeuwen and Muhardjo 2005, Thein et al. 2014, Maulana et al. 2016). Palu City is located in Central Sulawesi, near the neck, which connects the north arm to the western part of Central Sulawesi (Figure 2.2). The basement rock in this region consists of several metamorphic complexes overlain by volcanic sedimentary deposits and magmatic intrusions varying in composition from gabbro and diorite to granodiorite and granite (van Leeuwen and Muhardjo 2005, Watkinson 2011). Figure 2.3 provides a detailed map of bedrock geology of the area surrounding Palu City and Palu Bay.

The most prominent geologic structure in Central Sulawesi is the strike-slip Palu-Koro Fault (PKF) oriented NNW-SSE, which extends more than 300 km through Palu Bay and the city itself and connects to the North Sulawesi Trench subduction zone north of the island (Figure 2.2). The fault strikes along the western edge of the valley in Palu City and dips 50 to 80 degrees to the east (Walpersdorf et al. 1998, Socquet et al. 2006). The offset of geomorphic features, such as streams, Quaternary alluvial fans, etc., indicate left-lateral offsets (Bellier et al. 2001, Bellier et al. 2006). The PKF was believed to penetrate the thin lithosphere and be seismically interlocked to a depth of 12 km. Monitoring of the PKF with GPS demonstrated the fault had a high slip rate, accommodating approximately 39 mm/yr. of strike slip and 11 to 14 mm/yr. of extension (Socquet et al. 2006). Though the fault had been characterized as having a relatively low level of seismic activity, palaeoseismicity results indicate three major earthquakes with $6.8 < M_w < 8$ occurred in the last 2,000 years, indicating an recurrence rate of 700 years (Bellier et al. 2006). Prior to the most recent earthquake, Walpersdorf et al. (1998) highlighted that no significant earthquake ($M_w > 4.5$) had occurred in the last 100 years (prior to 1998). They also pointed out that displacements had accumulated to at least 3m, which would produce an $M_w 7$ earthquake if the displacements occurred along 50 to 100 km of the fault, similar to the $M_w 7.5$ earthquake that affected Palu City

on September 28, 2018, which was believed to extend over a length of 150 km according to USGS. Interestingly, mapped north-south displacements along the fault by Valkaniotis et al. (2018) ranged between 3m and 4m adjacent to the fault.

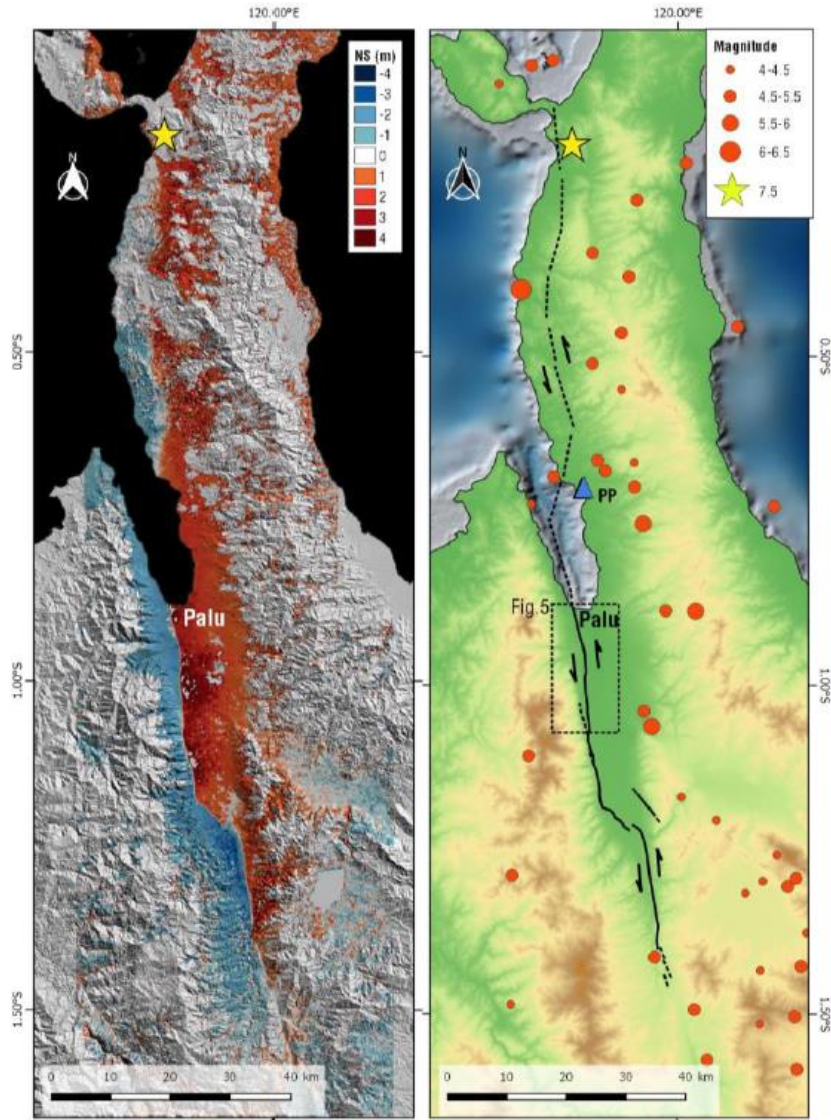


Figure 2.1. North-south displacements mapped along the Palu-Koro Fault from optical satellite data after earthquake (Valkaniotis et al. 2018).

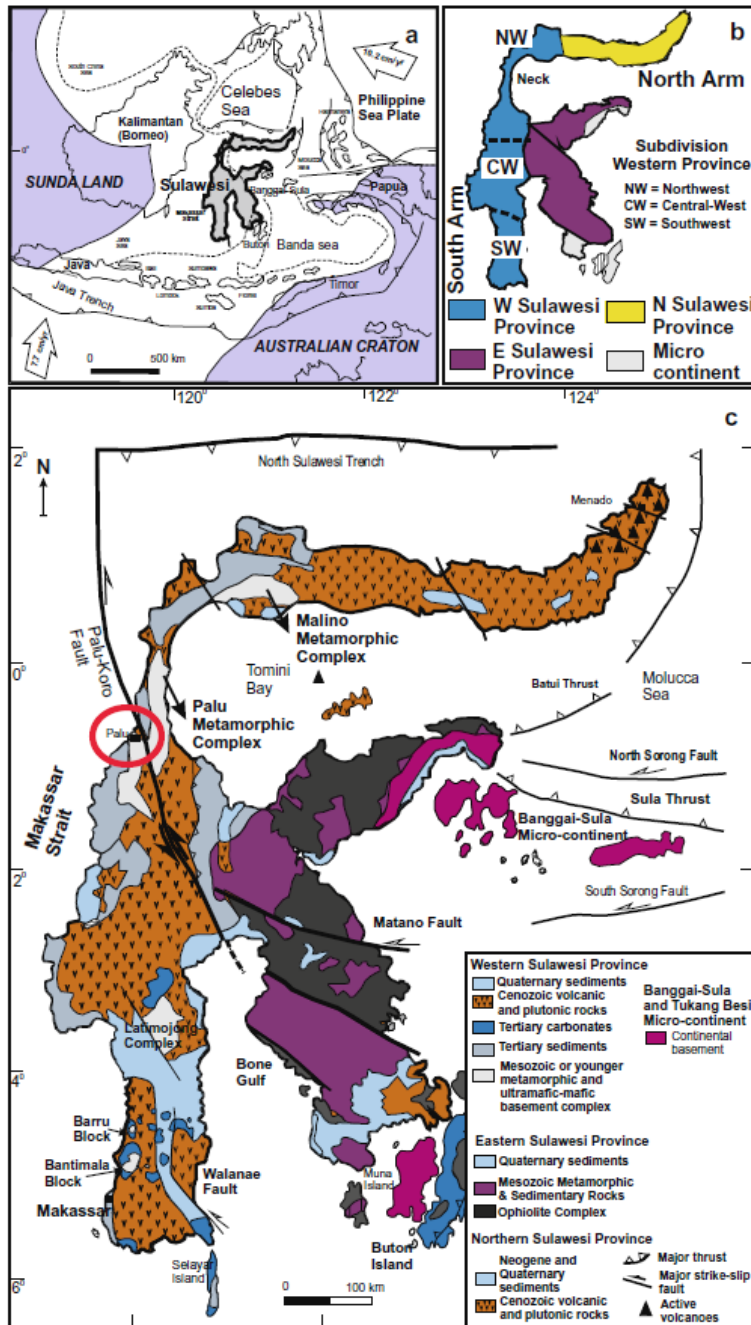


Figure 2.2. Geology of Sulawesi showing principal structures and geographical features (from Maulana et al. 2016).

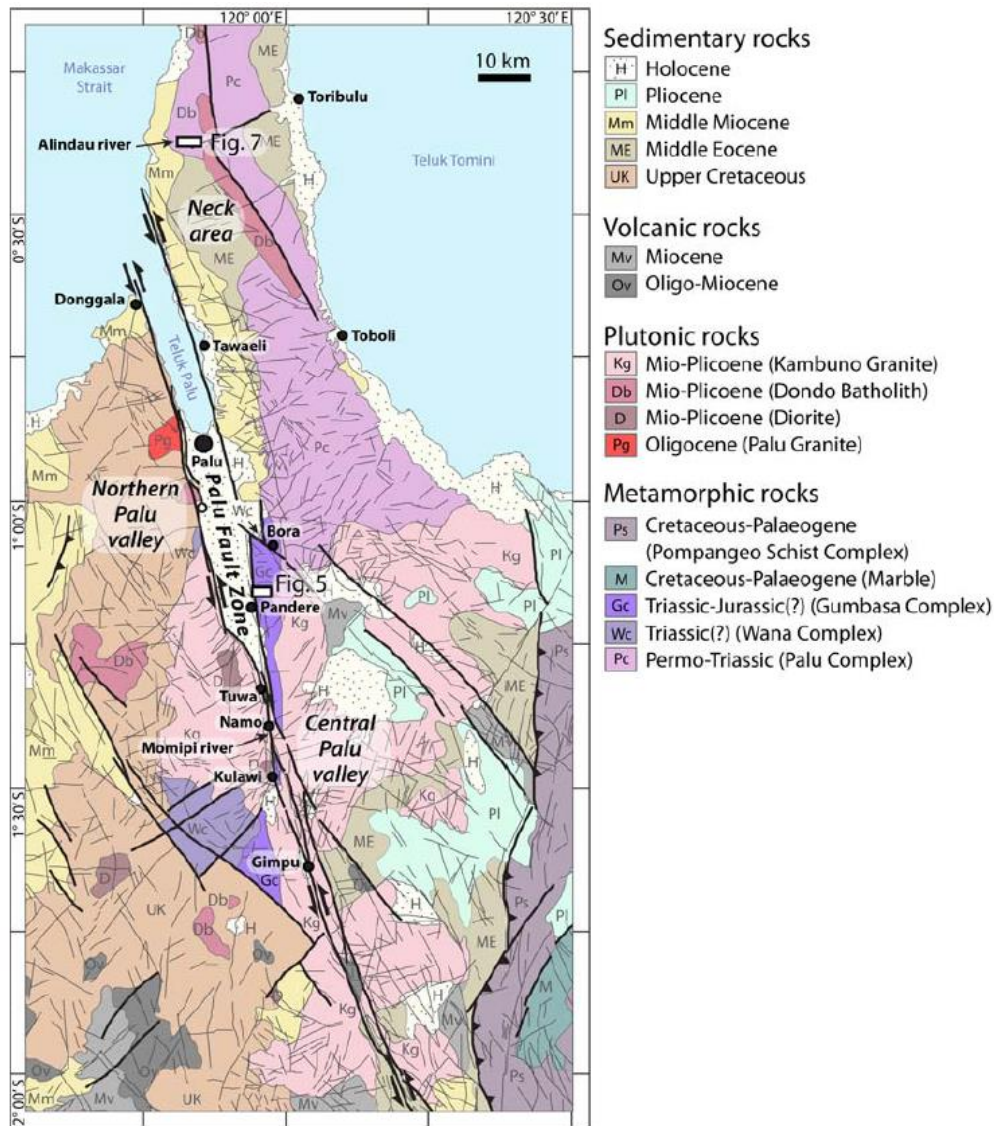


Figure 2.3. Geologic map of the Palu area (from Watkinson 2011).

2.2 Surficial Geology: Palu Basin

The Palu Basin is filled with Quaternary sediments (Figure 2.4). Clay, silt, and sand constitute alluvial flood and old river channel deposits that follow the Palu River at lower elevations near the center of the valley. Young and old alluvium fan deposits constitute surficial sediments in low relief hills extending up the west and east sides of the valley. Colluvium debris deposits of gravelly sand are common occurrence at higher elevations. Landslides studied by the GEER team during this reconnaissance generally intersect the boundary of unconsolidated, gently sloping alluvium fan material that extends from tributary drainage systems near the base of the mountains, and unconsolidated alluvial flood deposits from the Palu River (Figure 2.4). In the foothills and mountains surrounding the Palu Valley are Tertiary granite and granodiorite rock and pre-Tertiary

sedimentary and metamorphic rock. Sediment thickness (i.e. depth to bedrock) varies between less than 25m to greater than 125m, and generally increases at lower elevations towards the center of the valley (Thien et al. 2014). Sediment thickness also increases moving north and is greatest at the mouth of the Palu River where it empties into Palu Bay (Figure 2.4).

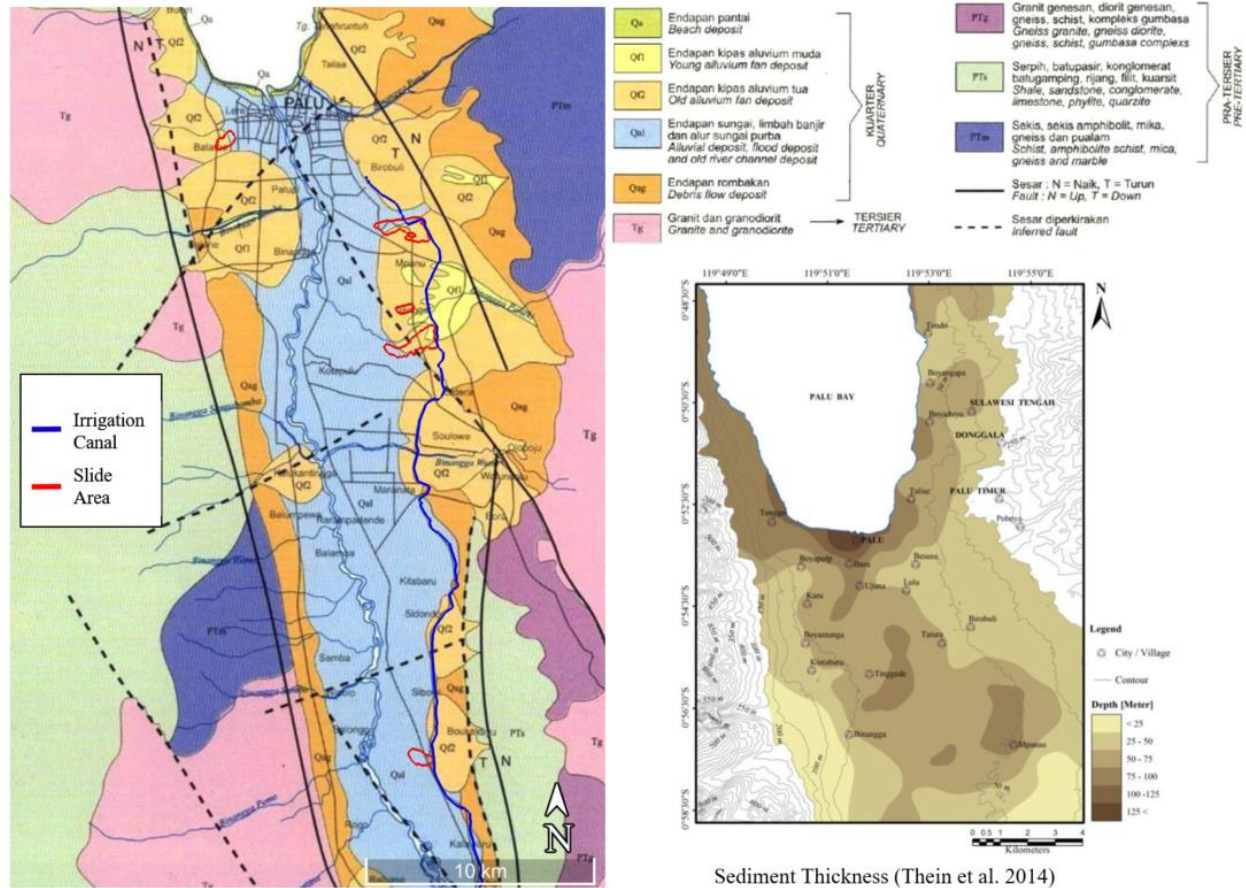


Figure 2.4. Surficial geology and sediment thickness in the Palu Valley (adapted from Hanifa 2018 and Thein et al. 2014).

2.3 Seismicity

The seismicity of the general Palu area, along with detailed interpretation of the mechanisms behind this earthquake, is given by Socquet et al. (2019). A unique feature of this earthquake is that it has been classified as a supershear event due to very high rupture velocities. This may have contributed to the intensity of the motion in the Palu area (Socquet et al. 2019). As noted in the §1, there is a paucity of strong motion data available in the Palu area, which hindered the GEER team's interpretation of the large landslides. Figure 2.5 shows the contours of peak ground acceleration (PGA) estimated by the United States Geologic Survey (USGS) based on the limited data. The maximum estimated PGA is approximately 0.7 g, which is likely a reason so much

damage was seen in the greater Palu area. Unfortunately, there was only one ground motion station in the Palu Basin. This station is located within Palu City (PCI-PALU; -0.90554, 119.83666) approximately 80km from the epicenter and just to the west of the large landslide in the Balaroa neighborhood. The recordings from this station have not been made available in digitally, but data plots shown to the GEER team showed horizontal PGAs of 0.286g in the east-west direction and 0.207g in the north-south direction. This discrepancy with this USGS estimates is important and requires further investigation. The GEER team hopes that the strong motion data from the Palu station, along with characterization data for the site, may eventually be released, which would motivate an addendum to the current report.

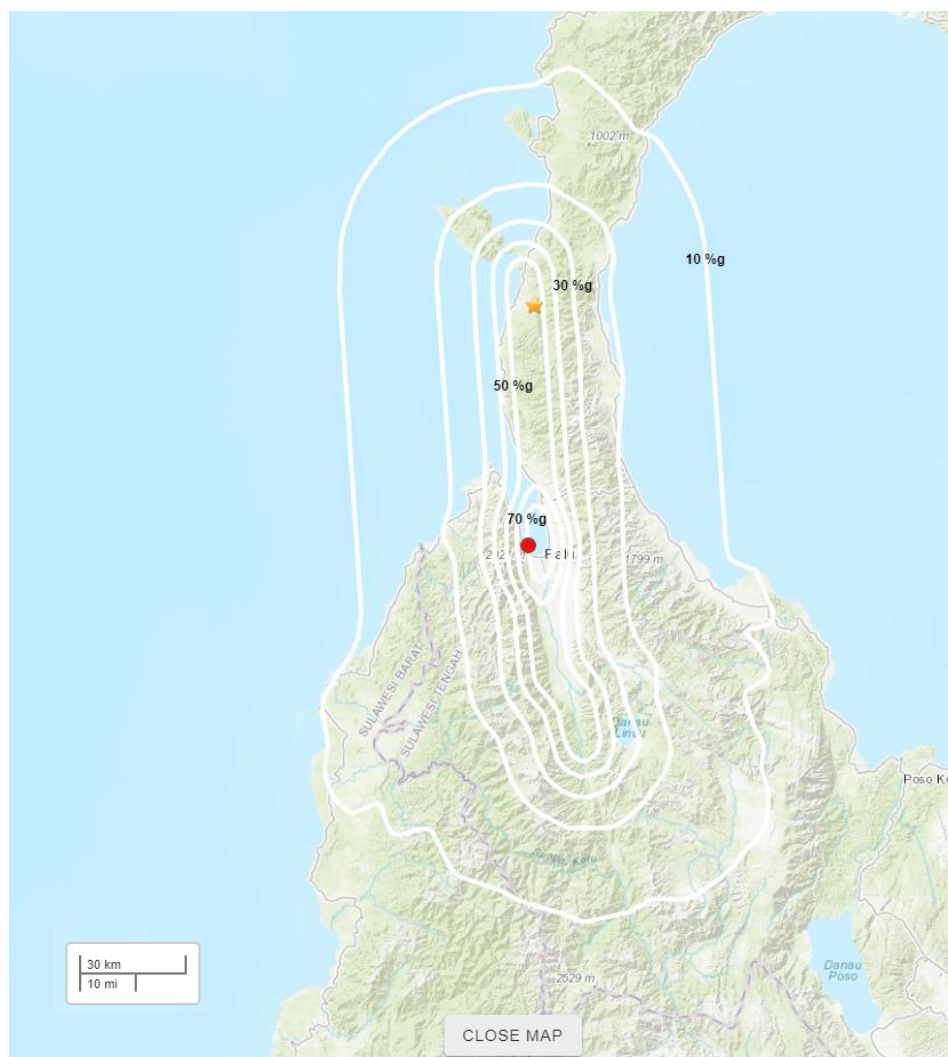


Figure 2.5. Contours of peak ground acceleration (PGA) given by the United States Geologic Survey (USGS). The star is the earthquake's epicenter and the red dot is a "Did You Feel It?" respondent, which is near Palu City (after USGS; <https://earthquake.usgs.gov/earthquakes/eventpage/us1000h3p4/shakemap/pga>; accessed 1 April 2019).

3 LANDSLIDES IN THE PALU BASIN

The 2018 Palu-Donggala Earthquake triggered four massive landslides (*flowslides*¹) located in or near Palu City (Figure 3.1). All of the slides are situated along the margins of the valley where alluvial fan deposits met the alluvial valley of the Palu River (Figure 2.4). The northernmost slide occurred on the west side of the valley in the densely populated *Balaroa* neighborhood. The Indonesian National Agency for Disaster Management (BNPB) estimated 2,895 buildings were damaged or destroyed in Balaroa. The remaining three flowslides in the northern part of the basin are located on the east side of the valley (Figure 3.1) and are referred to by the name of the community where they occurred (from north to south, these are *Petobo*, *Lolu Village* and *Jono Oge*). These three slides stretched approximately 7 kilometers south from the Palu (Mutiaras Al Jufri) Airport. Land use in the east side of valley consists of a mixture of rice paddies and residential and commercial buildings. The eastern margin of the flowslides is bounded by an agricultural canal used to irrigate local rice paddies. At the time of the earthquake, the canal reportedly contained water with an estimated depth of 2.0 m to 2.5 m. The BNPB estimates that the eastern flow slides damaged or destroyed 3,334 buildings in Petobo and 340 buildings in Jono Oge. Rapid damage mapping performed by Copernicus Emergency Management Service (2018) showed that approximately 150 buildings were damaged or destroyed in the area of the Lolu Village slide. Approximately 25 km south of the airport a fourth flowslide occurred in the village of *Sibalaya* (Figure 3.1). Copernicus damage mapping (Copernicus 2018) indicates that 147 buildings were damaged or destroyed by the Sibalaya slide. Similar to the flowslides in Palu, the eastern margin of Sibalaya slide was bounded by the irrigation canal.

The reconnaissance team used a combination of satellite imagery, unmanned aerial vehicle (UAV, or drone) high-resolution aerial photograph surveys, ground-based field surveys, and eyewitness interviews with local residents to investigate each flowslide. Key morphologic features were mapped, including head scarps, back-rotated soil blocks, extension zones, localized compression, block uplift, sand boils, flow channels, and scour. Pre- and post-earthquake satellite images provided through the Digital Globe Open Data program (Digital Globe 2018) were used to map the displacement of structures to identify the direction and magnitude of ground deformations. These satellite images form the background for most of the maps shown in this report. With the exception of Balaroa, the sites were well generally preserved and fully accessible at the time of the reconnaissance. Surveys at the Balaroa site were limited, because significant clearing and debris

¹ The Hungr et al. (2014) classification system is adopted in describing the landslides as flowslides, defined as "very rapid to extremely rapid flow of sorted or unsorted saturated granular material on moderate slopes, involving excess pore-pressure or liquefaction of material originating from the landslide source. The material may range from loose sand to loose debris... and silt. Usually originates as a multiple retrogressive failure."

removal had occurred before the reconnaissance team visited the area. The clearing activity involved the use of earthmoving equipment to remove or bury damaged buildings and to level the ground surface. Morphological mapping of the slides at Jono Oge and Sibalaya was impacted by canal breaches, which resulted in erosion, and in the case of Jono Oge, a major mudflow that damaged two villages downstream of the main failure.

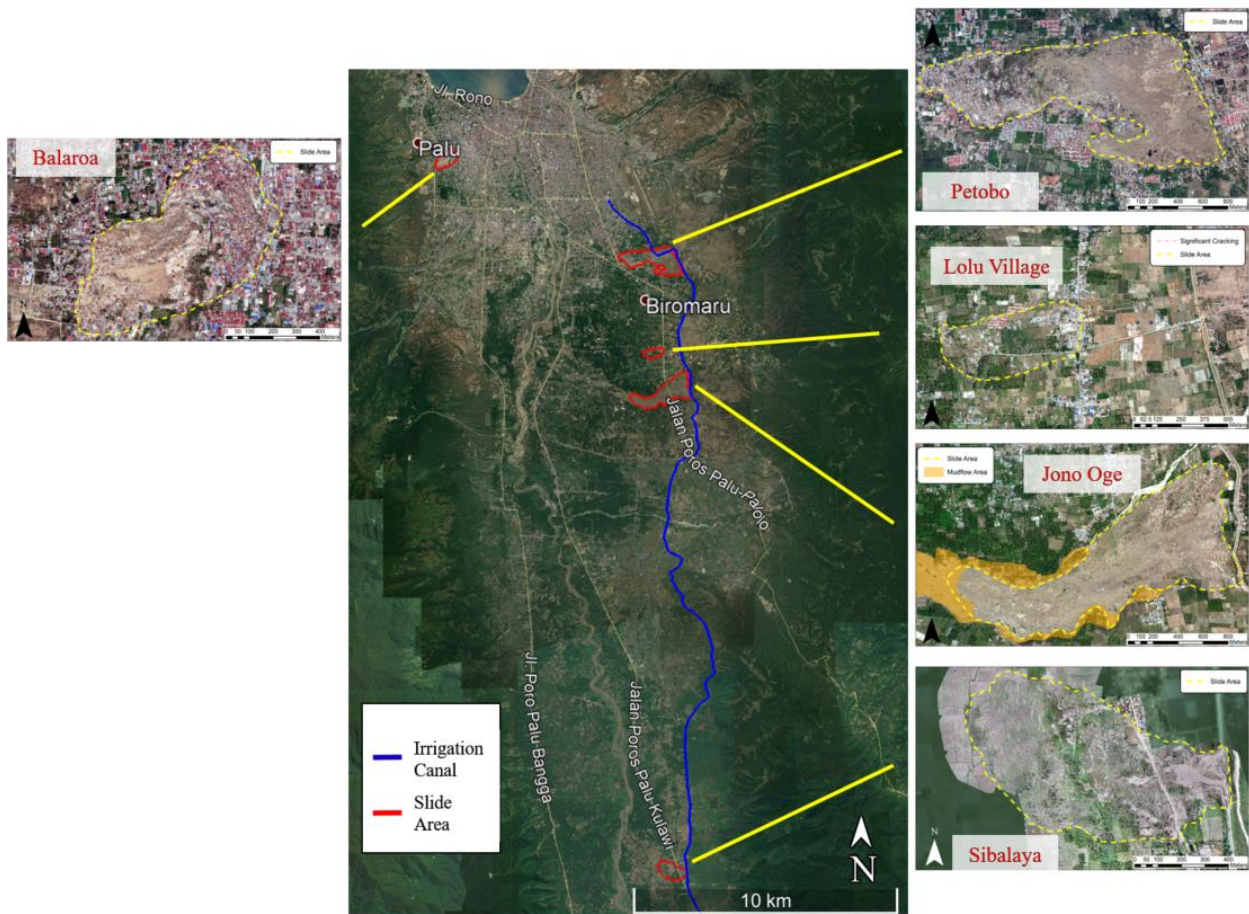


Figure 3.1. Locations of landslides in the Palu Basin surveyed by the GEER Team.

Mapped displacements from optical satellite imagery over the entire basin (Valkaniotis et al. 2018) indicate appreciable ground deformations outside the footprint of the massive flowslides investigated by the GEER team and their collaborators (Figure 3.2). Generally, the GEER team observed that ground deformations move west and east towards the Palu River on the eastern and western sides of the basin, respectively. Areas of larger ground deformations generally surround the areas where large flowslides occurred.

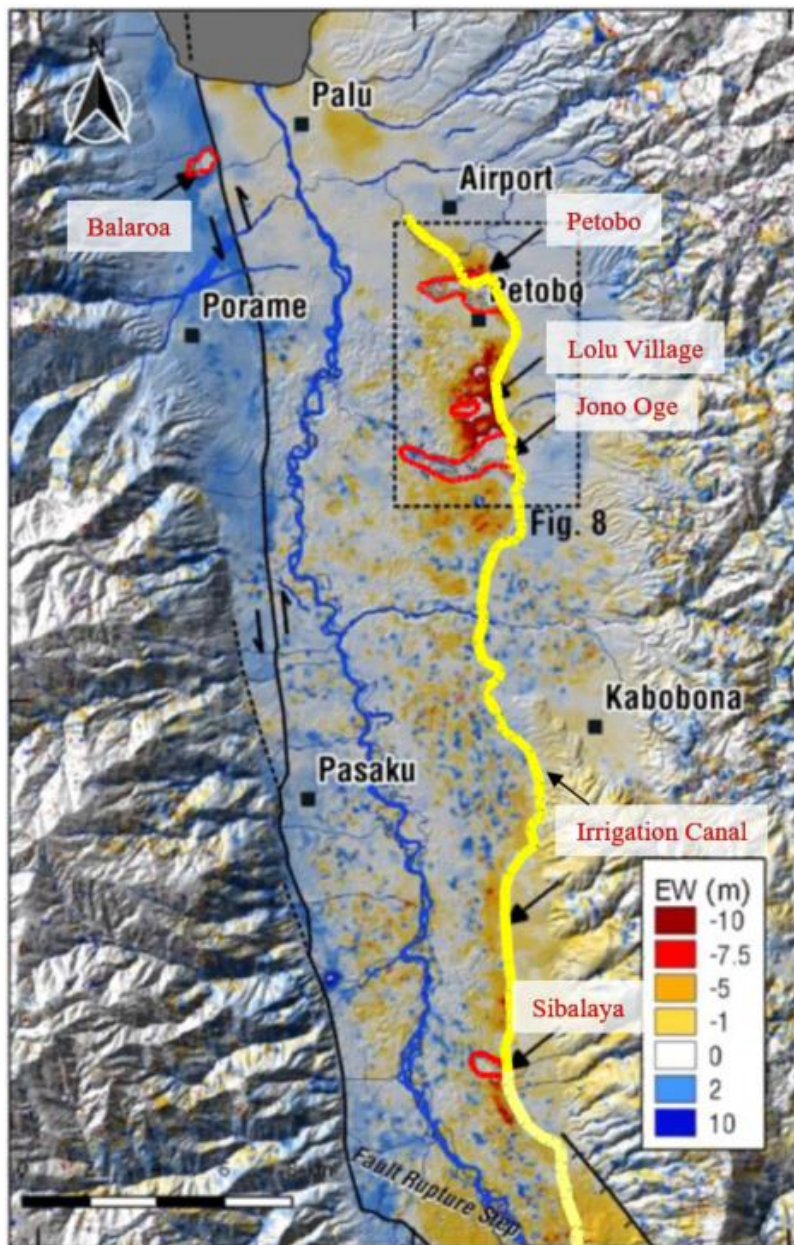


Figure 3.2. East-west ground deformations in Palu Basin interpreted from optical satellite data (adapted from Valkaniotis et al., 2018).

Global Perspective of East Basin Landslides South of Palu Airport

The three flowslides that occurred just south of the airport on the east side of the Palu Basin were situated within a region of large ground deformations (Figure 3.2). Land use includes a mixture of agricultural (e.g., rice paddies) and residential communities. Displacement maps (Figure 3.3) were generated by identifying locations of structures in pre- and post-earthquake satellite images and measuring displacements to better understand regional patterns of movement in this area. To document the movement of a building, a vertex, or other well-defined point, was chosen on both

images. The methods described above were used to map the displacement of 1,220 structures, which were then contoured using inverse distance weighting (Figure 3.3). The preceding mapping was performed using satellite images provided by DigitalGlobe’s Open Data Program. DigitalGlobe provides open access to pre- and post-earthquake images for natural disasters to support response and recovery efforts. For this study, the pre-earthquake image (ID 1030010078CD4A00) was taken on February 20, 2018, while the post-earthquake image (ID 1040010042376D00) was taken four days after the earthquake on October 2, 2018.

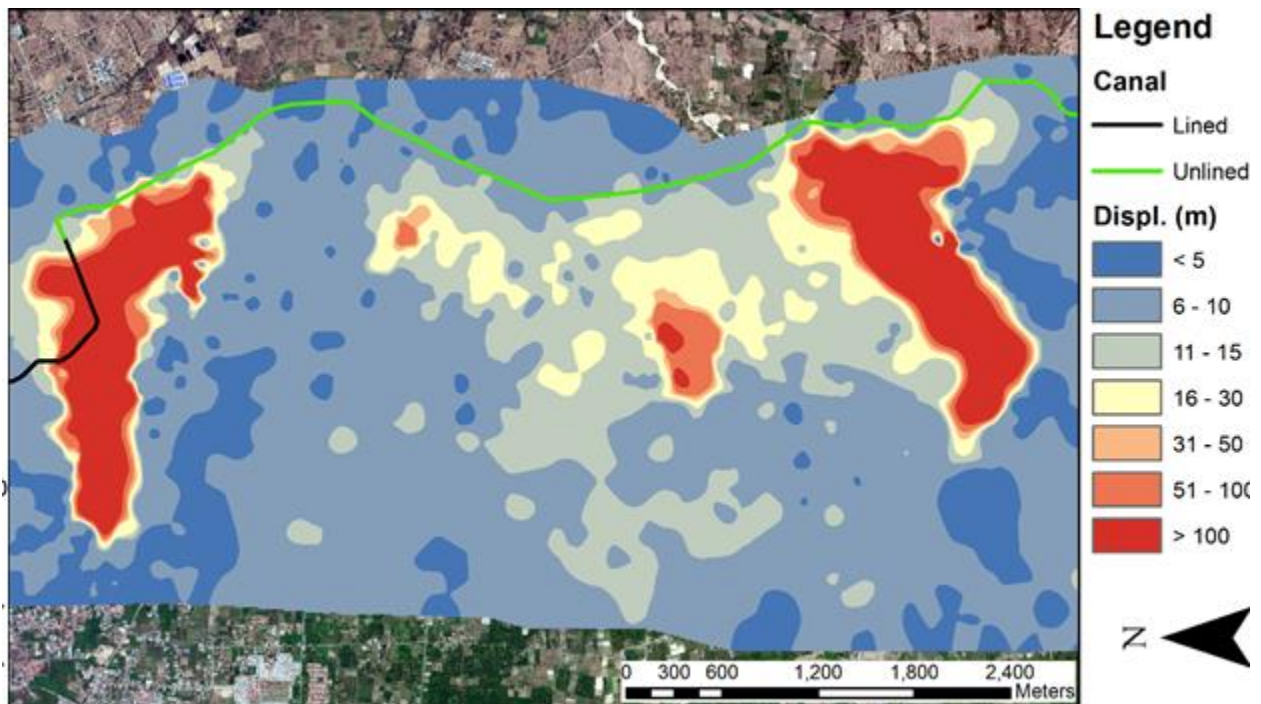


Figure 3.3. East-west ground deformations on western edge of Palu Basin interpreted from optical satellite data.

Displacements within the region shown in Figure 3.3 (i.e., the east side of the Palu Valley) were generally oriented west, which is downhill towards the Palu River. Deformations greater than 50 meters occurred at four locations, including the flowslides of Petobo, Lolu Village, and Jono Oge. A smaller, less pronounced flowslide also occurred in rice paddy fields between Petobo and Lolu Village, but was not investigated during the GEER reconnaissance effort. Outside the footprint of the four flowslides, displacements as great as 30 meters resulted in significant ground cracking and damage to roadways and structures in the region shown in Figure 3.3. In short, on a regional scale, relatively small displacements were observed east (i.e. uphill) of the irrigation canal, and much greater displacements were observed west (i.e. downhill) of the irrigation canal. Notably, the irrigation canal provided water for agricultural activities and was unlined until it reached the northern edge of the Petobo slide, which marks the northern extent of significant ground

deformations in this area. The unlined channel allowed water to seep downhill towards the river, which undoubtedly contributed to a higher groundwater table, saturation of alluvial fan deposits, and increased potential for liquefaction, and strength loss during earthquake shaking.

The pattern of ground deformations south of the airport also appears to be influenced by regional topography and geology. Flowslides occurred near the intersection of younger alluvial fan deposits and alluvial sediments comprising the floor of the basin near the Palu River. Petobo and Jono Oge, which constitute the northern and southern margins of significant ground deformations in this region, respectively, are located at the northern and southern edge of an alluvial fan (Figure 2.4). Additionally, the gently sloping ground in this area had an average grade between 2 and 4 percent, although flowslides appear to have *initiated* where relief was greater locally (approximately 4 to 6 percent), which also coincides with locations where the elevation transitioned from 60 to 80 m (i.e. transition from green to red contouring in Figure 3.4, which is the same region and elevation range where the greatest deformations were observed outside the footprint of the flowslides shown in Figure 3.3. Similarities between the incident elevation and increased relief is an intriguing observation, and may suggest similarities in the depositional environment contributed to the location where the landslides initiated. The size of the flowslides is more closely correlated with the extent of continued relief beyond the region where the landslides initiated. All slides terminated in areas with little to no relief, or in localized regions near the margin of the slide footprint where topography briefly ascended, impeding flow and continued progression of the flowslide downhill (initial topography for each slide is presented later in a detailed discussion of each landslide).

The preceding discussion focused on the larger patterns of movement surrounding the three flowslides just south of the Palu airport on the eastern side of the valley; however, similarities exist for the other landslides. For example, failures at Balaroa and Sibalaya, which are located on opposite sides of the valley, also occurred near the interface of alluvial fan and alluvial flood deposits from the Palu River (Figure 2.4). Sibalaya was also bound on its eastern margin by the irrigation canal, similar to Petobo, Lolu village, and Jono Oge. Subsequent sections presented herein provide a detailed discussion of each landslide visited by the GEER team, including key observations, geomorphic expressions, and eyewitness accounts that facilitate a better understanding of the slide progression at each location, and general mechanisms contributing to the landslides.

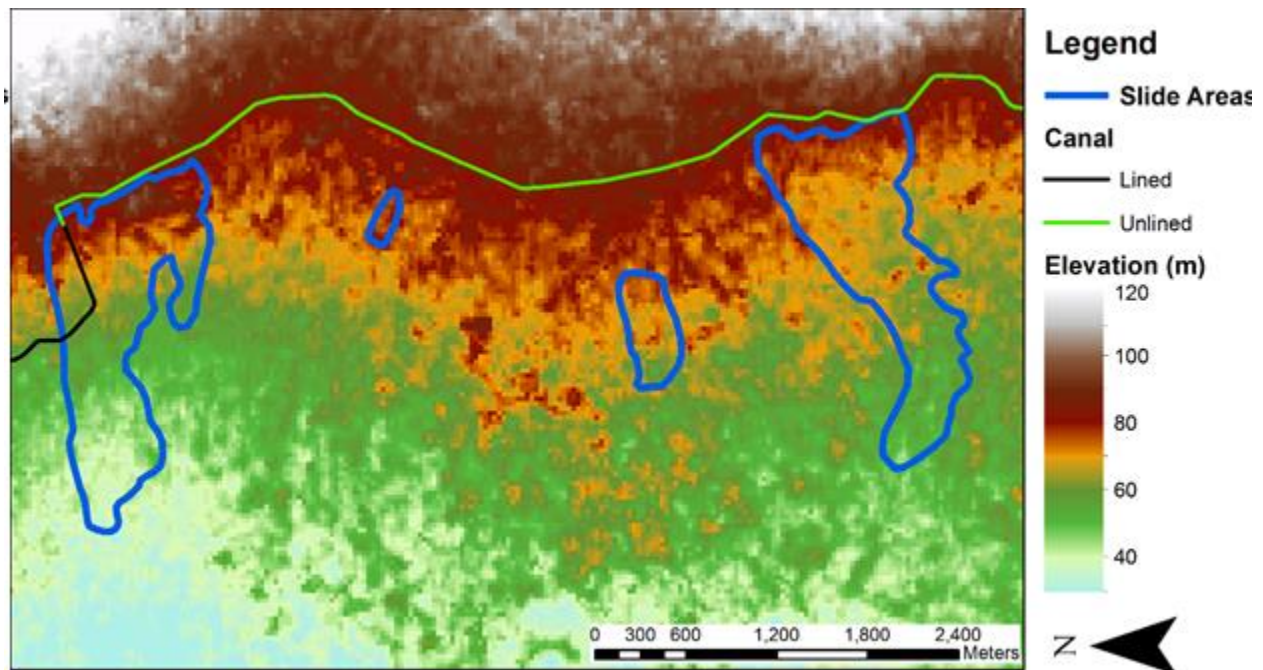


Figure 3.4. Elevation contours interpreted from optical satellite data on the western edge of the Palu Basin in the vicinity of the Peotobo, Lolu Village, and Jono Oge flowslides.

3.1 Petobo Landslide

Petobo was a residential district where most of the landslide-related casualties occurred. Loss of life and bodily injuries mainly resulted from inundation and subsequent burying of buildings in the middle to western portions of the slide, and from rapidly moving ground (with resulting displacements of up to 800 meters) that carried people and collapsed buildings from the middle to upper (eastern) portions of the slide. At least several hundred homes were destroyed in this densely populated community. The Petobo flowslide is centered approximately 1 km south of the Palu (Mutiara SIS Al Jufri) International Airport and situated along the western side of the valley. The total area of the slide — including the source, runout, and deposition zones — is approximately 1.43 km², with a perimeter of approximately 6.7 km. The length of the slide extended more than 2 km from the crest near the irrigation canal to the runout zone on the western margins of the slide area. The slide generally flowed east to west, with the largest movements occurring in the northern portion of the slide. Building displacements in the southern part of the slide footprint were not as large.

The GEER team has divided the flowslide into five distinctive zones in Figure 3.5 (A through E), which are characterized by unique morphologies with different styles of ground deformation (horizontal and vertical, and rotational), cracking, surface roughness, and soil block shearing, and reworking. Larger buildings and infrastructure in the eastern half of the slide footprint were generally well-preserved and relatively undisturbed. Pre- and post-earthquake satellite imagery

and digital elevation models (DEMs) processed from drone images² collected by the reconnaissance team aided the identification and interpretation of morphological features and the delineation of zones in the eastern portion of the slide (Figure 3.6). However, buildings and infrastructure in the western half of the slide area (mainly Zone E) were reworked and heavily disturbed by earth moving equipment brought onsite before the GEER team arrived. The earth moving equipment leveled the landslide mass and removed, demolished, and buried the remnants of displaced buildings destroyed by the slide.

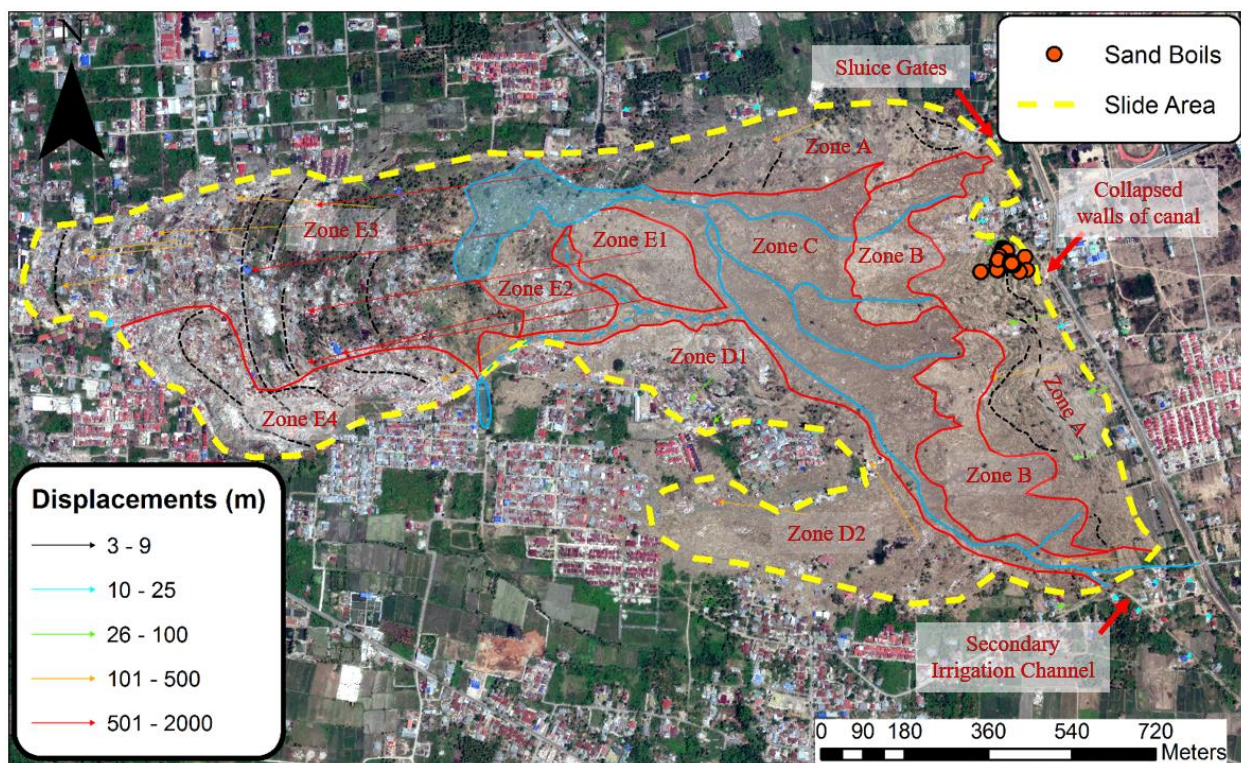


Figure 3.5. Orthomosaic map indicating limits of Petobo landslide, location of sand boils, vector displacements, and zones delineated by morphological features and key observations.

² Several commercial-grade unmanned aerial vehicle (UAV) or "drones" were used during the reconnaissance, but most of the high-resolution mapping was conducted using a DJI Inspire 2 platform mated with a Zenmuse X4S camera (1-inch sensor, with 20 MP resolution). Drone flights were typically flown at an elevation of 65 m (with nadir images having 75% overlap), providing a ground sampling distance pixel resolution of ~2 cm. The drone images were processed using the software Pix4D mapper to develop high-resolution orthomosaic images and digital elevation models. The accuracy of drone surveys was enhanced by the use of ground control across the scenes. High resolution real-time kinematic GPS surveys were used to determine the coordinates of the ground control points.

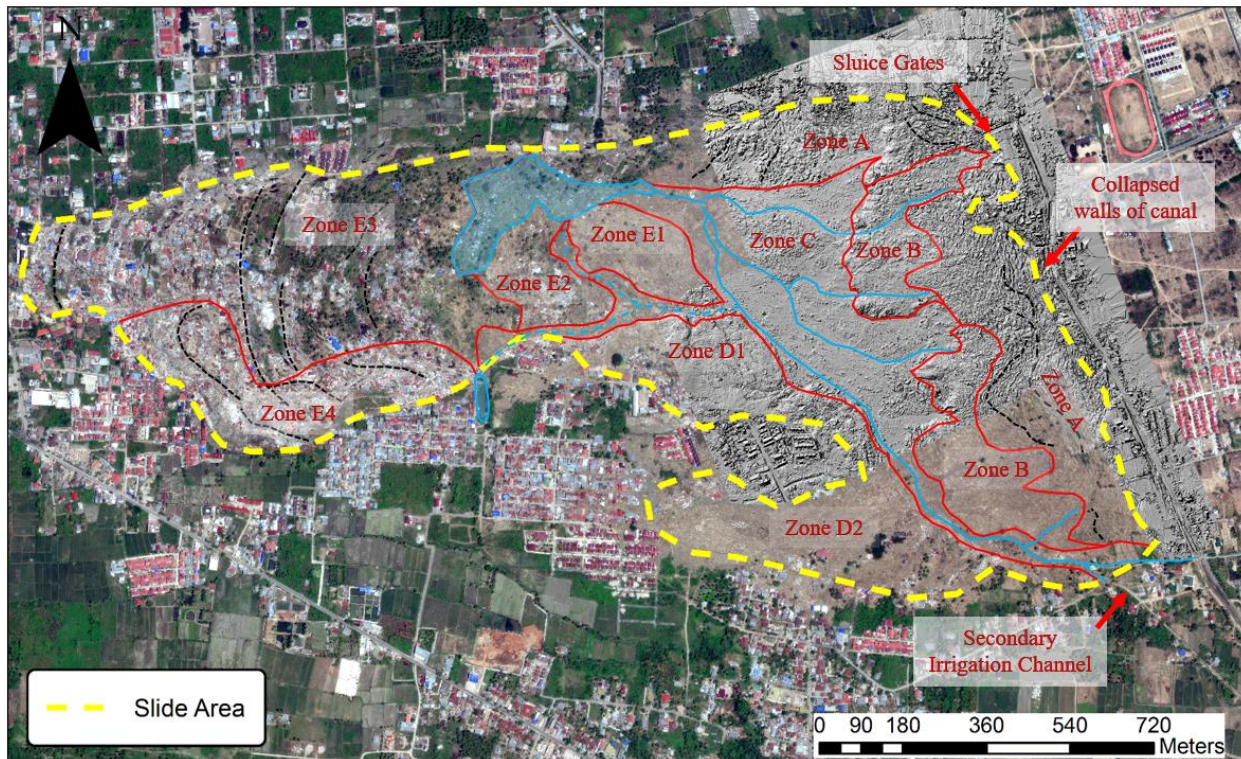


Figure 3.6. Digital elevation model illustrating 3D morphological features in the northeast section of the slide.

3.1.1 Field observations and landslide morphology

Zone A – Headscarp and Extensional Back-Rotated Block Field

Zone A consists of the Petobo landslide headscarp and immediately downslope (west) of this, a field of relatively well preserved back-rotated (i.e., rotated downward toward the west) angular soil blocks. The headscarp extends along the eastern margin of the landslide is adjacent to a previously active irrigation canal (Figure 3.5). A resident of Petobo estimated that the depth of water in the canal was approximately 2 meters at the time of the earthquake. It appeared that loss of lateral confinement in the headscarp region resulted in lateral extension (to the west) and severe tension cracking of the canal at multiple locations (Figure 3.7a), and in some areas, collapse of the canal side walls (Figure 3.7b). At the time of the reconnaissance, the canal was dry, and neither seepage nor water was present. It is worth noting that although the canal wall near the center of the Petobo slide was observed to have had completely collapsed (Figure 3.6), there were no readily identifiable scour or erosional features at this location, suggesting that the source of canal water was limited when the walls of the channel failed. As discussed later, this differs from the nearby Jono Oge and Sibalaya landslides, where significant scour and erosion was also observed at the locations of canal collapse. As shown in Figure 3.4, water in the canal previously flowed north, before turning sharply to the west and then turning again and resuming northward. The flow of

water in the canal was previously controlled by two sluice gates in the northeast corner of the slide, where the irrigation canal transitioned from an unlined system to a concrete-lined channel. Figure 3.7c illustrates the damage to the lined canal, sluice gates, and the lateral extension and vertical displacement of blocks in the northeastern corner of this site. The lined portion of the channel extending into the footprint of the slide was destroyed and buried beneath debris.

The headscarp mainly cut through rice paddy fields that were underlain by alluvial deposits that contained embedded seashells, indicating a former marine sediment. Large soil blocks (generally several meters high) were down-dropped and laterally extended near the headscarp. Ongoing raveling of these locally over-steepened blocks produced talus that was deposited in depressions between blocks. Most of the blocks were back-rotated, with vegetation was oriented uphill towards the headscarp (Figure 3.7d-f). The height and size of laterally extended blocks generally diminished with distance from the headscarp. The soil blocks appeared to have deformed across a series of imbricated failure surfaces during an initial stage of movement (visible near canal) before transitioning to rafted blocks that slid along a *décollement* of liquefied sandy material. Sand boils and associated soil ejecta were found between blocks in Zone A (Figure 3.5 and Figure 3.8), suggesting that elevated pore water pressure and liquefied soil in the soils below the blocks. The ejecta consisted of fine sand with silt and silty sand, similar to the material comprising the floor of Zone C.



Figure 3.7. Observations in Zone A: a.) cracking in the irrigation canal (-0.93791, 119.92157); b.) collapse of canal walls near head scarp (-0.93832, 119.92154); c.) damage and vertical displacement of gates in northeast corner of slide where the canal turns and runs east to west (-0.936019, 119.920635); d.) back-rotated blocks near head scarp at the center of the slide (-0.938349, 119.921008); e.) back-rotated blocks and head scarp in northeast corner of the slide (-0.93623, 119.92018); f.) overlooking back-rotated block field in the southeast corner of the slide (0.94071, 119.92258).

Zone B – Flowslide Materials with Disintegrated Soil Blocks and Mounds

Zone B is an area containing a mix of flowslide materials including highly softened soil masses and most conspicuously, soil blocks that were heavily reworked as the slide progressed, disintegrating into smaller, rounded mounds (Figure 3.6). Zone B also contains several large, isolated soil mounds. The blocks and mounds in Zone B were noticeably smoother and more rounded than the angular, back-rotated blocks found in Zone A (Figure 3.9a). The Zone B deposits appear to override the materials located downslope in Zone C. This is shown in the DEM by the localized over-steepened surface across the interface of Zones B and C (Figure 3.6). Comparing the surface conditions of Zone B (Figure 3.9b) and with those of Zone C (Figure 3.10a) indicates that the Zone B sediments were notably dryer at the time of reconnaissance. It is believed this is because the Zone B materials glided along the lower-lying sediments comprising the floor of Zone C, which were likely liquefied at the time of the slide.

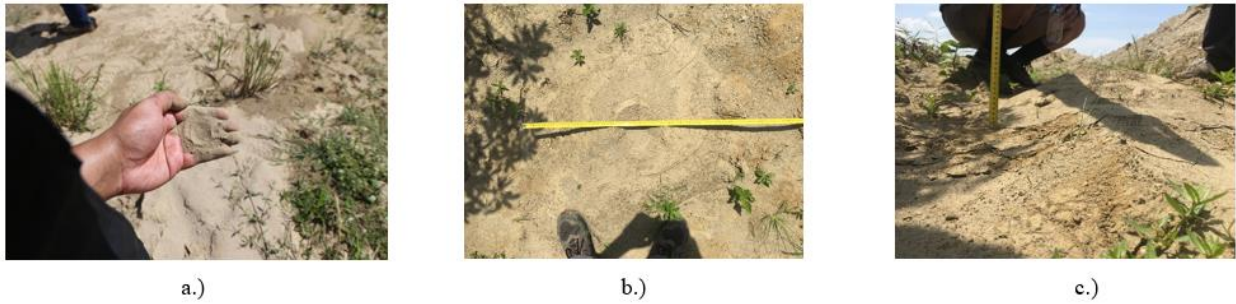


Figure 3.8. Sand boils: a.) typical sand boil ejecta (-0.93850, 119.92092); b-c.) representative height and width of typical sand boils found preserved between blocks (-0.938503, 119.920425).



Figure 3.9. Zone B: a.) relatively large block/mound in this zone with limited vegetation and a shape that is not as well-defined as blocks in Zone A (-0.939489, 119.917507); b.) debris flow deposits and mounds in the foreground of picture near the margin of Zone C, which forms an elevated plain at the boundary of these two zones (-0.939664, 119.918263).

Zone C – Highly Reworked Deposits

Zone C is a relatively flat, low-lying field of highly reworked (i.e., fully unstructured) soil deposits that separates the flowslide materials of Zone B from the more fluidized runout deposits in zones D and E. With the exception of several isolated locations, the soil blocks and mounds found throughout the upper region of the flowslide (i.e., Zones A and B) are absent in Zone C. The surficial sediments of Zone C consisted of saturated, fine-grained sandy soils with a modest silt content. These sediments were significantly softer (soils could not support the weight of team members) and wetter than those found in Zone B (Figure 3.10a-c). The high water content is indicated by the darker colors of Zone C deposits shown in satellite and drone-derived orthomosaic imagery (Figure 3.5).

At the time of the reconnaissance, an actively eroding rill network conveyed water across the surface of Zone C towards the northwest. The rill network channels extend upslope into Zone B (this is indicated by the discoloration shown in Figure 3.5) and reached into the lower part of the Zone A headscarp region. There are several possible sources of water in Zone C including: (i) seepage emanating from Zone B (this was visible during the reconnaissance), (ii) dissipation of earthquake-induced elevated pore water pressures within Zones A to C, (iii) surface flow from natural rivulet that previously ran through the southern portion of the slide footprint (visible Figure 3.3), and (iv) secondary irrigation channels that previously conveyed water from the main irrigation canal to rice paddy fields in the southern portion of the slide footprint (Figure 3.5). It is unknown if a breach of the secondary irrigation channel was a source of surface water that contributed to erosion and scour during and after the slide, or if it merely added to the saturation of sediments. If the secondary irrigation channel provided surface water Zone C immediately after the landslide, the gentle morphology of the zone suggests that flow was much less energetic than at other locations where the main irrigation canal was breached (e.g., Jono Oge and Sibalaya, see §3.2 and §3.4, respectively). The combination of the reworked sediments, wet conditions, and very low strengths together support the hypothesis that the sediments in Zone C liquefied during the earthquake, and served as a layer upon which groundmasses were carried during the flowslide.



a.)



b.)



c.)



d.)

Figure 3.10. Zone C: a.) view facing south-southeast at the margin of Zones B and C, with a clear difference in elevation and visible water in Zone C (-0.93971, 119.91859); b-c.) observed rill network and drainage channels carrying water through the zone (-0.939725, 119.918577 and 0.93974, 119.91859); d.) an erratic, relatively intact, block in the zone (-0.940918, 119.917806)

Zone D –Southern Runout Zone

Zone D consists of flowslide runout materials deposited across the southern part of the landslide. The deposits largely consisted of thoroughly reworked (i.e., fully unstructured) fine sandy sediments that appeared to have been highly fluidized at the time of the flowslide. The zone includes a range of surface features including disintegrated soil blocks and mounds, and rafted blocks of soil reinforced by the root mass of low-lying vegetation and trees (Figure 3.11a). Many of the surface features traveled several hundred meters before being deposited in Zone D. As they slid these surface features became rotated, tilted, sheared, and fragmented. The ground surface of Zone D is marked by north-south oriented compression ridges, uplifted ground, stacked and overridden surface features, and emplaced soil mounds. The runout deposits collided with and inundated numerous buildings and infrastructure elements in Zone D. Across the middle to the east part of the zone, buildings were torn from their foundations and carried by the fluidized deposits. In other nearby locations, buildings were entirely buried by the deposits (Figure 3.5). Along the western margin of the flowslide, homes were uplifted many meters along compression ridges. At the distal edge of Zone D, flowslide deposits fanned out and flowed through streets, penetrating through the walls, doors, and windows of residential structures lining these roads (Figure 3.11b).

At the time of the reconnaissance, most of the undamaged or partially damaged residential structures proximal to Zone D were unoccupied and appeared to have been abandoned.



a.)

b.)

Figure 3.11. Zone D: a.) compressed and uplifted blocks, ridges, and mounds along the western margin of the zone (-0.941527, 119.917471); b.) evidence of debris flow through a home in Zone D1 (-0.940627, 119.912096).

Zone E – Northern Runout Zone

Parts of Zone E were disturbed by post-earthquake rescue and recovery efforts by the time the reconnaissance team arrived in Palu. Excavation and earth moving equipment was used to demolish structures and level the runout zone and debris field (Figure 3.12a). As such, morphologic features were interpreted based both on direct reconnaissance observations and satellite imagery captured shortly after the earthquake. To help interpret the satellite images, the team related morphological features observed on the ground in adjacent Zone D to their expression in the images. This understanding was then used to develop the descriptions below for Zone E. It is worth noting that Zones D and E share many common characteristics including: (i) thickness of runout deposits (Figure 3.12d), (ii) spillover of fluidized materials along the distal edge into adjacent neighborhoods (with penetration into homes) [Figure 3.12e,f], and (iii) thoroughly reworked (unstructured) nature of the previously fluidized deposits. One significant feature observed in the satellite images of Zone E, a large area of ponded water (near the northern and southern edges of the zone, Figure 3.12b,c), was still present and observable at the time of the reconnaissance.

The Zone E runout distance was much higher than in Zone D. Many of the buildings and infrastructure elements impacted by the fluidized runout materials were carried over 500 meters. Debris along the eastern edge of Zone E (shown as subarea E1 on Figure 3.6) was similar to that in Zone D and consisted of a heterogeneous mix of reworked sandy and silts soils with an

increasing amount of anthropogenic material interbedded towards the west edge of the subzone E2. Mapped displacements indicate that structures carried into subzone E3 underwent the most significant movements, and were previously located in what is now Zone C and the eastern portion of Zone D (Figure 3.5). The orientation of compression ridges observed in post-earthquake satellite imagery provides insight into the interaction between subzones E3 and E4. In subzone E3, compression ridges are oriented north-south and consistent throughout the area. In subzone E4, the compression ridges are rotated, suggesting that the landmass was “shoved” as it impeded the flow of the rafted landmass in subzone E3. The satellite imagery also indicates that a debris flow occurred throughout the streets of subzone E4, suggesting at least partial overlap and deposition of ground from subzone E3 over subzone E4 as the flowslide progressed. Additionally, the western portion of subzone E3 sheared through the northwestern section of subzone E4 as the slide advanced, extending the length of the northwest corner for this portion of the slide (Figure 3.5).



Figure 3.12. Zone E: a.) reworked areas in the center of the zone where earthwork has made morphological features unrecognizable (-0.93952, 119.90387); b.) flooded areas on the northern margins of Zone E (-0.94672, 119.90939); c.) flooded are on the southern margin of Zone E (-0.94090, 119.91040); d-f.) area along the southern margins of Zone E4 where debris flows infiltrated adjacent neighborhoods (-0.94072, 119.90413; -0.94141, 119.90977; -0.94150, 119.9068).

3.1.2 Interpreted slide progression

Before the earthquake, Petobo was a densely populated neighborhood. The earthquake occurred in the early evening (approximately 6:00 PM) when many residents were at home or in their community. The reconnaissance team interviewed eyewitnesses who directly observed the

flowslide and its westward progression and advancement. Because of the large size of the flowslide, most of the observers witnesses only a portion of the event; however, one individual who was located on an elevated plane in the northeast corner of the flowslide (Figure 3.13) viewed nearly all the event as it progressed over several minutes. In general, the eyewitness accounts, which were provided voluntarily, were remarkably consistent and provided significant detail on the timing, sequencing, and progression of the flowslide. These accounts are also compatible with other sources of information about the flowslide including: (i) eyewitness videos posted to social media, (ii) pre- and post-earthquake satellite imagery, (ii) drone-derived images and DEMs, and (iv) morphologic expressions observed on the ground.

The eyewitnesses generally described the earthquake shaking as an initial period of intense horizontal ground movement, followed by a brief quiescence with no shaking (a few seconds), and then violent vertical motions and a significant vertical drop at the end of shaking. Several witnesses also provided a visual description of the ground motion sequence by first moving their hands laterally, followed by a vertical bouncing motion to visually articulate the transition to vertical motion, and then a rapid downward movement with both hands to describe the final vertical drop. Based on the eyewitness account from the individual who witnessed the landslide from the northeast corner of the slide area, the slide did not initiate until after ground motions had subsided. Sliding was first observed (via movement of coconut trees) in the southern portion of the site and progressed northward. The width of the slide footprint in the southern portions is greater than 1 km; therefore the witness could not provide an exact description of where the failure initiated (e.g., proximity to the southern and western margins). However, their account suggests movement was first observed away from the canal but in the eastern portion of the affected area (i.e., Zone B or C).



Figure 3.13. Perspective of eyewitness account (facing west-southwest) from northeast corner of slide (-0.93622, 119.920207).

A unique feature of the Petobo slide is the formation of two “legs” (northern and southern leg) during the earthquake. Figure 3.14 shows the pre-earthquake elevation profile for two cross-sections, A-A’ and B-B’, running through the northern and southern legs, respectively. The cross-section C-C’ shows the elevation profile along the eastern portion of the slide. Notably, the southern leg is significantly shorter, which is attributed to an elevated ridge encountered at the bottom of the south leg that obstructed the slide mass from extending as far west as the northern leg. It is likely that the continuous downhill topography along the north leg fostered greater displacements and runout distances after the slip initiated uphill in topography with greater relief.

The elevation profile across the eastern footprint of the slide (section C-C’) also helps elucidate observed geomorphic expressions and explain why the two legs manifested in this manner. In the southern portion of the flowslide, there is a rise in elevation or knoll-like feature that transitions to a shallow, channelized depression to the north (Figure 3.14). The flow of debris in the north appears to have been funneled towards this lower-lying area, which is also supported by extensive scarp development along the northern margins of the slide (i.e., an extension of Zone A west on this margin). Unlike the northern margin, a significant amount of debris flowed towards (not away from) the southern limits of the flowslide footprint. Deposits likely cascaded in multiple directions off the knoll (e.g., west, southwest, and northwest) as the flowslide progressed in the southern portion of the site, as there was no natural topography to funnel it in any single direction. Flowslide deposits obscured the scarp along the southern boundary. Note how scarp development (Zone A) extends much further west on the northern margin and runout deposits (Zone D) extend further

east on the southern limits of the slide. An understanding of pre-earthquake topography helps reconcile these observations.

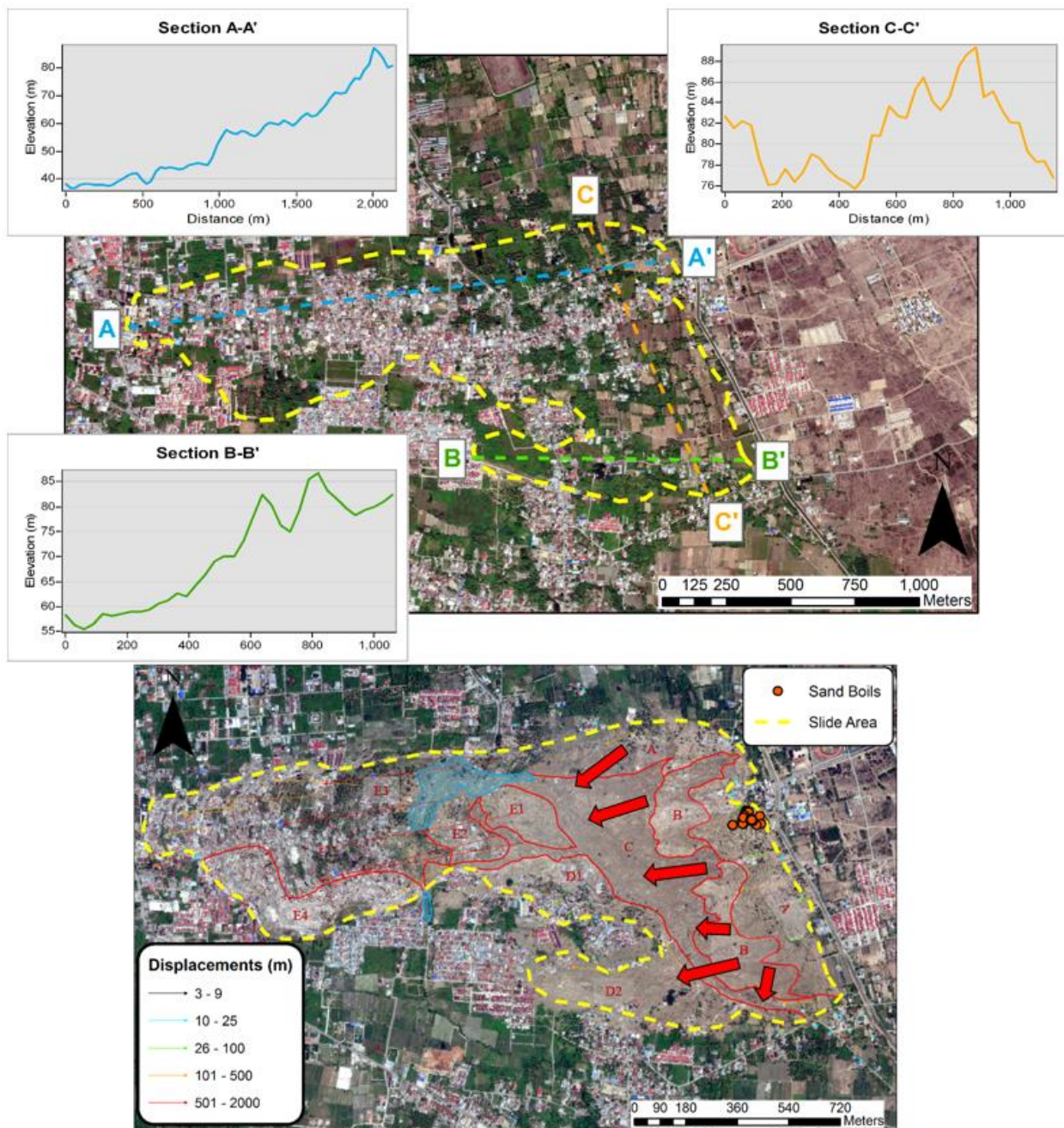


Figure 3.14. Pre-slide cross-sections and topography and post-earthquake satellite imagery of slide at Petobo.

3.1.3 Factors contributing to and hypothesized mechanisms of the Petobo flowslide

Pre-earthquake data at the site of the Petobo flowslide (e.g., high-resolution topography, groundwater levels, monitoring information, and subsurface conditions) is limited, and therefore

complete knowledge of the exact conditions at the time of the flowslide will never be fully known. As such, the precise mechanisms responsible for the initiation and progression of the flowslide can not be known with absolute certainty. Nevertheless, reconnaissance data collected during and shortly after the earthquake (including field observations, mapping and imagery, and eyewitness accounts) provide significant insight to triggering and sequencing of the flowslide. (Note that as part of a post-earthquake investigation, Indonesian partners are currently collecting subsurface information in and near the flowslide; however, these data remain incomplete at the time this report was written). Based on the available data and analyses conducted to date, the reconnaissance investigation team has identified factors contributing to and a hypothesized mechanism responsible for the initiation and progression of the Petobo flowslide. The interpretation presented below is based upon: (i) the team's understanding of conditions at the time of the earthquake, (ii) direct observations made during the reconnaissance, and (iii) multiple eyewitness accounts, among other sources of information. The key findings are as follows.

1. It is believed that the flowslide initiated at the base of alluvial fan deposits that had been transported from areas of higher elevation in the surrounding mountains. These deposits are, in turn, underlain by (and possibly interbedded with) alluvial flood deposits extending from the Palu River (Figure 2.4). This geologic environment would not have been highly energetic, promoting deposition of finer sands and silts (observed in sand boil ejecta) in a loose configuration (Youd and Hoose, 1977) on a sloping ground surface.
2. Based on interviews with public works officials in the city of Palu (and corroborated by eyewitness accounts), the irrigation canal was close to full at the time of the earthquake. This description is supported by the presence of and height to grass and vegetation (above the base) along the walls of the canal (e.g., Figure 3.7a). The bottom and walls of the main channel were unlined (i.e., without a hydraulic barrier) along the eastern boundary of the flowslide. The unlined canal, in combination with the relatively high hydraulic conductivity of alluvial deposits, would have resulted in significant artificial recharge of the groundwater system immediately below (west) of the canal, contributing to saturation of the loose alluvial deposits. A secondary channel (extending from the main channel) conveyed water to fields located in the southeast corner of the slide footprint. This may have further contributed to the saturation of the alluvium in this area and further east.
3. Sand boils observed in the upper part of the flowslide provide compelling evidence of earthquake-induced liquefaction and elevated pore water pressures within the alluvial deposits. Cyclically generated excess pore water pressure in loose saturated sediment,

with attendant strength and stiffness loss, is believed to be the primary mechanism responsible for *initiating* ground movements.

4. Multiple eyewitnesses reported that they did not observe (large) ground deformations until some time (on the order of minutes) after earthquake shaking subsided. Therefore, it is known that the flowslide did not initiate co-seismically (i.e., along with ground shaking), but instead occurred *progressively* soon after the earthquake. Delayed, liquefaction-induced flow-type failures, which are well-known in the geotechnical case-study literature (e.g., Gu et al. 1993), have been attributed to the redistribution of stresses resulting from dissipation of excess pore pressure (e.g., Seed 1979).
5. The flowslide appears to have initiated near or within sloping ground (Figure 3.4). Sloping ground imparts static (i.e., non-seismic) in-situ shear stresses within soils underlying slopes. It is known that cyclically-induced pore pressures will rapidly generate (in loose soils) in the presence of initial in-situ shear stresses (Seed and Harder, 1990). Moreover, it is well established that flow-type failures may occur when the in situ stresses exceed the residual (liquefied) strength of the soil (e.g. Boulanger 1990).
6. Together, these findings suggest that the failure may have initiated in the loose alluvial deposits that had been artificially recharged by seepage from the unlined canal (Zone B). The initial failure mechanism was likely cyclically induced pore pressure generation, which may have caused a redistribution of stresses due to pore pressure dissipation immediately after the earthquake. The sloping ground would have imparted in situ shear stresses that may have exceeded the strength of the liquefied soils, triggering the onset of the flow slide. As the ground began to move west, the toe region located downslope may have offered little buttressing or resistance, also due to liquefaction in this immediate area (Zones B/C). Together, these softened, masses may have coalesced into a large fluidized mass of soil, which traveled hundreds of meters, quickly engulfing the lower part of the flowslide (Zones D/E). The fluidized nature of the mass is indicative of an "undrained" soil response, which may have been promoted by the silt content of the alluvium. It appears that in some part of the flowslide, the fluidized soil mass carried of thin [on the order of several meters] "crust" of unsaturated ground close to the surface). As the flowslide traveled downslope, the steeper ground immediately below the canal may have been de-buttressed, resulting in an eastward expansion of the landslide, and causing the failure and back rotation of intact soil blocks in this upper area (Zone A).

3.2 Jono Oge Flowslide

The Jono Oge flowslide extended over a footprint of 1.35 km², making it the largest slide caused by the earthquake. The length of the slide extended more than 2 km from the crest near the irrigation canal to runout deposits along the western edge of the slide area. The flowslide also destroyed the main road connecting Palu and Palopo city, which was one of the primary roads in Central Sulawesi. The area where the flowslide occurred is primarily agricultural with residential communities covering less than 5 percent of the area. The features of the slide area were less preserved at Jono Oge due to a breach of the irrigation canal, which occurred at the southeastern corner of the flowslide where the failure intersected the canal (Figure 3.15). The failure destroyed a water gate and the water from the canal drained into the slide area. The rapid drainage led to significant scour within the slide area and a mudflow that traveled to the Palu River. Details of the damage caused by both the flowslide and subsequent mudflow are discussed in the following sections.



Figure 3.15. Aerial view of destroyed water gate and breach point captured by drone.

The failure process and morphology of Jono Oge is largely similar to Petobo with the exception of the canal breach. Due to the erosion from that breach and the large area, the reconnaissance team primarily relied on pre- and post-earthquake satellite images to map displacement of structures and identify morphological features (Figure 3.16). The satellite images were supplemented by aerial maps and high-resolution DEMs created from drone flights conducted by the reconnaissance team (Figure 3.17). UAV images from immediately after the earthquake were

available from BNPD and were used to confirm post-earthquake locations of structures. The slide area was divided into five zones (A through E), which shared similar displacement patterns and morphological features. A sixth zone (F) was included to describe the areas that did not experience significant displacement, but were inundated by the mudflow. Displacements were largest in the central area of the flowslide (Figure 3.16). The structures within this zone were all destroyed by the earthquake and only two buildings from the central portion of the slide (the Patra Poultry Market and the church Pusdiklat GPID Patmos Jono Oge) could be reliably identified in post-earthquake imagery. The final location of the Patra Poultry Market was photographed by the reconnaissance team (Figure 3.18a) and the final location of the church was identified by comparing post-earthquake satellite images with photos of the images of the collapsed church published online (Figure 3.18b). Pre-earthquake locations for these structures were determined using Google Street View images from December 2015. Based on these sources, the displacement of the poultry market was measured as 1,230 meters and displacement of the church was measured as 1,080 meters. Many other buildings located in this same area likely experienced similar magnitudes of displacement, but were too damaged to be reliably identified in post-earthquake imagery.

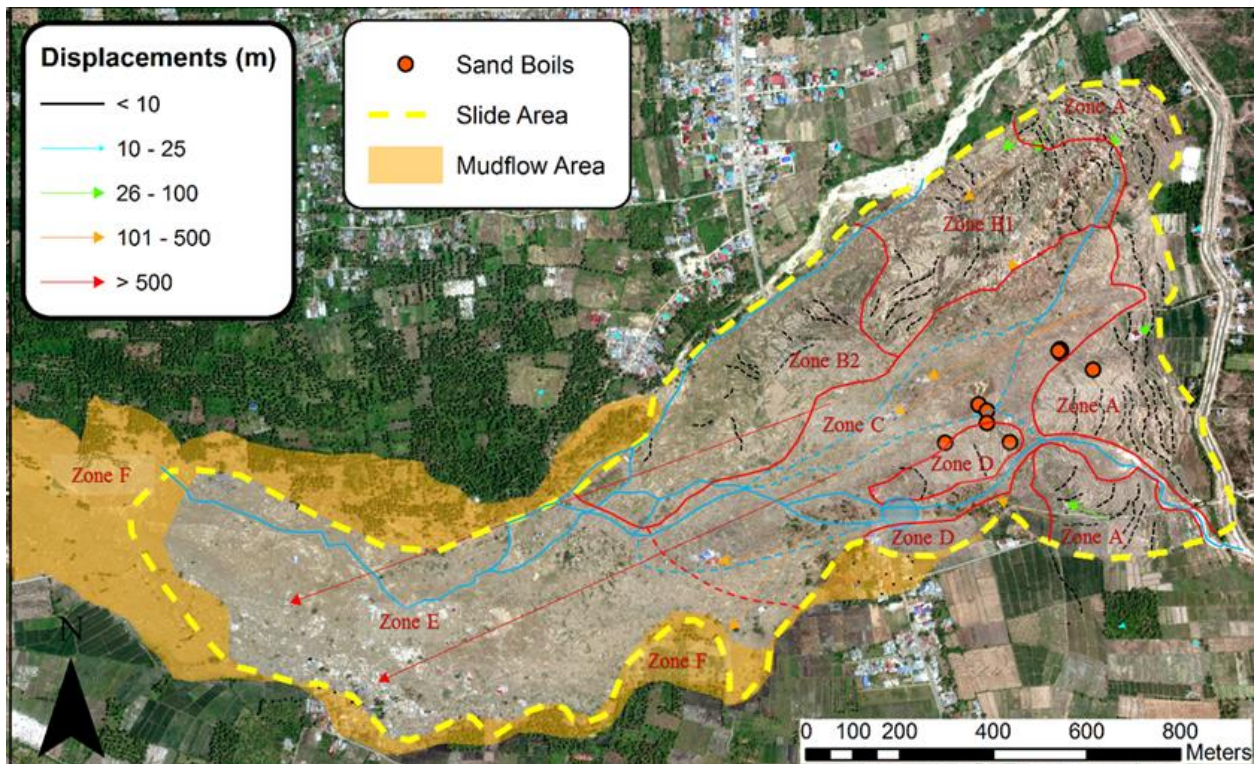


Figure 3.16. Orthomosaic map indicating limits of Jono Oge landslide, location of sand boils, vector displacements, and zones delimited by morphological features and key observations.

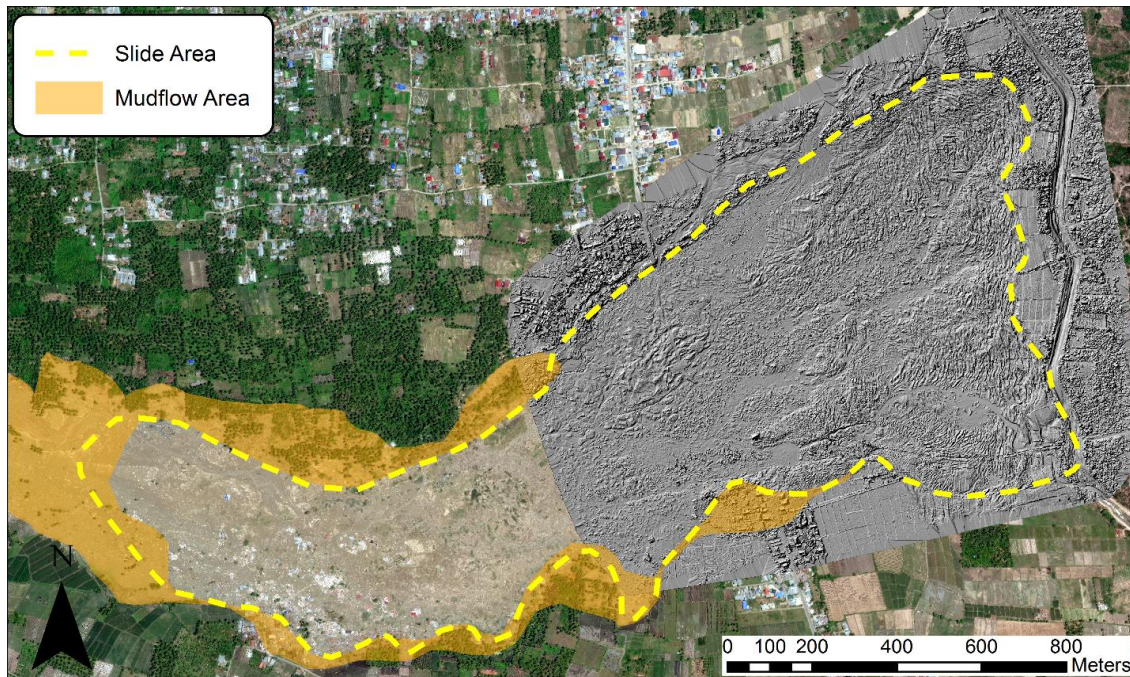


Figure 3.17. Digital elevation model and drone-derived shaded relief image illustrating 3D morphological features in the eastern region of the slide.



Figure 3.18. (a) Final location of the Patra Poultry Market (-0.98786, 119.90844), which displaced approximately 1,230 m ; (b) final location of the Pusklat GPID Patmos Jono Oge (-0.98942, 119.91007), which displaced approximately 1,080 m (image from Antara Foto 2018).

3.2.1 Field Observations and Morphology

Zone A – Head Scarp and Back-Rotated Blocks

Similar to the slide at Petobo (described above), Zone A at Jono Oge (Figure 3.16) encompasses the head scarp region of the flowslide. Zone A was primarily rice paddies (Figure 3.19a) with few structures. The head scarp extends along the western margin of the slide and intersected the canal

in multiple locations (Figure 3.19b). At the southernmost intersection with the canal, the breach led to a significant release of water (Figure 3.15). The flow of water led to significant scour within the failure and a subsequent mudflow that affected downstream communities, as previously discussed. The movement of the flowslide led to a lack of confinement on the rice paddies near the canal, which led to the formation of extensional cracks and rotated blocks of intact material (Figure 3.19c). Along the southern margin of the slide, blocks formed, but there was significantly less extension than observed in other areas of Zone A (Figure 3.19d).



Figure 3.19. Zone A: (a) View of an intact rice paddy and the head scarp of the flowslide at Jono Oge (-0.98540, 119.92580); (b) intersection of the head scarp with the canal (-0.98423, 119.92607); (c) formation of rotated blocks and extensional cracks in the area of the canal breach (note the sand deposited by the subsequent flooding; -0.98478, 119.92423); (d) damage to a road along the southern edge of the flowslide (0.98623, 119.92383).

Zone B – Laterally Extended, Rotated, and Rafted Blocks

Zone B is located on the northern side of the flowslide and consists primarily of rafted blocks, which moved into the failure area after the Palu-Palopo road and buildings that were previously located here were displaced by the slide. The blocks in Zone B were less coherent than those in Zone A (Figure 3.20) due to the significantly larger displacements that occurred within Zone B. Zone B was also impacted by subsequent flows of the river that runs along the northern edge of the failure area. Zone B1 can be distinguished from Zone B2 primarily from the coherence of the remaining blocks. Movements within Zone B1 appeared to be smaller Zone than B2, and Zone B1 was less affected by flows from the river. Both factors led to blocks being better preserved in Zone B1.



Figure 3.20. Zone B: Zone B consists of rafted blocks that moved into the main failure area after the soil in this area was displaced (-0.98211, 119.91760).

Zone C – Failure Region, Flood Area, Scour, Erosion

Zone C describes the main failure area of the slide and locations where subsequent scour and erosion occurred. The primary direction of movement was to the southwest. Zone C is bordered by Zone A on the east, Zone B on the north and Zone D on the south. Zone C transitions into Zone E, which contains the compression blocks and runout deposits from the failure. The exact location of the transition is unknown, because much of the material in Zone C was disturbed by the flood from the canal breach. Zone C comprised the lowest elevation within the slide and the central

portion was very wet due to both seepage of groundwater and flow from the river along the northern edge of the failure (Figure 3.21a). The blocks within Zone C were generally small and had been reworked by both displacement and the subsequent flooding.

Several damaged structures were located within Zone C (Figure 3.21b). The structures were transported on relatively intact blocks of crust. In some cases, trees that had been next to the structure before the failure remained essentially upright and in the same location relative to the structure in the displaced location (Figure 3.21c). The subsequent flooding made it difficult to map displacements of individual structures, but six structures within this area could be identified on before and after satellite images. The displacements of the structures ranged from approximately 270 meters along the southern portion of the failure to more than 1200 meters within the central portion (Figure 3.21a). The structure shown in Figure 3.21c was estimated to have moved 470 meters.

Sand boils were observed near the central portion of Zone C (Figure 3.21d). The sand boils were generally less than a 30 cm in diameter and the material within the sand boils was primarily fine sand. The sand boils were all located in flat areas between rafted blocks, similar to Petobo, suggesting that elevated pore water pressure and liquefied soil were confined at depth. Many of the low-lying areas had been affected by the water from the canal breach, which may have washed away evidence of other sand boils.

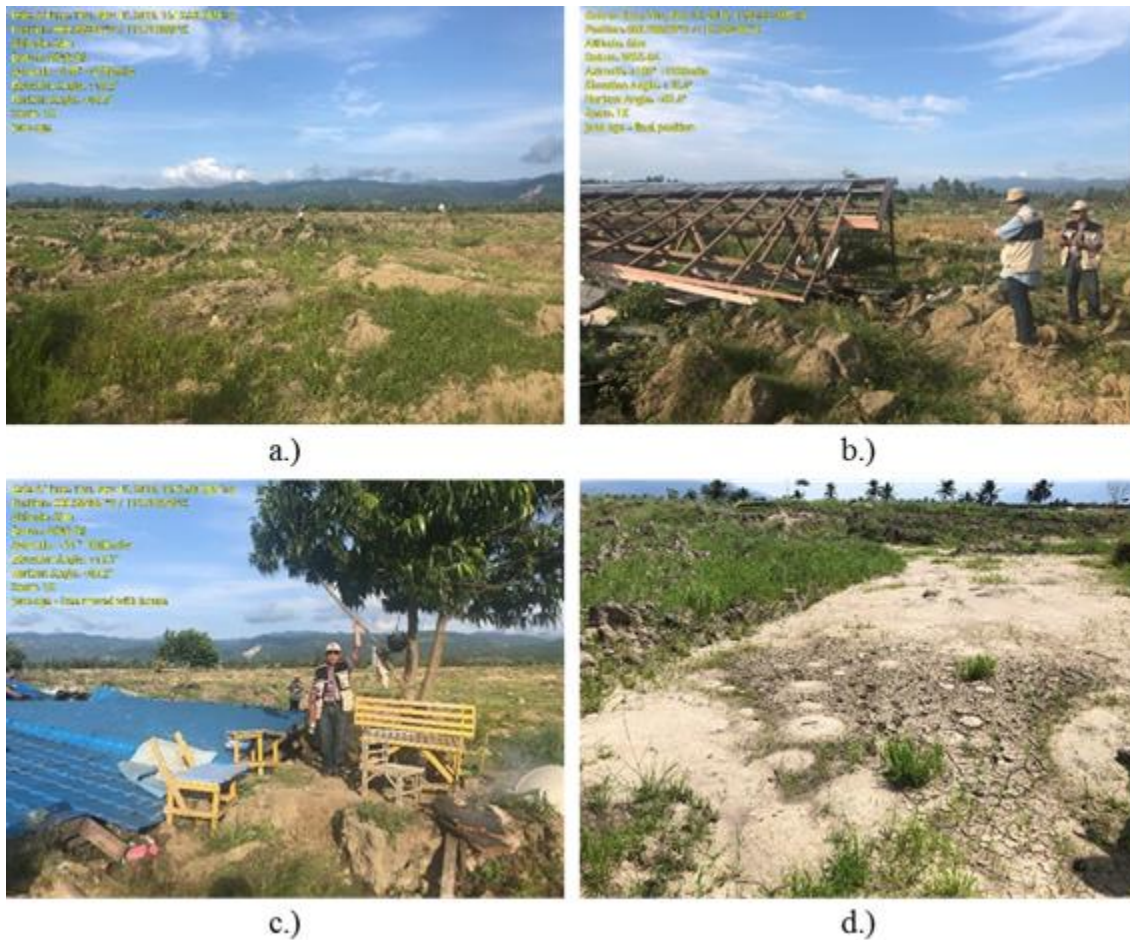


Figure 3.21. Zone C: (a) Much of Zone C was low-lying and areas between blocks were often saturated (-0.98539, 119.91938); (b) collapsed structure located in Zone C (-0.98364, 119.92071). The metal roofing was removed after the earthquake; (c) collapsed structure and tree, which had moved approximately 470 meters on a relatively intact block of crust (-0.98436, 119.91995); (d) cluster of sand boils between two blocks of crust (-0.98410, 119.92163). Note the pen on one of the sand boils in the foreground is approximately 15 cm long.

Although the main failure zone occurred within the center of the slide, a secondary failure zone was observed on the south side of the slide in the middle of Zone D (Figure 3.22). Video taken during the failure shows that the homes that were previously located in this area of Zone C were still in their original locations while the initial failure mass was moving (Figure 3.23). The homes eventually moved 330 meters (Figure 3.16).

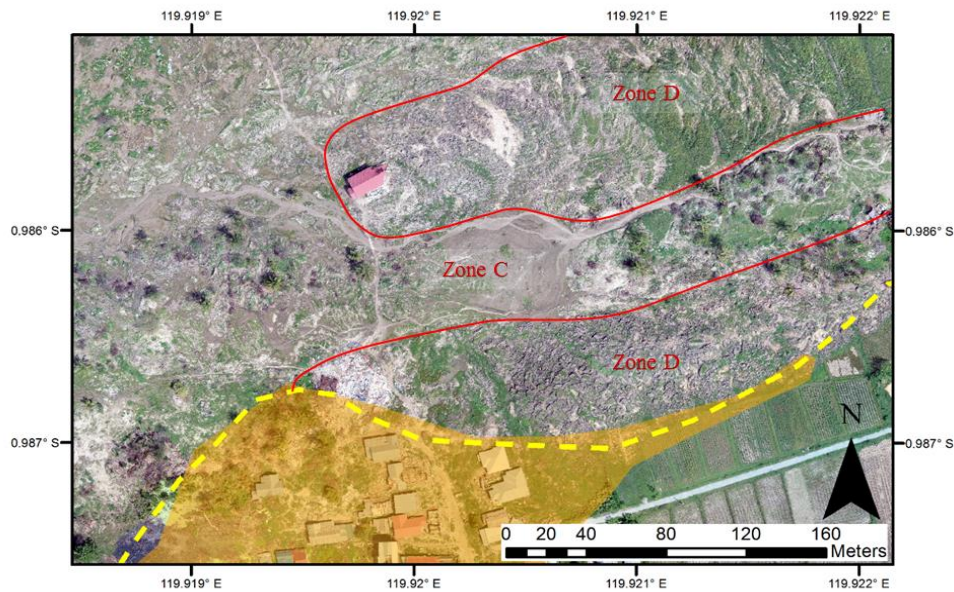


Figure 3.22. Drone imagery of the secondary failure zone along the southern edge of the flowslide at Jono Oge.



Figure 3.23. Screenshot of a video recorded during the initial failure. The person recording the video is standing on the roof of a building, which is moving. The red roofed house in the video is not moving and is located at -0.98579, 119.91965. The buildings behind the red roofed house have not moved at the time the video was recorded, but were displaced by a secondary failure.

Zone D – Laterally Extended, Rotated, and Rafted Blocks

Zone D is similar to Zone B1 in that it is composed mostly of rotated and rafted blocks that moved away from the head scarp area of the slide (Zone A). The initial movement in Zone D appears to have been primarily to the northwest, but the secondary failure discussed previously altered this movement pattern. Zone D is distinguished from Zone C because the movements are smaller and the blocks within Zone D are well-preserved (Figure 3.24a). Displacement of one structure was measured within this zone at approximately 130 meters. Some sandboils were located between

blocks on the northeastern edge of Zone D (Figure 3.24b). These sandboils were smaller than those observed in Zone C.

One unique feature within Zone D was the red-roofed home that did not move during the failure (Figure 3.24c). This was the only structure within the area of the flowslide that did not move. The flowslide did cause significant damage to the home (Figure 3.24d). The scrap marks on the side of the home indicate that the flowslide material was more than 2.5 meters thick (measured from the final ground surface to the top of the scrap marks) when it moved past the house. The house does appear to have a strong mat foundation (Figure 3.24d) of which approximately 65 cm was visible above the final ground surface. The GEER team does not know how deep the foundation extends below the ground surface.



Figure 3.24. Zone D: (a) Tree in between two intact blocks of rice paddies (-0.98554, 119.22403); (b) small sand boils in a low-lying area between blocks of crust (-0.98483, 119.92223); (c) view of the red roofed house looking northeast (-0.98595, 119.91951); (d) damage to the side of the red roofed house looking southwest (-0.98566, 119.91973). The person in the photo is approximately 1.87 meters tall.

Zone E - Compression Blocks, Debris flow, Runout Deposits

Zone E encompasses the depositional part of the Jono Oge flowslide. The transition from Zone C to Zone E was not well-preserved due to subsequent flooding of the site and so an approximate transition was determined based on the easternmost location of debris from Zone C. Similarly, the transition from Zone E to Zone F (mudflow deposits) is uncertain and the boundary shown in

Figure 3.16 was determined based on the westernmost location of large debris. The morphological features of Zone E were not studied in detail due to very large area and the erosion caused by the subsequent flood and mudflow.

The GEER team visited the community located near the western edge of Zone E. In this area, the team observed structures damaged by the runout from flowslide (Figure 3.25a and b) and structures that had been transported on the runout (Figure 3.25c). Scrap marks on the sides of the structures in this area were approximately 1 meter thick (Figure 3.25a; measured above the final ground surface elevation). The structure shown in Figure 3.25c was a market that had previously been located along the Palu-Palopo road through the center of the flowslide. Its final location was more than 1200 meters from its original location (Figure 3.18a), representing the largest measured displacement from any of the flowslides. Splashes of mud can be seen on the side of the building, which is believed to have occurred when the subsequent flood passed through this area. Debris from other displaced structures was present throughout this area of Zone E (Figure 3.25d).

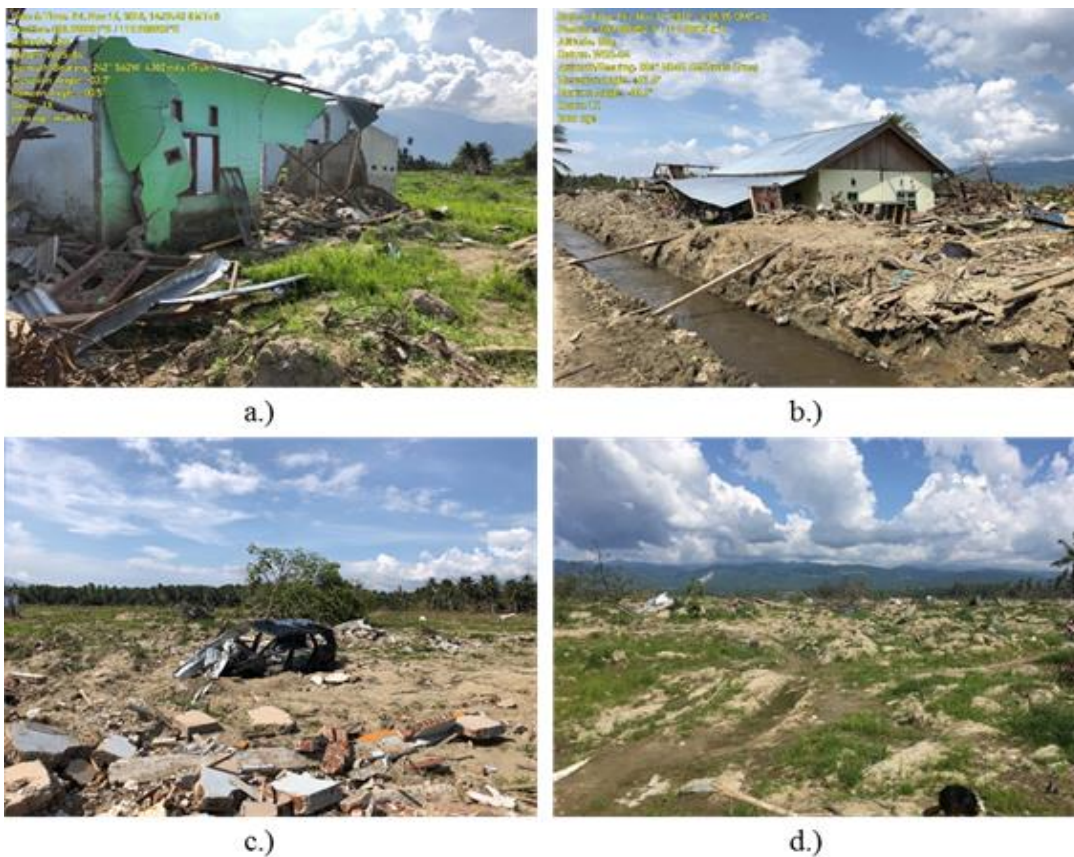


Figure 3.25. Zone E: (a) Structure damaged by the flowslide deposits (-0.98898, 119.90891); (b) Existing structure surround by debris and soil deposited by the flowslide at Jono Oge (-0.98985, 119.90922); (c) A vehicle damaged by the flowslide (-0.98838, 119.90895); (d) debris, blocks of crust and trees within the deposition area of the flowslide (-0.98893, 119.90881).

Zone F – Mudflow Deposits

After the flowslide occurred at Jono Oge, the canal breached at the southeastern corner of the slide, sending a flood of water from the canal through the failed area. The flood of water eroded significant amounts of the slide material and created a mudflow that traveled to the Palu River (more than six kilometers from the site of the breach). The approximate extent of the mudflow is shown relative to the slide area in Figure 3.26. The mudflow flooded multiple communities along the path that were not damaged by the flowslide (Figure 3.27a). The mudflow primarily followed the channel of the river that ran along the northern edge of the slide (Figure 3.27b). In two locations, the river channel was constricted by bridges (Figure 3.27c), which caused the mudflow to back-up and flood the surrounding community (Figure 3.27d).

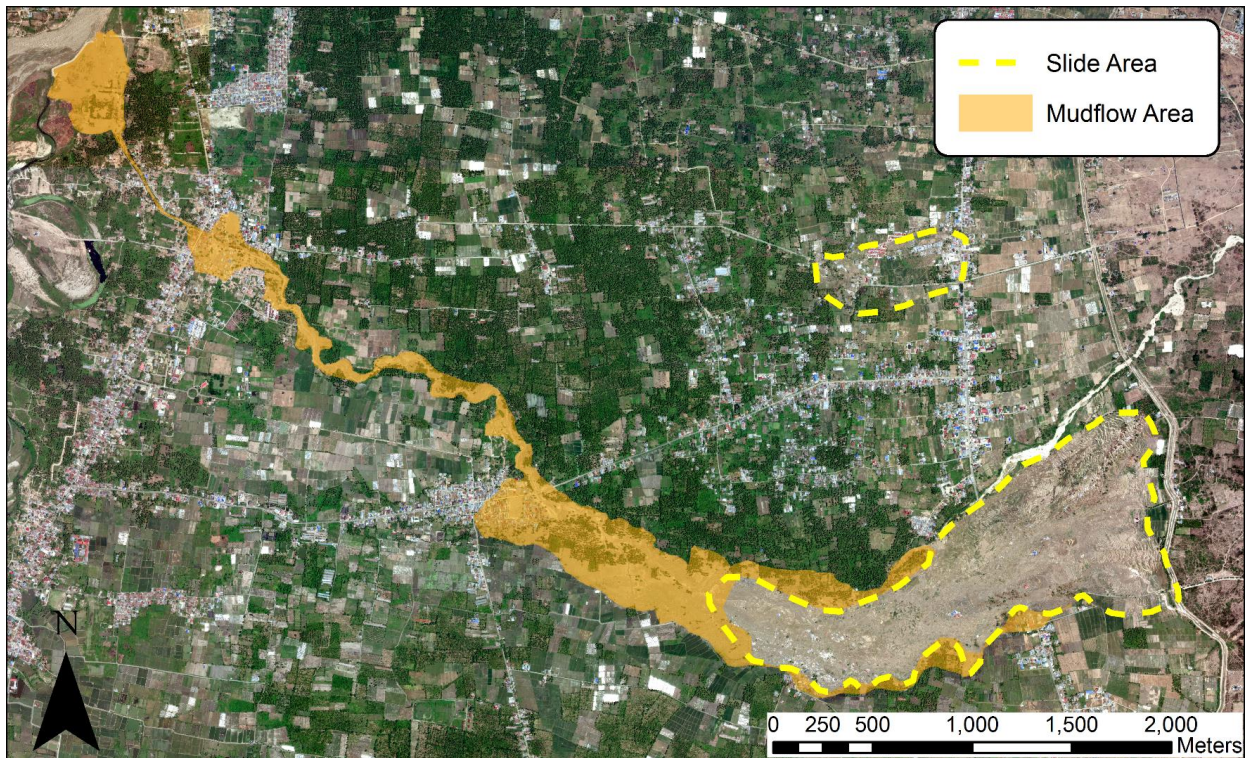


Figure 3.26. Approximate extent of the mudflow caused by the canal breach at Jono Oge.



Figure 3.27. (a) Mudflow deposits filled the streets, but left structures undamaged near the margins of the slide (-0.99025, 119.90926); (b) mudflow deposits within the river channel (-0.98440, 119.90143); (c) mudflow deposits left the river channel and flooded the surrounding community after reaching a bridge (-0.98279, 119.89848); (d) height of the mudflow on one of the homes near the bridge (-0.98253, 119.89817). The person in the photo is approximately 1.75 meters tall.

3.2.2 Eyewitness accounts

The GEER team’s interpretation of the slide mechanism and timing of the failure was based on interviews with eyewitnesses and recorded videos from the failure. Two eyewitnesses were interviewed and both described the flowslide beginning soon after the earthquake shaking stopped. The witnesses also described the failure as having initiated on the east side of the Palu-Palopo road and then progressed back towards the canal. The flow of water from the canal did not reach the lower end of the slide area until after movement had stopped. The most helpful video was recorded by a person who experienced the flowslide while standing on the roof of a structure (<https://youtu.be/c4sZlz8GuMI>; accessed 1 April 2019). The person recording the video is moving along with the flowslide and the red-roofed house seen in the beginning of the video is stationary. The velocity of the slide is slow enough that the person recording the video is able to stand and

hold the phone steady. A second video appears to show the initiation of the slide (<https://www.facebook.com/slamet.moeljono.75/videos/vb.100025552757715/243309053197518/?type=2&theater>; accessed 1 April 2019). When the video begins the person is standing across the street in front of the original location of Patra Poultry Market (-0.98424, 119.91858). The street is clearly cracked at the start of the video and it appears that shaking has ceased, although it is not known how long after the earthquake this recording began. Approximately 17 seconds into the recording, the person recording the video begins running and screams can be heard, along with some loud cracking and popping sounds. This is believed to be the initiation of sliding in this area. Attempts to reach the author of the video were unsuccessful.

One of the witnesses interviewed by the reconnaissance team was working in the fields near the eastern edge of the failure when the earthquake occurred. He observed trees moving and dry cracks opened in the fields running north-south. He was able to run to his son's house (final location shown in Figure 3.21c), which had not moved or collapsed during the shaking. He then saw coconut trees moving closer to the Palu-Palopo road and then his son's house began gradually sliding. He described hearing a loud noise after the movement had begun, which was likely the canal breaching. The second witness lived near the Palu-Palopo road was transported, along with ten other individuals, by the flowslide while standing in a grove of banana trees that floated on the slide material like a raft. Everyone on the raft of trees was able to survive the flowslide, but one member of his family was swept away by the mudflow that followed. The flow of water continued for three hours after all movement had stopped.

3.2.3 Interpreted slide progression and hypothesized mechanisms

The interpreted progression of the flowslide at Jono Oge is shown in Figure 3.28. The eyewitness accounts and video recordings suggest that the failure began somewhere in the eastern portion of Zone C after earthquake shaking had ended (shown with red arrows in Figure 3.28). The failure then moved southwest before depositing many of the structures along the southwestern corner of the slide area. The direction of movement was driven by the topography (Figure 3.29), which pushed the failure to the south. Movement stopped when the topography flattened out. After the initial movement started, the surrounding areas lost confinement and began to move into the zone left behind by the initial failure mass. The secondary movements are shown with yellow arrows in Figure 3.28. Progressive failures eventually reached the canal and initiated the breach. One area where the progression is uncertain is along the southern edge of the slide near the red-roofed house (Figure 3.22). The video recording (Figure 3.23) shows that this area failed after the initial movement took place, but it is not clear if this was simply part of the progressive failures that were occurring across the eastern edge of the slide area or if this represents a secondary failure that may

have been partially driven by the canal breach. The scour from the canal obscured any morphological features in this area, so the order of movements is unknown.

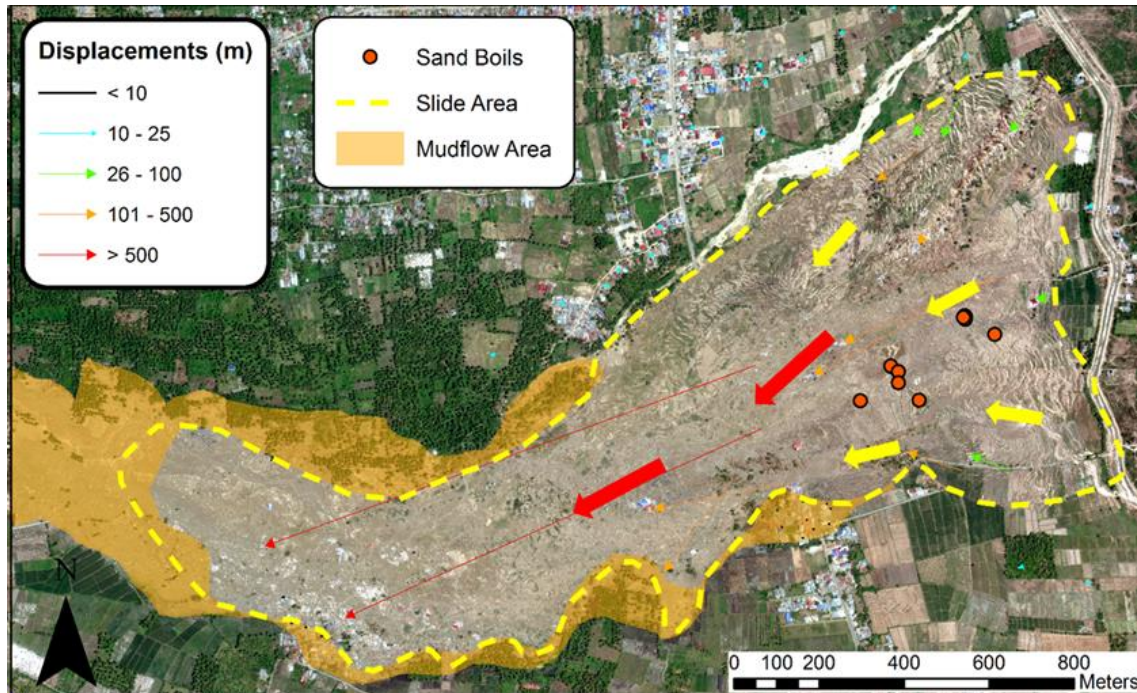


Figure 3.28. Interpreted progression of the flowslide at Jono Oge. The large red arrows indicate initial movements, while the yellow arrows indicate secondary movements.

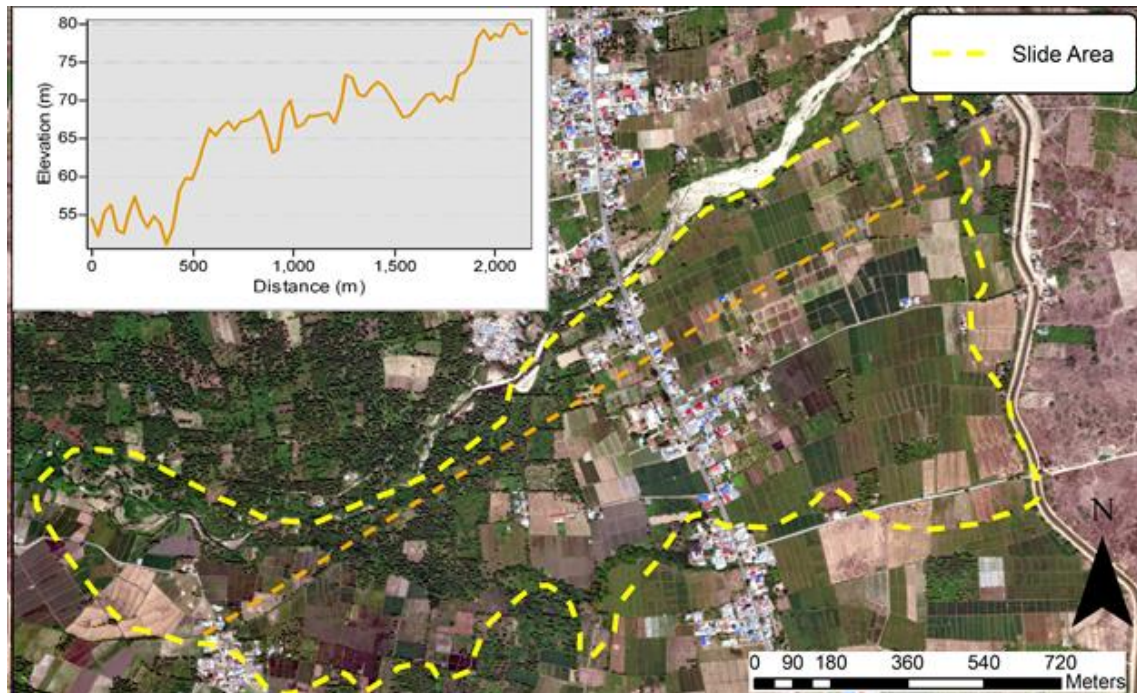


Figure 3.29. Pre-earthquake profile of the Jono Oge flowslide.

The hypothesized failure mechanisms at Jono Oge are the same as those previously described for Petobo. Sand boils were observed in low-lying areas of the site, which indicates that liquefaction likely occurred at depth and the sand boils manifested when the overlying material was removed by the slide. Liquefaction is believed to be the primary driver behind the flowslide. The initiation of the flowslide itself seems to have been driven by locally steeper terrain (Figure 3.29) and the termination of the flowslide occurred where the topography became relatively flat. The distinguishing feature at Jono Oge was the breach of the canal and the subsequent mudflow. The mudflow caused further damage to areas affected by the flowslide and inundated communities that were not affected by the original flowslide. The breach of the canal had a larger effect at Jono Oge because it was the southernmost breach on this section of the canal and a much larger volume of water drained through this failure than Petobo.

3.3 Lolu Village Landslide

Lolu Village was the location of a partially mobilized flowslide characterized by smaller ground displacements and lower degrees of geomorphic destruction than Petobo and Jono Oge. This failure affected 0.22 km² and stretched 750 m from the main road to the distal margins of runout deposits on the western edge of the slide (Figure 3.30). Although displacements were smaller, ground deformations were still as great as 150 m in some areas (Figure 3.30). The greatest displacements occurred below the main road approximately 650 m downhill from the irrigation canal, though laterally extended ground and partial scarp development was observed above the road and propagated up to the canal. Aside from repairs to the main road, which was impassable after the earthquake, geomorphologic expressions were preserved, including evidence of elevated pore water pressures and liquefaction via sand boils documented throughout the site.

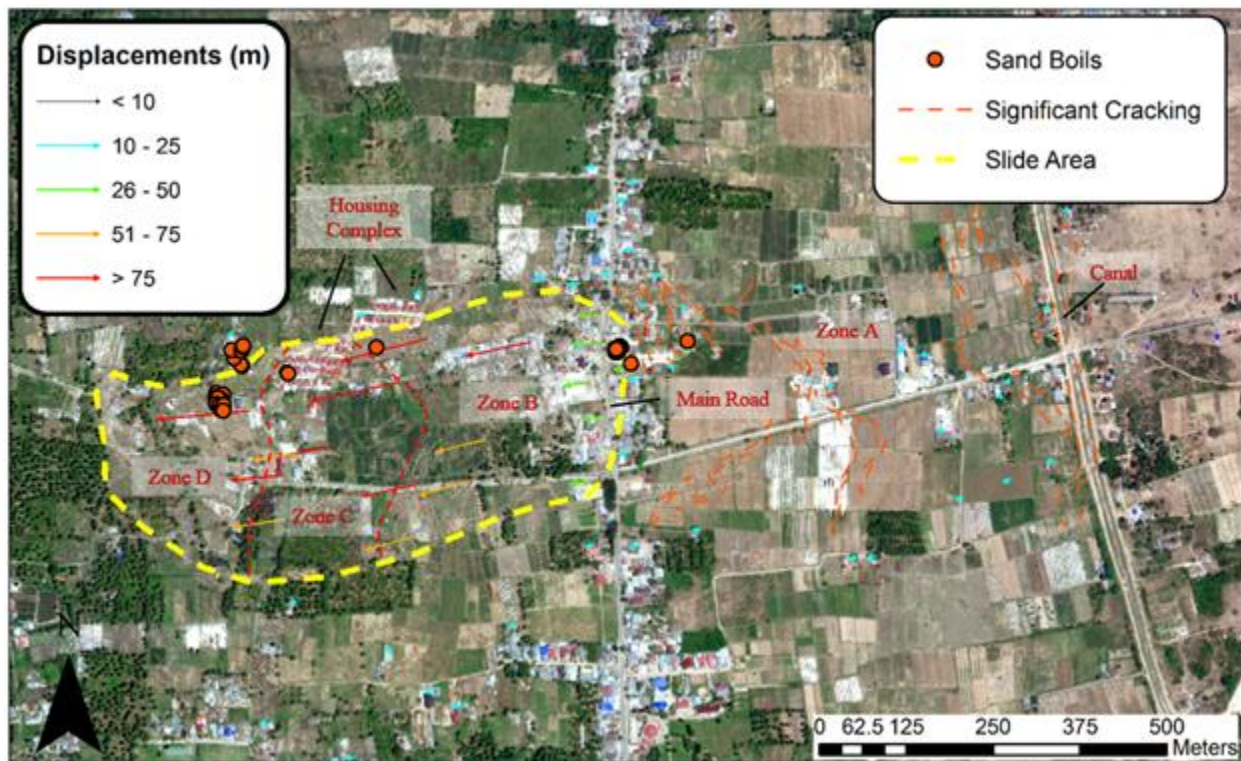


Figure 3.30. Orthomosaic map with sand boil locations and vector displacements at Lolu Village.

3.3.1 Field Observations and Morphology

Unlike the flowslides at Petobo and Jono Oge, ground movements at Lolu Village did not result in development of deep seated scarps, significant erosion, and heavy reworking of debris. The relatively “intact” nature of ground masses within the slide footprint is unique from other flowslides investigated by the reconnaissance team. The lower portion of the slide footprint (west of the main road), where the greatest displacements occurred, are more easily delineated by zones of relative movement, observed deformation patterns, shear ruptures, and visible extension seams (Figure 3.31). The uniquely intact nature of ground masses at Lolu Village aided interpretation of deformation patterns and rotation of ground masses. Pre- and post-earthquake satellite imagery and digital elevation models (DEMs) processed from drone data (Figure 3.32) collected by the GEER team aided the interpretation of morphological features and the delineation of zones for this discussion. Zones A is the include areas area above (east) of the main road up to the irrigation canal while Zones B through D are below (west) of the main road.

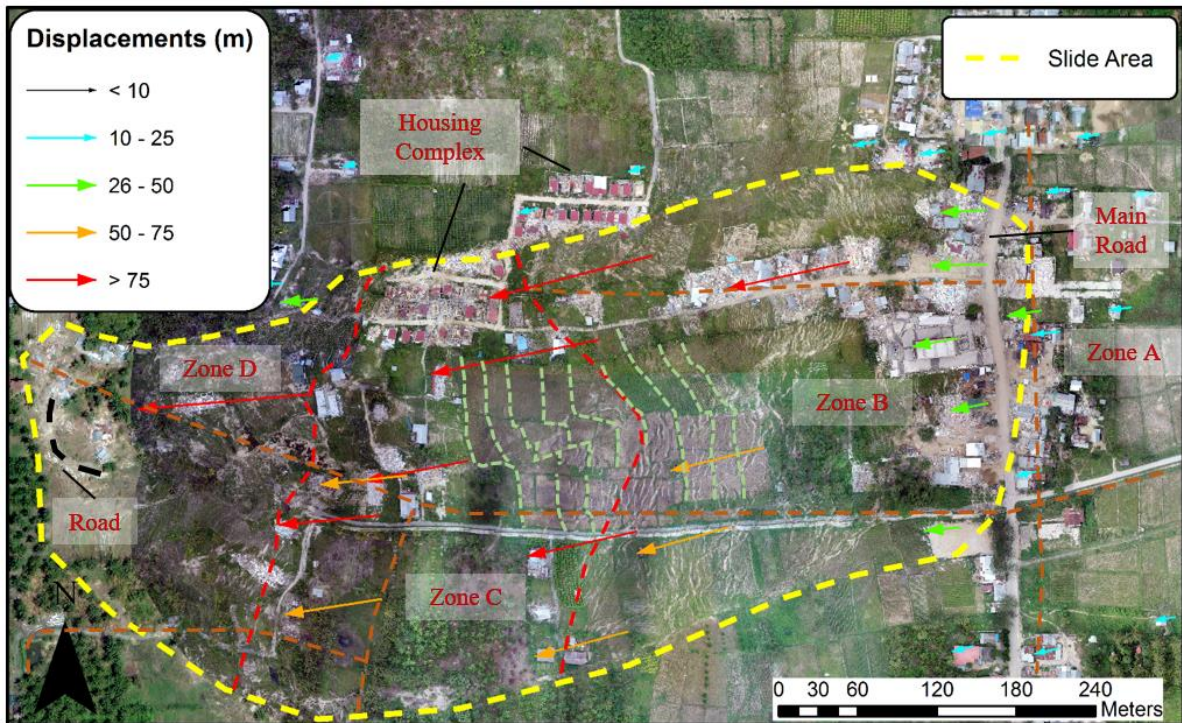


Figure 3.31. Orthomosaic map in area of the lower slide area indicating vector displacements. Also shown are the deformation patterns of ground masses near the center of the slide area (dashed green lines) and previous location of roads (brown dashed lines).

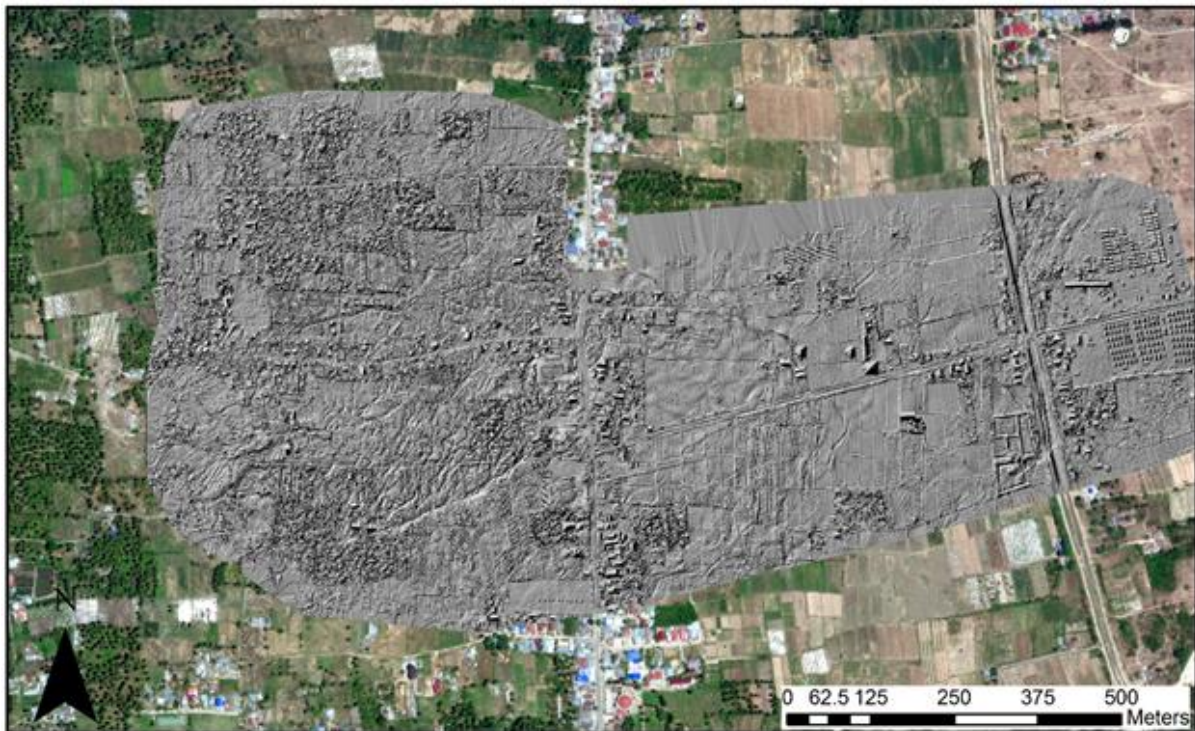


Figure 3.32. Drone-derived digital elevation model illustrating 3D morphological features at Lolu Village.

Zone A: Laterally Extended Ground and Partial Scarp Development (East of Main Road to the Canal)

The area east of the main road predominantly consists of large laterally extended cracks that propagated up to the irrigation canal (Figure 3.32). Unlike Petobo and Jone Oge, the flowslide did not result in complete loss of confinement and breaching of the canal walls, though significant cracking in the canal was documented (Figure 3.33a,b). A sluice gate located at the intersection of an access road remained largely intact (Figure 3.33c). Laterally extended cracks were also observed throughout previously irrigated agricultural fields between the main road and irrigation canal (Figure 3.34a). Vertical dislocation of laterally extended ground and partial scarp development is more apparent near the western margins of Zone A, where a series of imbricated failure surfaces are visible near the main road (Figure 3.34b,c). However, downhill displacements were not great enough for the loss of confinement to result in full separation and large, individually back-rotated blocks to form like the geomorphic expressions observed near the crest of flowslides at Petobo and Jono Oge. Documentation of sand boils near the main road also provide evidence of elevated pore water pressures in this region (Figure 3.35).

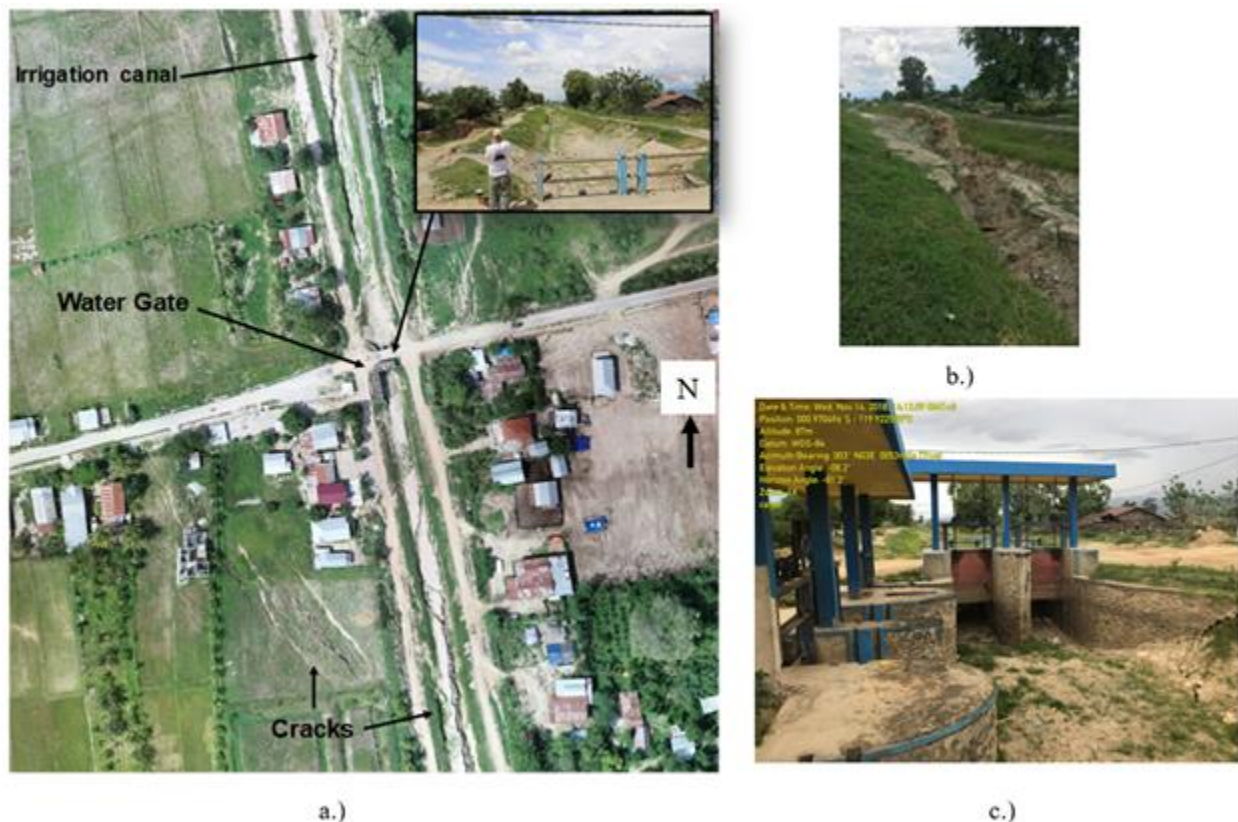


Figure 3.33. a.) Aerial view of cracking in irrigation canal; b.) crack in canal (-0.96974, 119.92249); c.) sluice gate that remained largely intact (-0.970496, 119.922598).

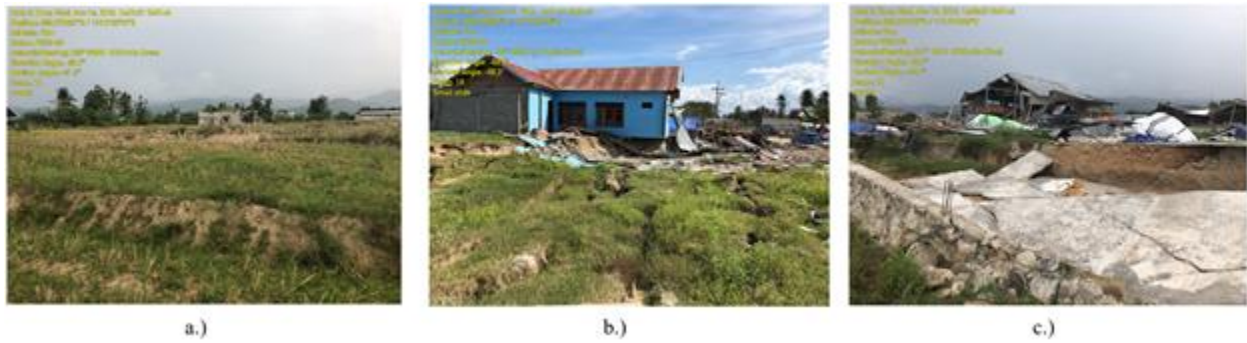


Figure 3.34. a.) Lateral extension of ground in fields above (east) of the main road (-0.970407, 119.918776); b.) damage to residential structure and laterally extended ground near main road (-0.970327, 119.916775); c.) damage to residential structure and partial scarp development near main road (-0.971073, 119.919248).



Figure 3.35. Sand boils between laterally extended ground above (east) of the main road (-0.970349, 119.916787).

Zone B: Laterally Extended Ground Mass

Below the main road transverse seams between laterally extended ground are visible in satellite imagery from immediately after the earthquake (Figure 3.31). The extension of blocks and width of depressed areas between blocks are generally greater than displaced groundmasses uphill, and recognized in aerial photographs by the decreasing density of vegetation. The preceding observations were used to delineate Zones A and B. On the eastern margin of Zone B (near main road) a gas station in Lolu Village displaced west and was severely damaged, causing cracking and splitting of the concrete pavement (Figure 3.36). Moving west (downhill), structures were subjected to greater displacements and either partially or totally collapsed (Figure 3.37). The foregoing observation is notable, because it supports the conclusion that ground was laterally

extended to a greater extent in the western portions of Zone B. Mapped displacements also corroborate the finding (Figure 3.31).



Figure 3.36. Damaged gas station on western side of main road: a.) view of facility (-0.970627, 119.916465); b.) splitting and cracking of concrete pavement (-0.970753, 119.916406).



Figure 3.37. Damaged structures in Zone B: a.) laterally extended ground and collapsed home (0.97051, 119.91515); b.) partially collapsed mosque and repaired access road left (-0.97050, 119.91492); c.) collapsed structures and rafted blocks in the foreground (-0.97037, 119.91531).

The GEER team spent a significant amount of time investigating the northern area of Zone B near the sheared housing complex. Full separation and rafting of individual blocks and mounds was observed and documented uphill from the complex (Figure 3.38a). Debris flow extended as far west (downhill) as the housing complex, where blocks were subjected to greater displacements and disintegrated more than blocks uphill (e.g. Figure 3.38b). Beyond the debris field was a relatively flat region of degradation that extends to the sheared housing complex near the western margin of Zone B. Sand boils were preserved and documented near the limits of debris flow deposits (Figure 3.38c). Ejecta consisted of fine silty to clean fine sand, similar to material ejected from sand boils documented further downhill in Zones C and D. However, sand boils appear to

have been partially eroded, likely from seeps and mudflow after the earthquake. The preceding observation, combined with the greater degree of geomorphic destruction observed in this region, supports a hypothesis that sediments comprising the floor in this region served as fluidized layer upon which the rafted housing complex was carried.



Figure 3.38. Area uphill and adjacent to sheared housing complex: a.) laterally extended and partially disintegrated blocks and mounds in field above housing complex (-0.97000, 119.91361); b.) extent of heavily reworked and disintegrated debris flow and rafted trees near margin of Zones B and C (-0.97034, 119.91374); c.) partially eroded sand boils near margin of debris flow deposits in Zone B (-0.97030, 119.91360).

Zone C: Rafted Area Compressed, Rotated, and Sheared (Sheared Housing Complex)

Zone C is a relatively “intact” area at the center of the slide footprint where some of the greatest displacements were observed. Zone C is distinguished from Zone B by fewer visible extension seams that ripple through this ground mass, and from Zone D by a lower degree of geomorphic destruction (Figure 3.31). Zone C appears to have slid on a bed of liquefied sediment, where compression ridges and uplifted features on the western margin of the Zone suggest movements were arrested by the buildup of debris (Zone D) as the flowslide progressed. Greater displacements were observed in the northern half of this area, resulting in shear ruptures and initial extension near the center of the Zone, and subsequent compression and rotation as that ground mass came to a halt. Perhaps the most compelling evidence that supports this hypothetical sequence of events is the deformation pattern of the agricultural field in this area, as shown in Figure 3.31.

The most notable evidence of shear rupture along the northern margin is the splitting of a housing complex, where rafted sections of homes displaced nearly 150 m. The separated portion of the complex appears to have been diverted around a papaya tree field as it flowed on a bed of liquefied silty to clean fine sand (Figure 3.39a). Movement of this rafted section was arrested as it abutted more stable ground on the northern margin of the slide and debris on the lower (western) side of the complex, resulting in compression, uplift, and rotation of alley or street corridors that separated the homes (Figure 3.39b,c). There was also significant evidence of compression and uplift via compression ridges just west of the housing complex, which may have initially extended before

coming to a halt. Evidence of liquefaction and debris flow was observed behind the housing complex in what is now a field adjacent to the separated portion of the complex (margin of Zone B and C). Sand boils, mudflow deposits, and disintegrated blocks and mounds that were laterally extended are shown in Figure 3.39d,e. The mounds and disintegrated blocks shown in Figure 3.39d,e are the remains of laterally extended blocks from Zone C. Note that visible vegetation (grass) is recent growth that occurred during the time period between the earthquake and the arrival of the GEER team. Though there was no breach of the canal, and significantly less erosion than what was observed at Petobo and Jono Oge, Figure 3.39f illustrates the height and subsequent consolidation of liquefied mudflow deposits in the separated portion of the housing complex.



Figure 3.39. Housing complex in Zone C: a.) view of split housing complex that slid around papaya tree field (-0.97025, 119.91304); b.) east-facing view showing rotated and uplifted street with papaya tree field still visible to the left (-0.97039, 119.91268); c.) view of destruction and evidence of compression and uplift in street in lower portion of apartment complex (-0.97069, 119.91304); d.) western view behind separated portion of housing complex showing sand boils and margin of debris flow and disintegrated blocks to the right (-0.97034, 119.91380); e.) west-northwest view of upper portion of housing complex with margin of debris flow and disintegrated blocks (-0.97036, 119.91375); f.) height of mudflow through lower portion of housing complex (-0.97040, 119.91292).

Zone D: Runout and Debris Flow

The greatest degree of geomorphic destruction and reworking of debris was observed in Zone D near the toe of the slide. Debris flow deposits consist of a heterogeneous matrix of fine sandy surface sediment with interbedded morphologic features, including intermittent occurrences of

partially disintegrated blocks and mounds, stacked or uplifted vegetation, downed or forward rotated trees, and compression ridges (Figure 3.40). Debris sheared through the eastern portion of an east-west trending road that previously cut through the center of Zone D (Figure 3.31). A remaining section of road, which was compressed and deformed, is still visible in Figure 3.31. The GEER team also documented extensive evidence of elevated pore water pressures and liquefaction in a sand boil field near the eastern margin of Zone D, where sand boils had diameters as great as 2.5 m (Figure 3.41).



Figure 3.40. Zone D: a.) sand boil field and heavily reworked and disintegrated debris (-0.97100, 119.91171); b.) compression ridge near margin of Zones C and D (-0.97048, 119.91188); c.) forward-rotated trees near toe of slide (-0.97091, 119.91104).



Figure 3.41. Sand boil field near the eastern margin of Zone D.

3.3.1 Interpreted Slide Progression and Hypothesized Mechanisms

The interpreted evolution and progression of the Lolu Village flowslide was made by corroborating eyewitness accounts, pre- and post-earthquake satellite imagery, drone data, and geomorphic expressions documented by the reconnaissance team. The landslide at Lolu Village occurred in a less densely populated area than Petobo, but several survivors with different vantage points described their account of the event. The accounts were translated by the GEER team's Indonesian colleague and/or the team's in-country partners from HATTI and PusGen. Although all witnesses were able to provide detailed descriptions of the ground motions during the earthquake, few actually had a good perspective to watch the entire flowslide that ensued (Figure 3.42). The eyewitness accounts, which were provided voluntarily, were consistent and provided significant detail on the timing, sequencing, and progression of the flowslide. The general mechanisms contributing to the initiation and progression of failure are similar to the detailed description provided in section 3.1.3.

Three eyewitness accounts were documented at Lolu Village. Two survivors witnessed the events unfold in the upper portion of the slide. The third eyewitness provided a detailed account from the toe and was able to describe the general progression of movements of the sheared housing complex (Figure 3.42). Similar to Petobo, earthquake shaking was described as an initial period of intense horizontal ground motions, followed by a brief quiescence with no shaking, and then violent vertical motions and a significant vertical drop at the end of shaking. One eyewitness witnessed the events unfold near a mosque located on an access road that extends west from the main road (Figure 3.42). In addition to the general ground motions, they also provided a detailed description of the ground rotating and the mosque "spinning" violently, followed by rolling ground, believed to be Love and Rayleigh surface waves, respectively. During the earthquake, they were running east (towards the main road) and recalled the ground continuously splitting and closing as they traversed this area during the event. The preceding observation is consistent with significant cracking observed in the lower portion of the access road. Note that the upper portion of this access road had been repaired when the reconnaissance team arrived, as shown in Figure 3.37b. The other eyewitness account from the top of the slide was from a relative of the first eyewitness, who was located on the eastern side of the main road across from the gas station during the event. They recall extensive cracking and lateral extension of the main road, and noted that these cracks were much greater than those that manifested on the eastern (uphill) side. This is consistent with a video recording taken in front of the gas station (<https://twitter.com/i/status/1049533431699234816>; accessed 1 April 2019). They described the road as impassable by traffic after the event, which had since been repaired when the GEER team arrived. The third eyewitness, located at the toe of the flowslide, first recalls the housing complex moving in unison before the southern half of the

complex sheared and slid towards their home. At some point during the flowslide the eyewitness also noted that the sheared portion of the complex began to move away (uphill). However, the GEER team believes this may be a perspective issue, and that ground where they were standing began to displace downhill towards the end of the event, giving the illusion that the sheared housing complex was moving away. As shown in Figure 3.42, ground displacements in the vicinity of this eyewitness were approximately 20 to 30 m.

Based on eyewitness accounts, mapped ground displacements, and geomorphic expressions, the flowslide appears to have initiated near the center of the flowslide area below the main road, followed by secondary movements and lateral spreading uphill (Figure 3.42). The direction, initiation, and termination of movements appears to be influenced, in large part, by topography. Movements initiated in areas with locally steeper terrain (Figure 3.42) and terminated downhill where there was little to no relief (i.e. flat terrain). Once movements initiated near the center of the flowslide, attendant loss of confinement uphill resulted in lateral extension and secondary movements. It is also noted that mapped displacements indicate secondary movements were greatest in areas where localized relief was steeper.

Generally, cyclic generation of excess pore water pressures and attendant strength loss during the earthquake are believed to be responsible for *initiation* of the flowslide at Lolu Village, similar to Petobo and Jono Oge. Sand boils observed near the toe and areas where flow appears to have initiated provide compelling evidence that support this mechanism. A global perspective of landslides in this region of the basin (Petobo, Jono Oge, Lolu Village) suggest flowslides initiated where elevations transition from approximately 60 to 80 m, as discussed earlier at the beginning of section 3 (Figure 3.4). However, this transition occurs at a greater distance from the irrigation canal than Petobo and Jono Oge. The foregoing observation is intriguing and further supports the hypothesis that the geologic and depositional environment of these alluvial fan deposits likely plays an important role in the initial conditions contributing to destabilization of this ground (section 3.1.3). However, given failure initiated much further away from the canal at Lolu Village, it is unclear whether artificial recharge or the natural groundwater table was responsible for saturation and subsequent fluidization of these deposits during the earthquake. Given there were no monitoring wells installed in this area before the earthquake, the initial groundwater table is not known. A shallow (hand) boring performed at the toe of the flowslide in Zone D indicates the groundwater table was approximately 1 m below the ground surface (Figure 3.42). However, without more groundwater information and post-earthquake elevation contours, the GEER team cannot yet conclude whether or not the soil only liquefied at or near the natural groundwater elevation.

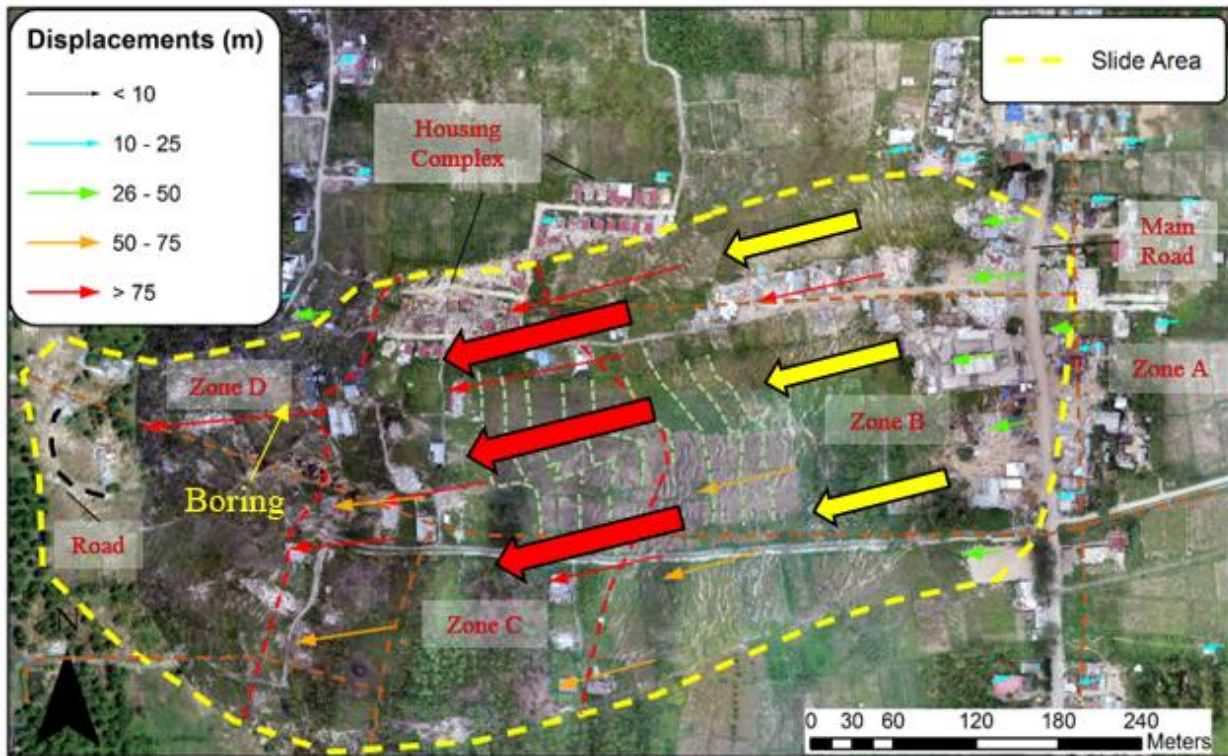
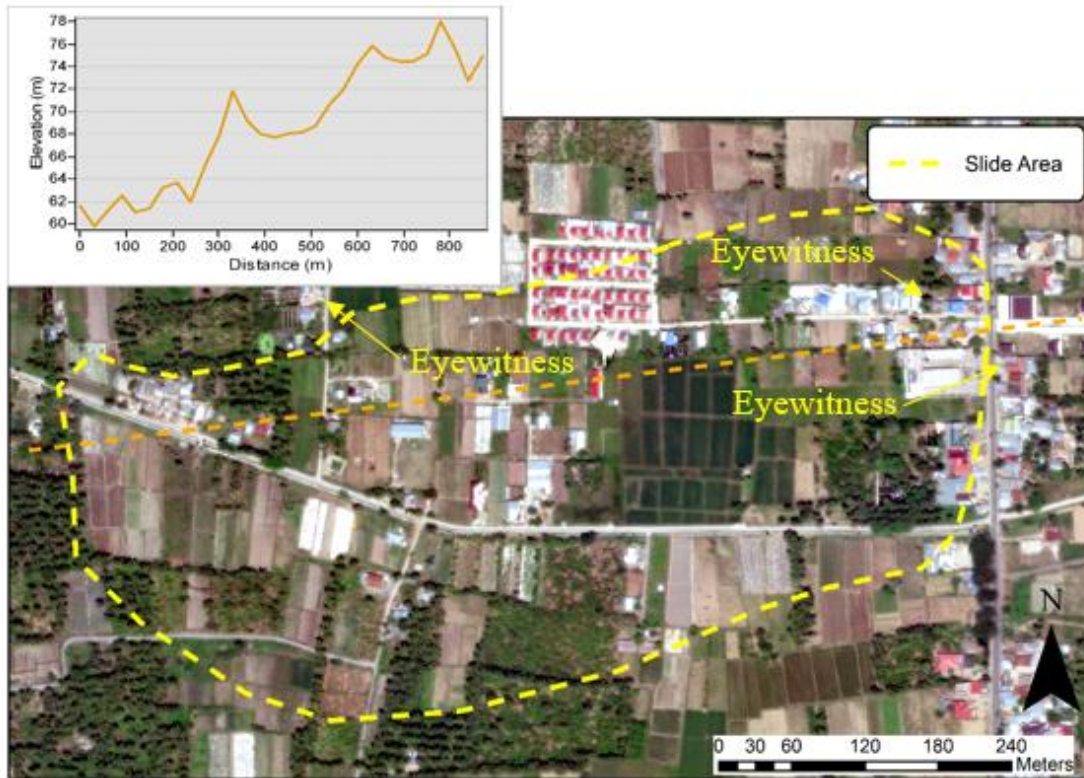


Figure 3.42. Pre-slide topography and interpreted slide progression indicating initial (red arrows) and secondary (yellow arrows) movements.

3.4 Sibalaya Landslide

Sibalaya is located 18 km in the south part of Jono Oge, and is also crossed by the irrigation canal. The width of the canal at this area is relatively large compared to Jono Oge and Petobo. This was the southernmost landslide investigated by the GEER team, and divided into five zones (A through E) based on morphological differences and key observations in each area. This failure affected 0.52 m² and extended more than 1.2 km from the irrigation channel to the distal margins of runout deposits on the western edge of the slide (Figure 3.43). A breach of the irrigation canal resulted in two scour channels that converged and split the villages of North and South Sibalaya. A portion of the roadway is clearly visible in Zone D, and remained largely intact during translation to its current location. Aside from minor repairs made to the main road to make it passable for traffic, there was little disturbance and most geomorphologic features were preserved after the earthquake. Sand boils and evidence of liquefaction were documented in several areas throughout this site.

Figure 3.44 shows the vector displacements of several structures, which indicate ground movements and runout distances as great as 400m at some locations. Based on the vector displacements shown in Figure 3.44, the slide generally flowed west-northwest and fanned out, spreading in the north south direction as the ground displaced. Displacements at the center of the slide are greatest and decrease near the margins of the affected area, though movements along the southern margin of the slide are significantly smaller but oriented in the general direction that the landslide masses flowed.

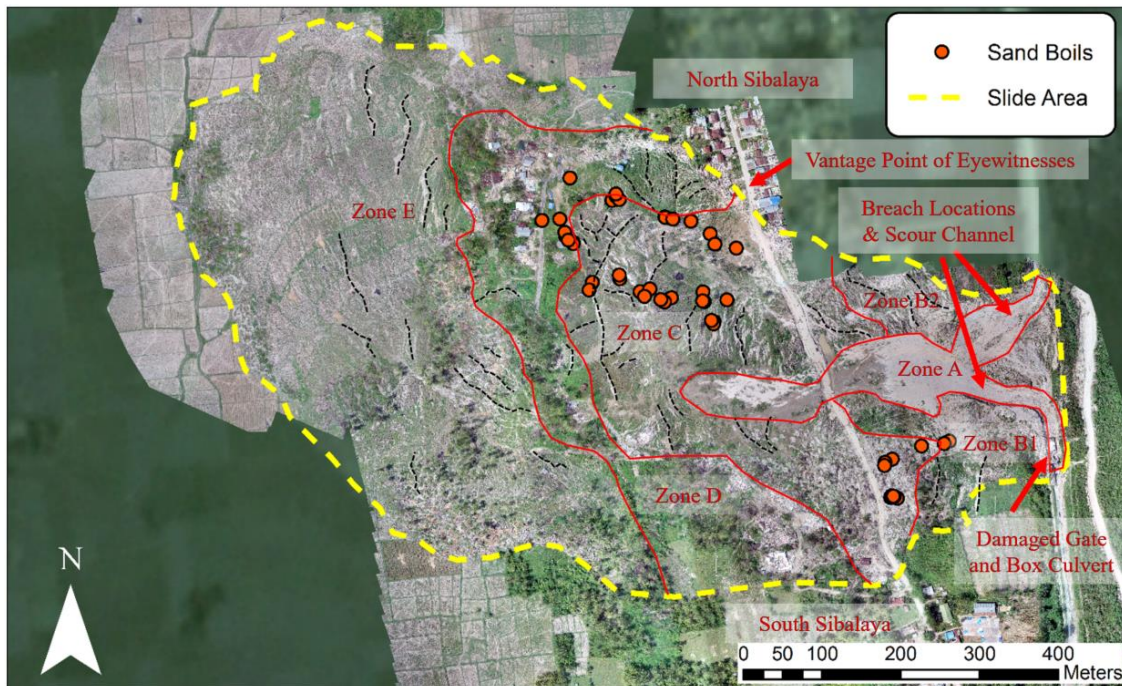


Figure 3.43. Orthomosaic map indicating limits of Sibalaya landslide location of sand boils, and zones delimited by morphological features and key observations.

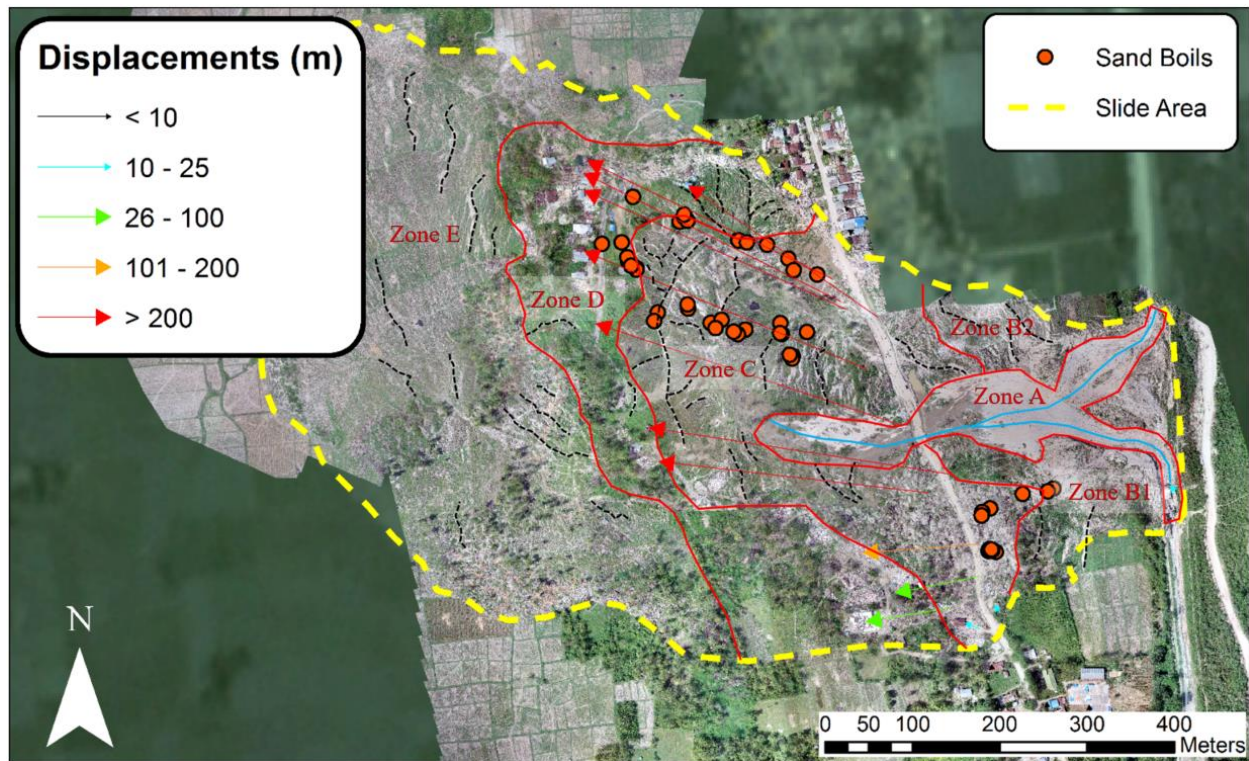


Figure 3.44. Orthomosaic map indicating locations of sand boils, vector displacements, and zones delimited by morphological features and key observations.

3.4.1 Field Observations and Morphology

Zone A – Scour and Erosion Area

Breach of the canal at two locations resulted in significant scour and erosional features, including development of two channels at the southeast and northeast margins of the slide that converge towards the center of Zone A. Scour channels in Zone A resulted in an unconformity in structural features observed in Zones B and C near the center of the slide (Figure 3.43). These scour channels made deep cuts roughly 4 to 6 m through what was previously gently sloping alluvial fan deposits of fine to medium sand and silty sand. The presence of gravel, cobbles, and boulders near the bottom of these channels suggest scouring mechanisms likely intersected older colluvium debris deposits underlying surficial sediments (Figure 3.45a,b). Finer sands and silts were eroded and carried by water draining from the canal and deposited towards the center and western margins of Zone A.

Other notable features include destruction of a concrete box culvert and steel framed gate near the southeastern breach of the canal. Lateral extension and cracking, which lead to the breach at this location, facilitated scour and erosion around these structures, as well as sloughing along the canal

walls. This also resulted in severe damage to a non-continuous, unreinforced concrete liner connecting the box culvert and gate (Figure 3.45a, c, d).



a.)



b.)



c.)



d.)

Figure 3.45. Zone A: a.) scour channel and damaged box culvert (-1,14844, 119.92477); b.) east-southeast facing perspective of southern scour channel where scour channels converge (-1.14788, 119.92281); c.) damaged gate and cracking in the canal on southeastern margin of slide (-1.149652, 119.924991); d.) damaged liner between box culvert and gate and sloughing of canal walls in the background (-1.14915, 119.92493).

Zone B – Head scarp and back-rotated blocks

This zone, located at the southeast and northeast margins of the slide (Zones B1 and B2) consist of head scarps and back-rotated blocks that cut through rice paddy fields adjacent to the canal (Figure 3.46). The head scarps consist of the same unconsolidated alluvial fan deposits that were scoured by breach of the canal in Zone A. Relatively large blocks near the crest were down-dropped at this location, and vegetation and trees were generally oriented uphill towards the crest of the head scarp. The size of down-dropped blocks generally decreased moving west away from the crest, and near the delineation with Zone A, where scour and erosion would have been more influential in the final structure of these blocks. Talus sediments partially filled depressions

between smaller blocks at lower elevations. Additionally, sand boils were identified and preserved/protected by smaller blocks and Talus at the base of Zone B1, verifying liquefaction and fluidization of material contributed to destabilization of the groundmass. (Figure 3.46c). Ejecta provided evidence that the liquefied layer consisted of fine sand with silt or silty sand. At this time the depth of the liquefied layer has not been identified. Sand boils were not observed in Zone A, though these features would likely have been eroded by flood waters in a high energy environment after the canal was breached, and would therefore not have been preserved like those features found in Zone B1.



Figure 3.46. Zone B1: a.) head scarp (-1.149536, 119.924125); b.) back-rotated blocks (-1.149580, 119.924053); c.) sand boils (-1.49620, 119.923225).

Zone C – Back-rotated and laterally extended block field

This area consists of back-rotated transverse ridges of alluvial fan deposits that were laterally extended throughout the zone (Figure 3.47a-c). Vegetation on the surface of these blocks largely remained intact, indicating they translated from the rice paddy fields that were adjacent to the canal prior to the earthquake (Zones A and B). While surficial sediments along the eastern portion of the slide are believed to be alluvial fan deposits that originated in the mountains and transported to the

basin via a tributary drainage network, original sediments in Zone C are believed to be alluvial flood deposits from the Palu River (Figure 2.4).

The extension of blocks and width of depressed areas between blocks are generally greater than displaced groundmasses west of this area, and a key feature that helps delineate this zone from others (i.e. Zones D and E). Aside from ground surveys, extension is recognized in aerial photographs by the decreasing density of vegetation (rice paddies) and greater visibility of sand in depressions between blocks (Figure 3.44). In some areas the floors of these lateral extension veins (e.g. black dashed lines in Figure 3.44) are filled with material carried by flood waters from the canal, especially near the center of this zone. An extensive number of sand boils were preserved in these depressed areas throughout Zone C, indicating liquefaction was widespread (Figure 3.43 and Figure 3.47c-f). Ejecta consisted of fine silty sand, similar to material ejected from sand boils in Zone B. Given sand boils manifest at locations where pore water pressures exceed overburden stresses, the prevalence of these features may suggest that the elevation of the fluidized layer is near (or at) the elevation of the depressed floor between extension blocks in this zone.

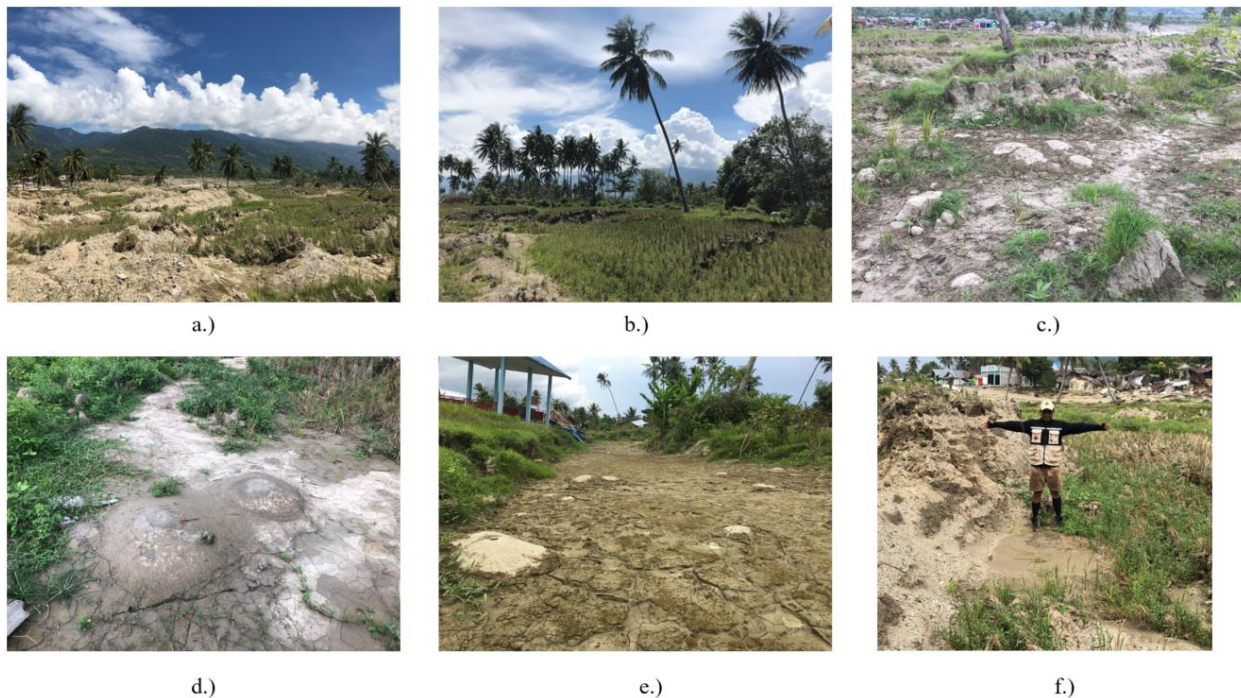


Figure 3.47. Zone C: a.) view facing southeast of back-rotated blocks (-1.146946, 119.919843); b.) view facing south of back rotated blocks (-1.146946, 119.919843); c.) view facing southeast of back-rotated blocks and sand boils (-1.146575, 119.919432); d.) sand boils (-1.146419, 119.920662); e.) sand boils near margins of Zone C and D (-1.146422, 119.919374); f.) large sand boil (-1.147622, 119.921125).

Zone D – Collision blocks and rafted landslide masses

Several observations and features in this area offer insight into the evolution of movements and progression of the landslide mass in this zone. Groundmasses in this area transition from an area of extension in Zone C to compression, characterized by closure of cracks and extension features, and where blocks may experience uplift and/or rotation as blocks collide. Evidence of this is observed in aerial photographs by the increased density of vegetation and width of areas with exposed sand, which indicates closure of extensional depressions between blocks (Figure 3.44). For instance, in the northeastern limits of Zone D the roadway and blocks appear to have initially rotated clockwise before sliding and colliding with the northern margins of the slide. Collision with the northern limits of the slide and Zone E appears to have at least partially compressed cracks and extension features. Aside from displacements, the predominant orientation for some of these compressed veins are interpreted in Figure 3.44 to illustrate the general movement of landslide masses in the northeast area of Zone D. Additionally, blocks are no longer consistently back-rotated, and instead uplifted and/or forward-rotated in many instances (Figure 3.48a).

The condition of pavement and residential homes were beneficial in interpreting the progression of the landslide mass near the center and northwest margins of the zone. Near the central portion of Zone D, the landslide mass appears to have effectively behaved as a raft that underwent relatively limited extension or rotation as it was displaced. Trees and root systems running along the western margins of Zone D likely reinforced the ground mass, holding it together as it was displaced. This is supported by the condition of the original roadway, which remained largely intact. An extension crack near the edge of the intact portion of road appears to have closed (left side in Figure 3.48b), suggesting this area may have been subjected to collision and compression on the eastern margin from extending landslide masses in Zone C. Furthermore, the roadway and landslide mass in this areas is at a higher elevation based on visual observation, and may have been uplifted in the final stages of the slide (e.g. Figure 3.48c).

Residential homes near the center of the zone and intact portion of roadway were also largely intact, indicating fewer signs of distress than structures clustered in the northwest limits of Zone D, many of which collapsed entirely (Figure 3.48d vs. Figure 3.48e-f). The central portion of Zone D was relatively flat compared with the northwestern area of the zone. Several undulations within this area may be evidence of greater initial extension and partial closure of blocks during the final stages of the slide. This hypothesis also explains greater distress or complete collapse of residential homes in the northwest corner of Zone D.

There continues to be fewer, easily recognizable extension features and increased tree vegetation along the southern margin of Zone D, similar to the central portion of the landslide mass in this area. Displacements were roughly 50 to 100 m based on movements tracked near the southwestern corner of the zone, which are significantly less than displacements observed near the eastern (central) and northern portions of the zone. Based on the interpreted limits of Zone D in Figure 3.44, the central area of Zone D appears to have dislodged from the southern portion during the slide. Greater tree density within and outside the southern margins the slide may be attributed to greater resistance and smaller displacements in this area.

Another notable observation is the displacement of a field in the southwest corner of Zone D, which appears to have only shifted 25 to 50 m. Given displacements at the southeastern corner were 50 to 100 m, there was likely lateral spreading in the southeast corner as the slide initiated, with some possible recompression and collision during the later stages of the event. Greater distress to residential homes and a mosque in the southeastern corner of Zone D (relative to structures in the central portion of Zone D) supports this interpretation of sliding progression, similar to discussion of the northeastern corner of the zone.

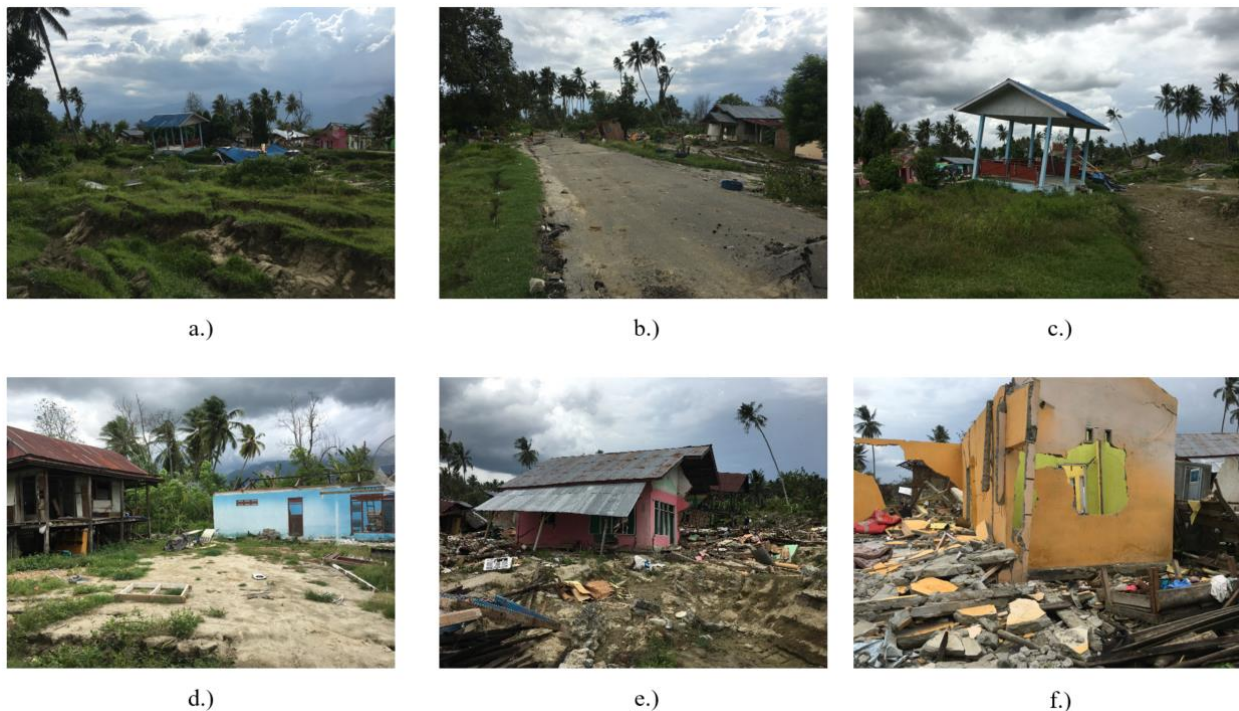


Figure 3.48. Zone D: a.) block compression and uplift near northern margin of zone C (-1.145940, 119.919559); b.) relatively intact portion of road and apparent closure of crack on left side (-1.146440, 119.919162); c.) notable difference in elevation immediately adjacent to depression in zone C (-1.146422, 119.919289); d.) relatively intact residential homes near the center of the zone D (-1.146385, 119.919055); e.-f.) greater distress and collapse of structures near the northwestern margins of zone D (-1.145904, 119.919079 and -1.145963, 119.918827).

Zone E –Runout Debris and Block Field

The runout zone consists of well-defined isolated blocks resting on a floor of fine silty sand that is visible in depressed seams separating these features (Figure 3.49a,b). The width of extension seams and the size and height of isolated blocks were generally uniform throughout the debris field. In localized areas where the width of extensional veins was greater, increased disintegration of blocks was observed. Material constituting the floor of this zone likely represents fluidized sediment that functioned as a lubricant and facilitated flow and large displacement of isolated blocks in this area of low relief (grades 1 to 2 percent). Away from the margins of the slide, the varying orientation of blocks suggests these features were rotated under the global and local forcing conditions provided by the viscous flow of fluidized sediment emanating across rice paddy fields in Zone E. The dispersion of fluidized sediment across this region of the slide likely caused the continuous formation of extension seams as the groundmass fanned out across the zone (Figure 3.44). Based on geomorphic expressions in other zones and eye witness accounts (discussed later), the slide appears to have initiated beneath this block field, which was displaced from the region just west of the existing road (now Zone C). Block uplift and forward rotation of trees and blocks provide evidence of collision near the distal margins of the zone where the slide terminated (Figure 3.49c,d).

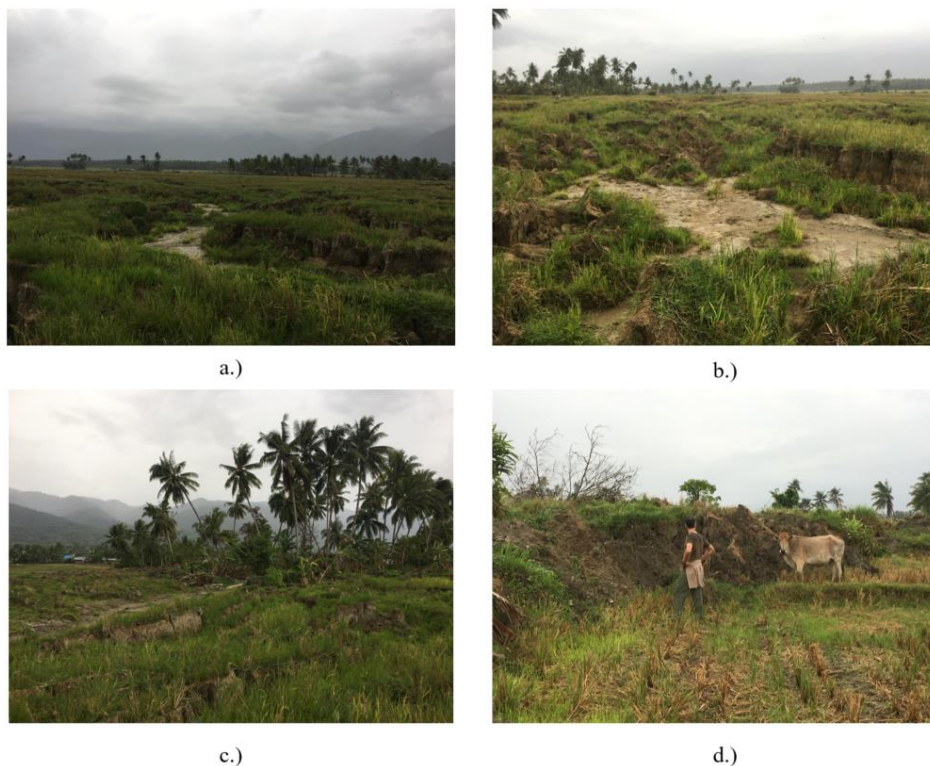


Figure 3.49. Zone E: a.) runout block field and seam of previously liquefied sediment in seam between blocks (-1.144891, 119.917555); b.) sediment in depressed seam between blocks (-1.14496, 119.91769); c.) forward-rotated and uplifted collision blocks near the terminus of the slide (-1.144893, 119.917708); d.) thickness of debris at the terminus of the slide (-1.144651, 119.915743).

3.4.2 Interpreted Slide Progression and Hypothesized Mechanisms

The interpreted evolution and progression of the Sibalaya flowslide was made by corroborating eyewitness accounts, pre- and post-earthquake imagery, and geomorphic expressions documented by the reconnaissance team. The landslide at Sibalaya cut through the (locally dense) villages of North and South Sibalaya, and several survivors provided eyewitness accounts from different vantage points. These accounts were translated by the GEER team's Indonesian colleague and/or the team's in-country partners from HATTI and PusGen. However, few actually had a good perspective to watch the entire landslide that ensued, with the exception of a group of young men (teenagers or older) who witnessed the event unfold in North Sibalaya (Figure 3.50). The eyewitness accounts, which were provided voluntarily, were consistent and provided significant detail on the timing, sequencing, and progression of the flowslide. The general mechanisms contributing to the initiation and progression of failure are similar to the detailed description provided in section 3.1.3 for Petobo.

The group of young men who witnessed the events unfold in North Sibalaya (Figure 3.50), which was mainly described by the eldest member of the group, recounted the sequence of strong shaking as an initial period of intense horizontal ground motions followed by vertical motions and a vertical drop at the end of the earthquake, similar to eyewitness accounts at other flowslide locations. The group did not begin witnessing (large) ground displacements until after shaking ceased. Ground movements were first observed west of the main road via sliding of coconut trees in the approximate location of what is now the laterally extended block field (Zone C), followed by clockwise "rotation" of a field (east of the main road) away from the canal. As the field rotated and displaced away from the canal an extremely loud noise was heard, presumably a combination of the canals walls being breached and subsequent destruction of the sluice gates and box culvert. Flooding then ensued and inundated the region west of the canal. A woman, whose home was initially adjacent to the main road, recalls the splitting of the structure's floor followed by flowing ground into the home. As she attempted to escape, the structure began to displace and she was forced to hold onto wooden slats in her window. The structure displaced approximately 400 m before coming to rest. She did not recall any flooding and inundation until after movement of her home ceased. The village leader of South Sibalaya provided second hand accounts of the event (he was not there at the time) and general displacements of structures in his village, which are consistent with mapped displacements.

Based on eyewitness accounts, mapped ground displacements, and geomorphic expressions, the Sibalaya flowslide appears to have initiated west of the main road, followed by secondary movements that include rotation and lateral extension of the field previously adjacent to the canal

(Figure 3.50). The direction, initiation, and termination of movements appears to be influenced, in large part, by topography. Movements initiated in areas near the “toe” of locally steep terrain. This location is approximately 800 m from the terminus of debris flow (Figure 3.50), and consistent with eyewitness accounts of where coconut trees were first observed moving. Once movements initiated just west of the main road, attendant loss of confinement east of the road resulted in lateral extension and secondary movements (Figure 3.50). Debris flow and runoff terminated in areas with little to no relief, or where there was a slight incline in the terrain.

Similar to flowslides north of Sibalaya (Petobo and Jono Oge), artificial recharge from the canal is believed to have saturated alluvial sediments, contributing to the initial conditions necessary for cyclic generation of excess pore water pressures and attendant strength loss during the earthquake. The prevalence of sand boils observed in the lateral extended block zone where flow is believed to have initiated provides compelling evidence that again support this mechanism instigated the landslide. Interestingly, the Sibalaya flowslide also occurred at the interface of alluvial fan and floodplain deposits, same as the other large flowslides at Petobo, Jono Oge, and Balarooa (discussed in the following section). Again, this suggests the geologic and depositional environment of these alluvial deposits likely plays an important role in the initial conditions contributing to destabilization of these materials. Another notable consequence of the landslide is the breach of the western walls of the irrigation channel, and subsequent erosion and degradation of material near the canal. Given this is the southernmost landslide investigated by the GEER team, it is also closest to the water source. Large volumes of water drained from the canal in two directions (up and downstream), making deep cuts (as great as approximately 4 to 6 m) through alluvial fan deposits. The depth of erosion for the southern breach was appreciably greater than the northern breach at Sibalaya, presumably because there was a greater volume (and source) of water that drained from the upstream portion of the canal. Flooding likely eroded and obscured many geomorphological features that may have existed immediately after the flowslide took place.

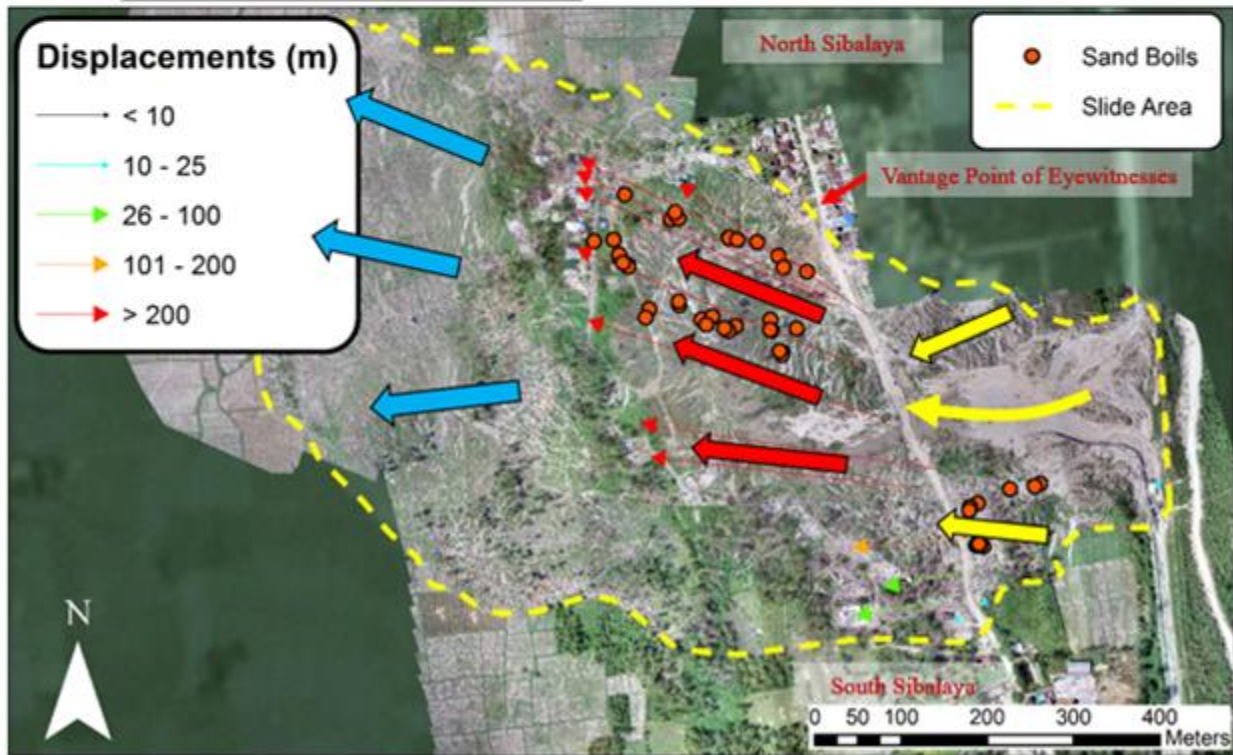
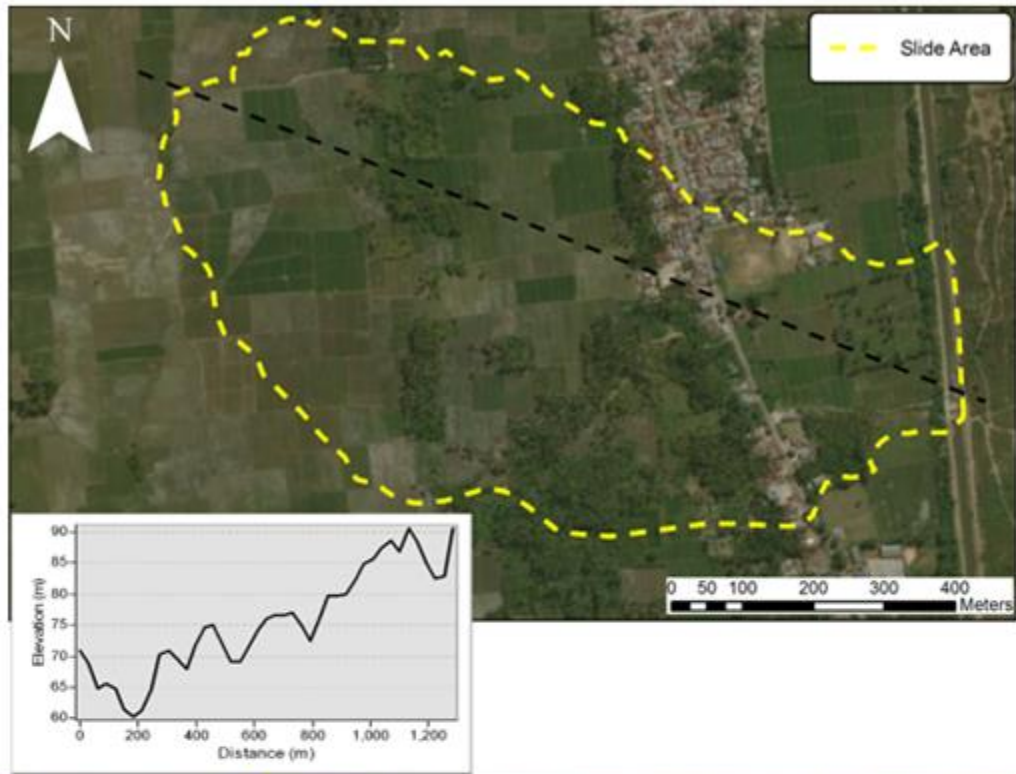


Figure 3.50. Pre-slide topography and interpreted slide progression indicating initial (red arrows) and secondary (yellow arrows) movements as well as runout displacements (blue arrows).

3.5 Balaroa Landslide

The Balaroa flowslide was the only failure observed on the west side of the valley. The landslide encompassed 0.4 km² with a length of approximately 980 m. The failure occurred in a very densely populated residential neighborhood (Figure 3.51) and BNPB estimated 2,895 buildings were damaged or destroyed. The toe of the landslide was located next to the fault rupture, so it was difficult to distinguish damage from the slide and damage from surface rupture in some areas (Figure 3.51). The GEER team visited this site on 14 November 2018, but many of the damaged structures had been removed and significant earthwork had been completed to level the site. The clean-up efforts made any detailed mapping of the site or morphological interpretations very difficult (Figure 3.52).

The general direction of movement of the Balaroa landslide was to the northwest (Figure 3.53). Displacement mapping of the landslide was performed by matching points on individual structures in pre- and post-earthquake satellite imagery (Digital Globe 2018) at the site. The displacement mapping showed maximum building displacements of more than 350 meters in the central portion of the failure (Figure 3.53). Many of the buildings could not be identified in the post-earthquake imagery, which led to incomplete mapping of the failure. The GEER team observed high groundwater during the site visit, including deep ponding of water near the toe (Figure 3.54).

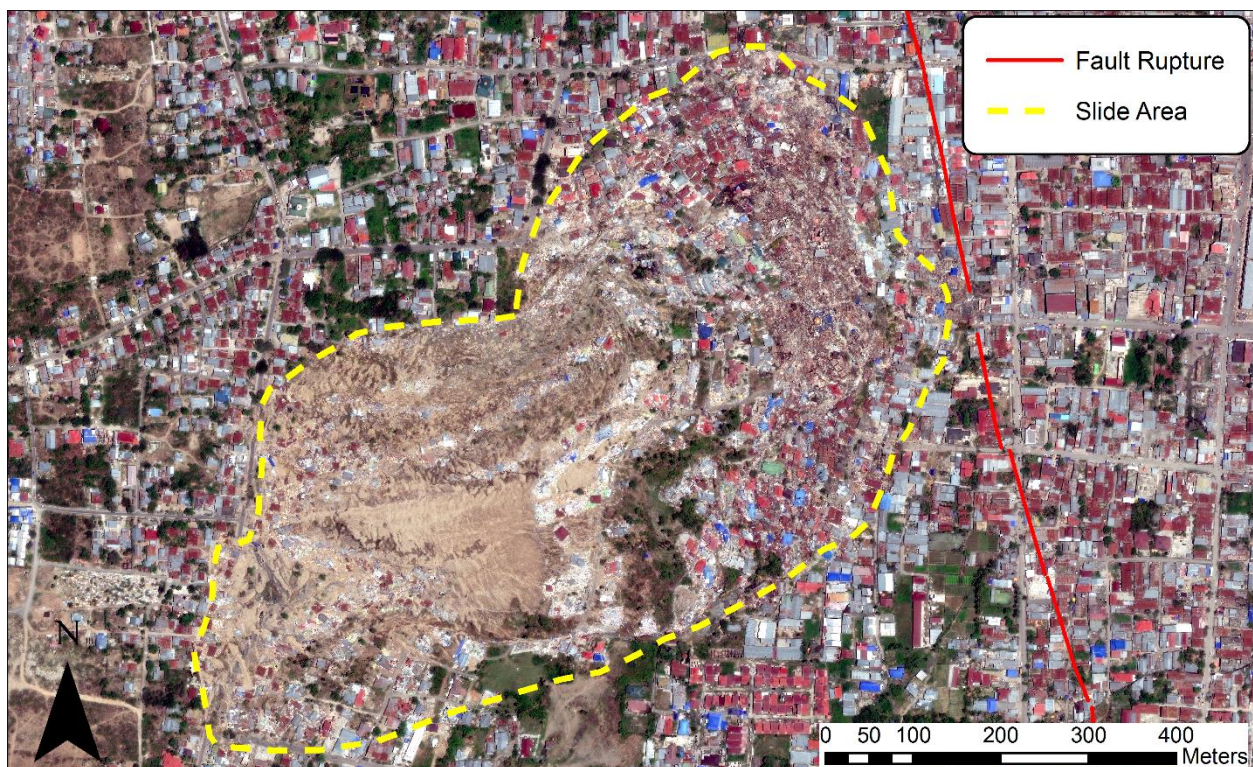


Figure 3.51. Landslide in the Balaroa neighborhood.



Figure 3.52. Photos of the scarp of the Balaroa landslide (left -0.906689° , 119.839557°) and of the slide area (right, -0.906687° , 119.839372°) after clean-up had occurred.

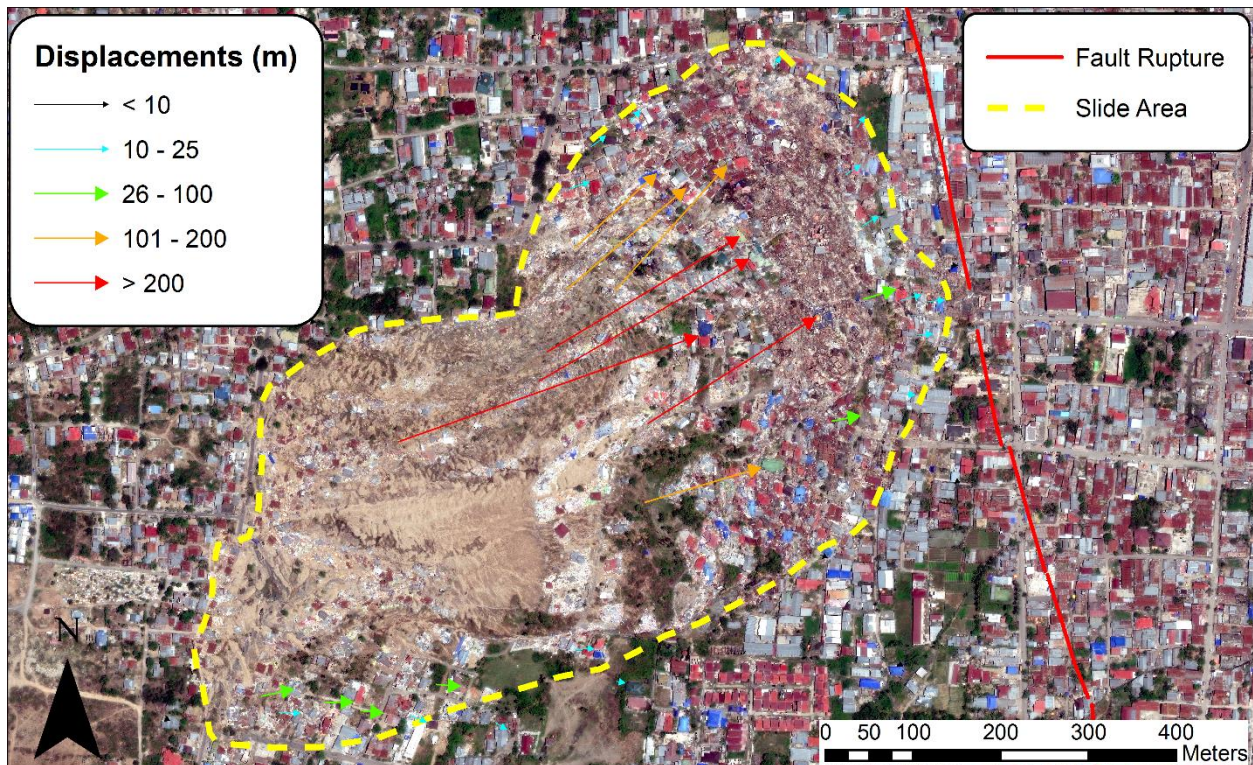


Figure 3.53. Displacement mapping of the Balaroa landslide.



Figure 3.54. Toe of the Balaroa landslide, showing multiple structures stacked on top of each other (-0.904367, 119.846528).

Eyewitnesses interviewed by the reconnaissance team described the failure initiating near the toe of the landslide. The initial failure was described as buildings sinking. People in the area had time to run uphill away from the initial failure, but then the sliding started. A video was recorded within the Balaroa failure (<https://twitter.com/i/status/1046445010231603200>; accessed 1 April 2019); although the original video could not be located and the sound suggests that this video may have been slowed down. Comparisons were made between the buildings and vehicles shown in the video with pre- and post-earthquake satellite imagery to determine the initial (-0.90447, 119.84291) and final locations (-0.90334, 119.84431) of the empty lot where the video was recorded. The locations would put this video recording along the northern edge of the landslide area. At the start of the video, the camera appears to be pointed to the southwest (large hills can be seen in the background). The camera then pans to the south, where buildings can be seen collapsing and beginning to slide. Approximately 20 seconds into the video, the buildings along the edge of the lot slide past. Although it is unclear how long after the earthquake this recording was taken, the video does provide evidence that the failure was progressive in nature and that the initial failures took place near the center of the slide.

The Balaroa landslide differs from the previously described landslides in some important ways. The first is that no irrigation canal is present on this side of the valley. Rice farming does still occur

in this area at a smaller scale, but the rice paddies are located near the toe of the landslide rather than the scarp (Figure 3.55). Satellite images from 2005 show that significantly more of this area was devoted to rice paddies in the past, but much of it was replaced by buildings. A second important difference at this landslide was that no sand boils were observed or reported. It is possible that sand boils occurred, but the GEER team was able to observe boils at the other four failure areas. A third important difference is the topography in this location. The previously described landslides occurred on relatively uniform slopes, which lead to long runouts relative to the area of sliding. The Balaroa failure occurred in an area with steeper slopes than those observed at the other sites, but the toe of the failure was very flat. This reduced the amount of runout and led to a piling up of debris at this location. In some cases, multiple buildings became stacked on top of one another (Figure 3.54).

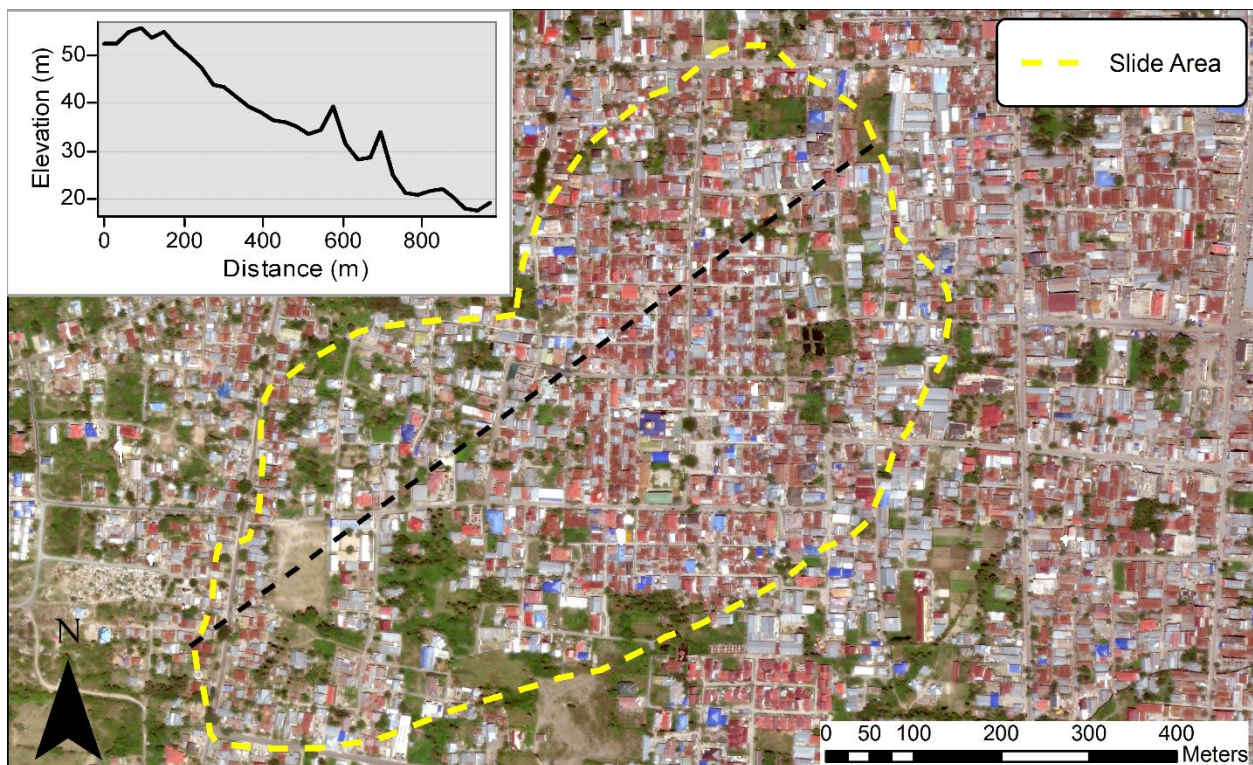


Figure 3.55. Pre-slide topography of the Balaroa landslide.

4 SUMMARY AND CONCLUSIONS

The M_w 7.5 Palu earthquake occurred on September 28, 2019 at 6:02 p.m. local time caused significant structural and geotechnical damage in Central Sulawesi. Much of the damage along the coastal areas was caused by the tsunami. Details of the damage caused by the tsunami are described by Robertson et al. (2019) and Yalciner et al. (2018). Outside of the coastal areas, damage was primarily caused by flowslides, which occurred along the margins of the Palu Basin. All of the flowslides, with the exception of Balaroa, occurred near an irrigation canal, which provides water for irrigating rice fields. Three of these flowslides occurred within a Zone of large ground deformation that extended for more than 6 km south of the Palu Airport.

The reconnaissance team, composed of engineers from GEER, HATTI and PusGen performed surveys in Central Sulawesi on November 13 to 18, 2018. The team collected a variety of data using digital cameras, GPS survey equipment, and UAVs. This data was supplemented by eyewitness interviews and satellite images from Digital Globe (2018) and Planet. The geomatic and photogrammetric data collected via drone and satellite images were used to assess ground displacements and generate digital elevation models that aided interpretation of geomorphological features. Eyewitness accounts provided insight into the progression of the landslides. Based on this information the following conclusions can be drawn:

- The most devastating geotechnical consequence that contribute to almost 80 percent of the total casualties was the large flowslides that occurred in densely populated residential areas. These residential areas were located in parts of the valley that were actively being used for rice farming or had been used for rice farming in the recent past.
- All of the flowslides occurred near the interface of alluvial fan deposits coming from the hills and fluvial deposits from the Palu River. These areas had relatively flat slopes (2 to 3 percent), although the flowslides appeared to have initiated in locations with locally steeper slopes (4 to 6 percent).
- An unlined irrigation canal, used to provide water for the rice fields, defines the eastern (uphill) margin of large ground deformations or flowslides on the eastern side of the Palu basin. Where the canal transitions to being lined, no significant deformations were observed.
- For the three flowslides just south of the Palu airport, the largest displacements and/or initiation of flowslides occurred where elevations transitioned from 60 to 80 m and the grade was greater locally than the average slope (Figure 3.4).

- Sand boils were observed within the margins of all of the flowslides, with the exception of Balaroo. The slide area at Balaroo had been heavily reworked by earth moving equipment and excavators by the time the reconnaissance team arrived, which may have obscured evidence of sand boils if any had been present. The sand boils that were observed generally occurred in low-lying areas between blocks of rafted crust. This suggests that elevated pore pressures occurred at depth and were only able to reach the surface once the crust was laterally extended by the deformations and loss of confinement.
- Eyewitnesses interviewed at each of the flowslides told the reconnaissance team that the large deformations initiated after the earthquake shaking stopped. This delay seemed to be on the order of minutes, but most of the witnesses had a hard time describing the exact length of the delay between the earthquake and the initiation of sliding. At Jono Oge and Balaroo, the delay was long enough for people to exit buildings and run towards open fields where some were able to survive the flowslide by riding on blocks of crusts or on roofs of collapsed buildings.
- Flowslides caused canal breaches at Petobo, Jono Oge and Sibalaya. At Jono Oge, the mudflow inundated multiple communities downstream of the flowslide that would have been unaffected otherwise. One eyewitness described how his family was able to survive the flowslide by riding on a raft of crust created by a cluster of banana trees, but his son was swept away by the mudflow that followed. He is now among the many people reported missing after this earthquake.

5 REFERENCES

- ASEAN Coordinating Centre for Humanitarian Assistance on Disaster Management (AHA) (2018). *Situation Update No. 15 M7.4 Earthquake and Tsunami Sulawesi, Indonesia*. Situation Report, AHA Centre, Jakarta, Indonesia. <https://ahacentre.org/situation-update/situation-update-no-15-sulawesi-earthquake-26-october-2018/>, last accessed April 1, 2019.
- Antara Foto. (2018). “Dampak Likuifaksi Tanah Pascagempa Sigi.” <https://www.antaraneews.com/foto/754873/dampak-likuifaksi-tanah-pascagempa-sigi/2>, last accessed March 19, 2019.
- Bellier, O., Sebrier, M., Beaudouin, T., Villeneuve, M., Braucher, R. Bourles, D., Siame, L., Putranto, E., Pratomo, I. (2001). “High slip rate for a low seismicity along the Palu-Koro active fault in central Sulawesi (Indonesia).” *Terra Nove*, 13, 463-470.
- Bellier, O., Sebrier, M., Seward, D., Beaudouin, T., Villeneuve, M., Putranto, E. (2006). “Fission track and fault kinematics analyses for new insight into the Late Cenozoic tectonic regime changes in West-Central Sulawesi (Indonesia).” *Tectonophysics*, 413, 201-220.
- Boulangier, R.W. (1990). *Liquefaction behavior of saturated cohesionless soils subjected to uni-directional and bi-directional static and cyclic simple shear stresses*. Dissertation, University of California, Berkeley.
- Copernicus Emergency Management Service (CEMS) (2018). “[EMSR317] Earthquake in Indonesia.” Grading Maps, CEMS, <https://emergency.copernicus.eu/mapping/list-of-components/EMSR317>, last accessed April 1, 2019.
- Digital Globe (2018). “Open Data Program: Indonesian Earthquake and Tsunami.” <https://www.digitalglobe.com/ecosystem/open-data/indonesia-earthquake-tsunami>, last accessed March 19, 2019.
- Gu, W.H., Morgenstern, N.R., Robertson, P.K. (1993). “Progressive failure of lower San Fernando dam.” *Journal of Geotechnical Engineering*, 119(2), 333-349.

- Hamilton, W. (1979). "Tectonics of the Indonesian region." *U.S. Geological Survey, Professional Paper, 1078*, 345 p.
- Hanifa, R. (2018). GEER – HATTI – PuSGeN Joint Survey on Palu Earthquake 2018 (M7.4) 13-18 Nov 2018. Presentation, Indonesian Ministry of Research, Technology and Higher Education, Jakarta, Indonesia, November 12, 2018.
- Hungr, O., Leroueil, S., Picarelli, L. (2014). "The Varnes classification of landslide types, an update." *Landslides, 11*(2), 167-194.
- Jakarta Post (2019). "Central Sulawesi disasters killed 4,340 people, final count reveals." <https://www.thejakartapost.com/news/2019/01/30/central-sulawesi-disasters-killed-4340-people-final-count-reveals.html>, last accessed April 2, 2019.
- Joint Research Centre (JRC). (2018). "M_w 7.5 Earthquake in Indonesia, 28 Sep 2018." JRC Emergency Reporting - Activation #02, Global Disaster Alert and Coordination System, European Commission. <http://www.gdacs.org/Public/download.aspx?type=DC&id=74>, last accessed April 1, 2019.
- Maulana A., Imai, A., van Leeuwen, T., Wantanabe, K., Yonezu, K., Nakano, T., Boyce, A., Page, L., Schersten, A. (2016). "Origin and geodynamic setting of late Cenozoic granitoids in Sulawesi, Indonesia." *Journal of Asian Earth Sciences*, 124, 102-125.
- Robertson, I., Esteban, M., Stolle, J., Takabatake, T., Mulchandani, H., Kijewski-Correa, T., Prevatt, D., Roueche, D., Mosalam, K. (2019). *StEER - Palu Earthquake and Tsunami, Sulawesi, Indonesia: Field Assessment Team 1 (FAT-1) Early Access Reconnaissance Report*. Structural Extreme Events Reconnaissance, DesignSafe-CI , doi:10.17603/DS2JD7T.
- Seed, H.B. (1979). "Considerations in the earthquake-resistant design of earth and rockfill dams." *Geotechnique*, 29(3), 215-263.
- Seed, R.B., Harder, L.F., Jr. (1990). "SPT-based analysis of cyclic pore pressure generation and undrained residual strength." Proc., H.B. Seed Memorial Symp., Bi-Tech Publishing Ltd., 351–376.

- Soquet, A., Hollingsworth, J., Pathier, E., Bouchon, M. (2019). "Evidence of supershear during the 2018 magnitude 7.5 Palu earthquake from space geodesy." *Nature Geoscience*, 12, 192-199.
- Socquet, A., Simons, W., Vigny, C., McCaffrey, R., Subarya, C., Sarsito, D., Ambrosius, B., Spakman, W. (2006). "Microblock rotations and fault coupling in SE Asia triple junction (Sulawesi, Indonesia) from GPS and earthquake slip vector data." *Journal of Geophysical Research*, 111, B08409.
- Tehusjarana, K.M. (2018). "Central Sulawesi quake, tsunami inflicted US\$911 million in losses: Govt." *The Jakarta Post*, Jakarta, Indonesia.
- Thein, P.S., Pramumijoyo, S., Brotopuspito, K.S., Kiyono, J., Wilopo, W., Furukawa, A., Setianto, A. (2014). "Estimation of seismic ground motion and shaking parameters based on microtremor measurements at Palu City, Central Sulawesi Province, Indonesia." *International Journal of Geological and Environmental Engineering*, 8(5), 308-319.
- Valkaniotis, S., Ganas, A., Tsironi, V., Barberopoulou, A. (2018). *A preliminary report on the M7.5 Palu earthquake co-seismic ruptures and landslides using image correlation techniques on optical satellite data*. European-Mediterranean Seismological Centre, 1-15.
- van Leeuwen, T.M., Muhardjo. (2005). "Stratigraphy and tectonic setting of the Cretaceous and Paleogene volcanic-sedimentary successions in northwest Sulawesi, Indonesia: implications for the Cenozoic evolution of Western and Northern Sulawesi." *Journal of Asian Earth Sciences*, 25, 481-511.
- Walpersdorf, A., Vigny, C., Subarya, C., Manurung, P. (1998). "Monitoring of the Palu-Koro Fault (Sulawesi) by GPS." *Geophysical Research Letters*, 25(13), 2313-2316.
- Watkinson, I.M. (2011). "Ductile flow in the metamorphic rocks of central Sulawesi." *The SE Asian Gateway: History and Tectonics of the Australia-Asia collision*, Geological Society of London, 355, 157-176.
- Yalciner A.C. et al. (2018). *The 28th September 2018 Palu Earthquake and Tsunami: ITST, 07-11 November 2018 Post Tsunami Field Survey Report (Short)*. International Tsunami Survey Team, International Tsunami Information Center, Honolulu, Hawaii.

Youd, T.L., Hoose, S.N. (1977). "Liquefaction susceptibility and geologic setting." Proc., 6th World Conf. on Earthquake Engineering, Roorkee, India, Indian Society of Earthquake Technology.